University of Naples Federico II
Department of Structures for Engineering and Architecture

PhD Programme in Seismic Risk
XXVIII Cycle

Coordinator Prof. Aldo Zollo

Maddalena Cimmino

PhD Thesis

SEISMIC RETROFIT OF PRECAST STRUCTURES

Tutor
Prof. Gennaro Magliulo

2016

A Stefano,
per averci sempre creduto,
per avermi spronato a combattere
da sola ma non sola.

Abstract

In the last decades, RC precast structures were extensively used in all Europe as industrial buildings. However, both the poor knowledge of their seismic behavior and the lack of specific code provisions led to a high seismic vulnerability of the existing precast estate. During recent seismic events, indeed, significant and extensive damages were exhibited by precast structures. These scenarios demonstrated that the structural safety of precast structures is an important issue for both the human safety and the social/economic management of whole regions/countries. Three significant losses items are imputable to seismic damage mostly for precast structures. The first one is related to the casualties, injuries and its amount is proportional to the exposure of the structure. The second losses item is strictly related to the structural damage, and it consists in repair/replacement costs. The last ones, instead, depends on the down time in which the productive activities are interrupted in order to allow the interventions of structural rehabilitation.

This work focuses on typical one-story precast buildings, designed without any seismic criteria, characterized by isolated columns fixed in socket foundations and connected to the beams by friction connections. Roof elements are arranged so that no rigid diaphragm is provided and the seismic force at the roof level is transferred to the lateral resisting system by masses proportional criteria which lead to plan irregularities.

For the above considerations, it is recognized that seismic retrofitting interventions are required for the existing precast structures. However, two main issues should be faced: first, the code recommendations for seismic retrofit of the precast structures are still poor; second, the retrofit strategies typically adopted for the reinforced cast-in situ buildings are not suitable to fix the specific vulnerabilities related to the structural scheme of the precast buildings.

The present work aims at presenting different retrofit strategies for the beam-to-column friction connections of existing precast structures. In particular, it aims at comparing two different strategies based on displacement or velocity activation. The seismic performance of the retrofitting solutions is demonstrated by means of experimental and numerical results.

Keywords

Precast structures; beam-to-column connections; seismic retrofit; hysteretic device; viscous device; energy balance; non-linear dynamic analysis.

Table of contents

List of figures

List of tables

Chapter 1

INTRODUCTION

1.1 Motivation

In the last decades, RC precast structures were extensively used in all Europe as industrial buildings. However, both the poor knowledge of their seismic behavior and the lack of specific code provisions led to a high seismic vulnerability of the existing precast estate. During recent seismic events, indeed, significant and extensive damages were exhibited by precast structures. These scenarios demonstrated that the structural safety of precast structures is an important issue for both the human safety and the social/economic management of whole regions/countries. Three significant losses items are imputable to seismic damage mostly for precast structures. The first one is related to the casualties, injuries and its amount is proportional to the exposure of the structure. The second losses item is strictly related to the structural damage, and it consists in repair/replacement costs. The last ones, instead, depends on the down time in which the productive activities are interrupted in order to allow the interventions of structural rehabilitation.

During some recent earthquakes, like L'Aquila (Italy) in 2009 (Faggiano et al. 2009; van der Harst et al. 2012), Van (Turkey) in 2011 (Ozden et al. 2014) and Emilia earthquakes (Italy) in 2012 (Belleri et al. 2015; Bournas et al. 2013; Magliulo et al. 2014), the poor seismic response of these structures was mostly caused by the inadequacy of the connection systems between both the structural elements and the structural and nonstructural components (Baird et al. 2011). In many structures, indeed, the connections were not designed for any seismic action and their premature failure during the seismic excitation caused catastrophic collapses and structural damages. For instance, during the Emilia earthquakes, most of the failures were caused either by the absence of mechanical devices connecting the structural elements (Magliulo et al. 2014)

or by the inadequacy of the connections of the nonstructural components (Biondini et al. 2013), i.e. the cladding panels.

During the last years several experimental and numerical researches on precast structures were developed in order to achieve: the improvement of modern seismic codes for the design of new structures (Fischinger et al. 2008; Toniolo 2012), the assessment of existing structures (Belleri et al. 2015; Bournas et al. 2013; Casotto et al. 2015) and the definition of new retrofitting solutions (Belleri et al. 2015; da Fonseca et al. 2011). With regards to existing buildings, Magliulo et al. (2008), performed several nonlinear analyses on existing precast structures in order to assess their seismic response. The analyses results demonstrated that the strength of the frictional beam-to-column connections can be lower than the seismic demand in low-medium seismic zones in Italy: in these areas the collapse of the structures could occur due to the loss of the support in the beam-to-column connections. Moreover, in the following years the same authors experimentally defined the frictional strength for the typical existing frictional connections (neoprene-concrete) (Magliulo et al. 2011) and they found out that the frictional coefficient values were lower than the values adopted in the previous study, giving an even lower structural safety.

Belleri et al. (2015) also performed an assessment study of existing precast buildings. By detailed field observations of existing buildings in Emilia Romagna region after the earthquakes, it was found that the connection systems were the crucial elements in the structural seismic response. In the study, the seismic performance of seven benchmark industrial structures with different construction ages were described in details. Some numerical considerations were also performed in order to justify the recorded loss of support phenomena under the recorded seismic loads in Emilia region.

Since the knowledge about the seismic retrofitting of RC precast structures is still poor if compared to the cast in-situ RC structures (Fardis et al. 2015; Lampropoulos and Dritsos 2011; Mazza 2015), both the scientific and the technical community are addressing growing efforts for the development of this topic. After the Emilia earthquakes, the Italian government regulated the retrofitting actions for the structures in the epicentral area by issuing a specific law (Legge 01/08/2012 n. 122 2012). Moreover, in order to give more detailed technical indications, the "Guidelines on local and global retrofitting systems of precast structures" (Gruppo di Lavoro Agibilità Sismica dei Capannoni Industriali 2012) were edited under the supervision of the Italian Department of Civil Protection. According to the reference law, the structural safety against seismic events can be obtained through a procedure consisting of two phases: a) the removal of the main structural deficiencies; b) extensive and systematic actions in order to achieve the required seismic performance, according to the current Italian code (Circolare 02/02/2009 n. 617 2009; D. M. 14/01/2008 2008). The first phase is crucial

and it requires quick emergency actions to obtain the positive usability judgment by removing the main deficiencies, as the lack of connections between structural elements and the inadequacy of connections between structural and nonstructural components. Some authors studied innovative retrofitting solutions for existing precast buildings; however, few efficient solutions were defined in the last years, such as mechanical devices for connections (Belleri et al. 2014), dissipative systems (Biondini et al. 2013) and retrofitting actions for vertical elements (columns) and foundations (Belleri and Riva 2012), typically used for RC frame structures.

1.2 Objectives and outlines

The present work aims at presenting different retrofit strategies for the beam-to-column friction connections of existing precast structures. In particular, it aims at comparing two different strategies based on displacement or velocity activation. The seismic performance of the retrofitting solutions is demonstrated by means of experimental and numerical results.

In the Chapter 2 basic principles of the existing retrofitting strategies are describe and the existing Code approaches are presented. Moreover, different retrofitting solutions for precast structures are described. In particular, retrofit solution at the structure level, element level and connection level are presented. Particular attention is paid to the existing retrofit solutions for the beam-to-column connection.

In Chapter 3 a case study is presented: it consists of an existing precast building situated in Mirandola (Emilia), which presents the main features of the typical one-story precast structure of the Italian industrial areas. Through numerical analysis the poor seismic performance of the existing building is demonstrated.

In Chapter 4 a retrofit solution for the beam-to-column connection is presented. It is based on a three hinged arc configuration which should avoid changes in structural schemes. It can be activated by relative displacements between beam and column. The possible damping source is related to the hysteretical behavior of the steel components.

In Chapter 5 a viscous damper retrofit solution is described by means of non-linear numerical analyses on a single frame of the reference building. Parametric analyses are performed to define the optimal configuration and mechanical characterization of the device.

In Chapter 6 the main conclusion of the present work are summarized.

Chapter 2

RETROFITTING SOLUTIONS FOR PRECAST BUILDINGS

2.1 Seismic retrofit of existing structures

2.1.1 *Retrofitting strategies*

In the last decades, wide scientific and technical researches dealt with the study of mechanical devices for the seismic retrofit of existing buildings in earthquake prone areas.

The main goal of the seismic devices consists in improving the seismic performance of the main structure according to two different strategies: damping the input energy absorbed by the structure during the earthquake (dampers) or limiting the absorbed input energy (isolation systems).

The isolation systems consist of slider bearings places between the foundations and the elevation of the main structure. They are designed so that their lateral stiffness is much lower than the lateral stiffness of the main structure so that they highly deform whereas the main structure rigidly moves without any source of hysteretic strains.

The dampers consist of mechanical devices, which activate during the structural movements and reduce the dynamic structural global response redirecting the energy content, due to the seismic event, towards these "sacrificial" elements, which can be easily inspected and replaced after damage. If the presence of the mechanical devices does not change the fundamental period of the main structure, it results in a reduction of the relative displacements. If the presence of the mechanical devices increases the lateral stiffness of the main structure, it results in a reduction of the fundamental period, which corresponds to the increase of absolute accelerations and the reduction of the displacements.

The energy damping can be obtained allowing inelastic mechanisms in the main structure or in the supplemental devices until the carrying capacity of the main structure, with respect to the gravity loads, is not yet compromised.

Concerning the request of power sources, the seismic dampers can be collected in three main categories:

- Active devices, which include monitoring systems to assess the structural response in run time through an electronic acquisition system, a control system which receives the collected data and selects decisions, an actuation system which physically realizes these actions. They need external power sources which can be interrupted during a seismic event;
- Semi-active, which have the same structure of the active devices but they need a low quantity of external power source since the control process is limited to local properties (i.e. the geometrical arrangement of the orifices in the fluid viscous damper, in order to prevent buckling);
- Passive energy dissipation systems are intended to dissipate part of the seismic input energy without external power sources, such as actuators, power supplies, computers, etc. necessary for active control technology. They are activated by the structural movements.

Concerning the working principles, the seismic passive dampers can be divided in three categories:

- displacement based dampers, which activate due to the relative displacements between the structural parts that they connect. The input motion frequency content does not influence the device response. The reaction forces in the device, transmitted to the main structure, are in phase with the internal forces generated by the input motion. For this reason, the maximum device response occurs with the maximum structural response and with the maximum transient structural deformations. Metallic, friction and self-centering systems belong to this category;
- velocity based dampers, which activate due to the relative velocity between the structural parts that they connect. The device response depends on the input motion frequency content and the reaction forces in the device, transmitted to the main structure, are not in phase with the internal forces generated by the input motion. For this reason, the maximum device response does not occur with the maximum structural response and this returns in lower design forces for the seismic dampers. Viscous and viscoelastic dampers belong to this category;
- acceleration based dampers, which change the energy flow to the main structure thanks to secondary tuning systems. The secondary system, design in terms of addition mass and stiffness, is tuned with the fundamental frequency of the main

structure. During the dynamic excitation, the input energy is moved towards the supplemental device and it is damped thanks to the inertial forces applied to the secondary structure.

Table 2-1 Supplemental Damping Systems

Conventional systems	**Passive Dampers**	**Semi-Active/Active Dampers**	**Isolation Systems**
Flexural Plastic Hinges	Metallic	Braces	Elastomeric
Shear Plastic Hinges	Friction	Tuned-mass	Lead-Rubber
Yielding Braces	Viscoelastic	Variable Stiffness	High-damping rubber
	Viscous	Variable Damping	Metallic
	Tuned-mass	Piezoelectric	Lead-extrusion
	Self-centering	Rheological	Friction Pendulum

2.1.2 *Code approach for the seismic retrofit*

The seismic performance of the industrial precast structures during recent earthquakes, pointed out structural vulnerabilities, especially for existing structures built in accordance with non-seismic criteria. For this reason, seismic retrofitting interventions should be performed but, whilst design building codes for new constructions provide methods and procedures to develop modern performance based structural responses, methodologies and guidelines are still poor concerning the retrofitting techniques.

The Italian building code (Circolare 02/02/2009 n. 617 2009; D. M. 14/01/2008 2008), following the Eurocode provisions (CEN 2005), gives general rules to perform the structural rehabilitation process of the existing structures. It should start with the assessment of the structural safety with respect to the external actions that the reference building should face during its life: if the current safety level does not follow the minimum requirements prescribed by the building code in force at this time, structural interventions should be performed. They should aim at restoring the initial conditions, exhibited before the performance degradation for external causes, or at improving the structural response to gain satisfactory safety levels.

In the specific section for the existing structures, the Italian building code limits the safety assessment and the design of retrofitting interventions to the ultimate limit states, i.e. with respect to the human life safety and with respect to collapse. Moreover, it defines the conditions in which the assessment of the existing structures is necessary:

- strength and stiffness degradation of the whole structures, or of some portions, with respect to environmental actions, material mechanical properties decay or with respect to special loads;
- change of the structural destination, which leads to different variable loads to be considered and different importance class of the structure;
- presence of non-structural interventions which interfere with the structural members, reducing their strength or stiffness;
- design or construction errors with respect to the code provisions and to the good practice.

The assessment procedure leads to the definition of one of the following conditions: (a) the structure can be used without any further intervention, (b) the structural destination and use should be limited, (c) the structural capacity should be improved. In this case, the Italian building code identifies three different categories of structural interventions: structural interventions which aim at the full compliance of the code safety levels, structural interventions which aim at improving the structural performance, local interventions which are applied to single structural elements or to limited portions of the whole building, with no modifications of the structural system.

Before the intervention application, the retrofitting procedure should include the assessment, in order to define the structural deficiencies and the level of seismic actions which cause the attainment of the ultimate limit state (and of the serviceability limit state, if requested). After that, the retrofitting strategy should be selected and motivated, with particular attention to the applied materials and techniques. The selection of the type, technique, extent and urgency of the intervention shall be based on the structural information collected during the assessment of the building. A preliminary dimensioning of the retrofitting technique and of supplemental structural elements should be performed and the structural response of the retrofitted building should be assessed, identifying the new level for external actions which leads to the attainment of the ultimate limit states (and of the serviceability limit state, if requested).

For more detailed indications, it should refer to specific technical publications (FEMA 2000; fib 2003) but there are still few recommendations for precast buildings.

2.2 Seismic retrofit techniques for precast structures

The seismic retrofit of precast structures requires specific criteria for the selection of the best solution: often, it is not possible to apply the strategies and the techniques used for reinforced concrete structures because of the peculiar issues related to the structural typology. In particular, when designed in accordance with seismic codes, the precast elements can exhibit higher performances due to the high mechanical properties of the

adopted materials and due to the high quality control during the production phase. Hence, typical structural deficiencies of the cast in situ reinforced concrete elements, such as the lack of transversal reinforcement area, inadequate overlapping lengths, discontinuities for longitudinal bars, etc., can be avoided. However, the precast structures can exhibit very poor seismic performance of the mutual connections between the structural elements. In particular, they can show: (a) a very poor reliability of beam-to-column connections, without any mechanical restrainers, i.e. friction connections, or without adequate seismic details which lead to ductile responses); (b) the lack or the inefficiency of the mutual connections between the roof elements, which reflect in flexible roof plans and in plane irregularities; (c) the presence of mutual constraints characterized by high stiffness, which are not compatible with high displacement requests and induce dangerous phenomena of dynamic interaction.

An important issue for the seismic retrofit of the precast structures concerns the high costs of interventions. First, it should be considered the wide extension of a typical precast building and the high number of elements, which need rehabilitations, especially for structures in which non-seismic criteria have been systematically applied (e.g. in order to fix the mutual connections between the roof elements of a typical industrial building, it could be necessary to realize hundreds of local interventions). Moreover, it should be considered that the application of the retrofitting techniques could be not easy due to the high span length of structural elements. For example, in order to check and operate in correspondence of the beam-to-column connections, skilled labor and specific equipment are needed: this results in high costs related to the installation procedures and to the facility breakdown.

The retrofitting techniques for precast structures can be divided in three main categories: they can be addressed at improving the global structural response (structure level), at increasing the seismic capacity of the structural members (element level) or at allowing the mutual transmission of the external loads (connection level).

2.2.1 *Structure level retrofit*

The retrofitting techniques, which can influence the global structural response, include interventions on the superstructure or on the substructure. The main issues that this kind of global techniques should face are the absence of lateral resisting frames in both the directions and the presence of flexible diaphragms.

Typical examples of superstructure interventions to improve the lateral shear strength are the bracing systems or the shear walls. However, the application of shear walls appears to be not very convenient for the precast structures, which are usually characterized by wide dimensions, in plan as well as in elevation.

In some cases, if urgent intervention is required, a global retrofit technique applied at the superstructure can consider to connect the top ends of the vertical columns with metallic strands or with ropes, which work only for tensile forces and not for compression. Hence, this kind of retrofitting technique should be carefully selected and accurately verified and integrated after the emergency phase.

In Belleri et al. (2015), the authors focus on the typical configuration for the horizontal diaphragms in the industrial precast buildings: the roof elements are connected directly to the supporting beams through mechanical connections or by friction and no cast in place topping is poured mainly due to the presence of large openings. In these conditions, the diaphragm action is not provided and the behavior of adjacent precast frames is basically decoupled during the seismic event. The lateral frames are more rigid than the internal ones because of the presence of cladding panels and therefore adjacent frames could move out-of-phase so that roof-to-beam and beam-to-column connections experience displacements and rotations that could cause premature fall. Moreover, the beams are subjected to out-of-plane bending and additional torque due to the seismic roof loads and to the column top rotations. The authors present a possible retrofitting global solution aiming at reducing the lateral load demand: it consists in providing a diaphragm at roof level, which will act as a deep beam in carrying the horizontal loads. This could be realized adding interconnecting adjacent elements (Figure 2-1(a)), introducing a planar steel truss or introducing diagonal tendons (Figure 2-1(b)).

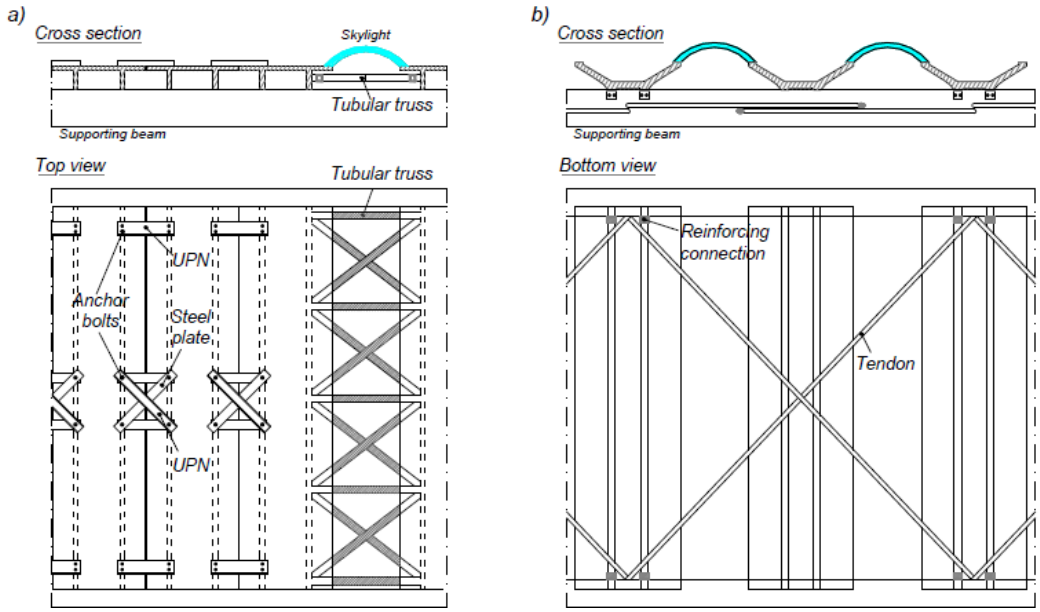

Figure 2-1 Possible retrofitting solutions for flexible diaphragms (Belleri et al. 2015)

Another possible intervention on the superstructure could consider the presence of an external steel frame, fixed at the base and connected to the existing building at the horizontal diaphragm level. The external frame provides, at the same time, a supplemental structure for absorption of the seismic actions and an effective restrain to the horizontal diaphragm in order to perform a rigid horizontal level.

Concerning the retrofitting techniques applied to the substructure, the isolation systems could be considered. In this case, the retrofitting system could lead to high costs for installation and maintenance after damage.

2.2.2 *Element level retrofit*

Considering the typical structural scheme of precast structures, consisting in isolated columns fixed at the bottom end by socket foundations and connected at the top end to the beams through isostatic restrains, the only ductility source is related to the plastic behavior of the columns. For this reason, the retrofitting techniques addressed to the element level mainly consist in structural interventions for the increase of the column bearing capacity, for the increase of the column flexural and/or shear strength, for the increase of the column deformation capacity and of the overall structural ductility. Typical techniques applied to the precast structures in order to join these goals can be derived from reinforced concrete structures, e.g. concrete or steel jacketing and FRP plating or wrapping (Figure 2-2). However, also in this case, the effects of the retrofitting techniques should be considered for the specific structural typology and the related issues. For example, due to the presence of industrial equipment or racks, it could be

difficult to install the retrofitting systems at the column base and it could be impossible to increase the cross sectional area. Moreover, jacketing or wrapping techniques improve confinement and increase deformation but high column base rotation can result in high value of the lateral drift or of the relative displacements between beam and column with consequent damage to the non-structural components as well as to the roof elements.

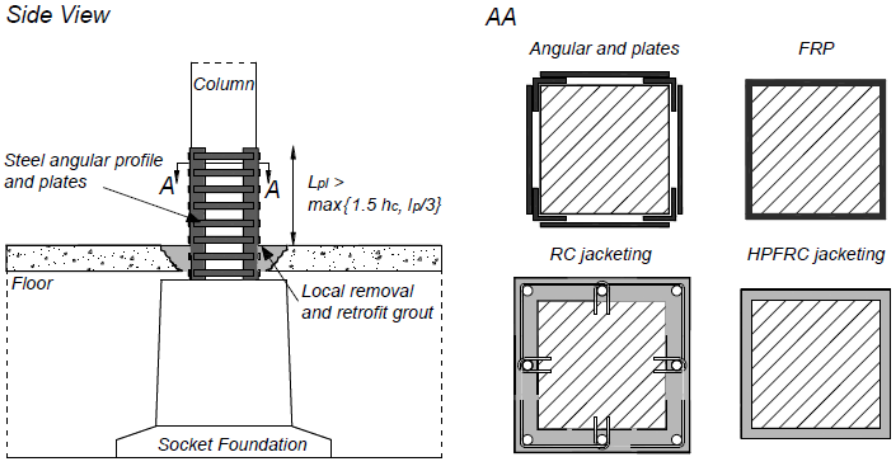

Figure 2-2 Column strengthening solutions (Belleri et al. 2015)

2.2.3 *Connection level retrofit*

The retrofitting techniques addressed to the connection level should: limit relative displacements where unseating phenomena can occur, create new effective restrains, limit relative rotations, which can lead to out-of-plane mechanisms, avoid overturning of the cladding panels, etc. However, the application of these techniques should avoid the increase of lateral stiffness and the structural scheme modification. In fact, this may result in the increase of the external actions (in the range of periods of interest, a higher lateral stiffness corresponds to a lower fundamental period and results in higher seismic actions) and of internal forces (in presence of statically indeterminate restrains the structural elements can be subjected to external actions for which they are not designed).

As mentioned before, the mutual connections between precast elements represent a high seismic vulnerability source. For this reason, after the recent seismic events which hit precast facilities, different solutions are carried out. In the following, some remarkable examples are described in order to define the recent state of art and knowledge about seismic retrofitting of different types of structural connections in precast structures. Finally, particular emphasis is dedicated to the beam-to-column connections.

In Belleri et al. (2014), the authors investigate the use of ductile connections between precast beams and roof elements. These connections are able to transfer the horizontal inertial loads and to accommodate deformations arising from seismic displacement compatibility. In fact, the typical precast beam-to-column connection adopted for precast building consists of L-shaped steel plates, bolted to the roof elements and connected to the beam by means of anchor headed bolts placed in steel channel profiles embedded in the concrete element. This connection is intended to perform a hinge connection. However, during the seismic event relative rotations reduce the gap between the two structural elements and when the elements keep in contacts, the connection gains rotational stiffness. This results in additional forces in the connection which induce brittle failures associated with the concrete crushing or with the prying action of the anchor headed bolts.

On the contrary, the investigated connection, thanks to an arch shaped configuration (Figure 2-3), accommodates relative displacements and rotations. If designed with a dissipative approach, the proposed connection could be used to dissipate energy during the seismic event.

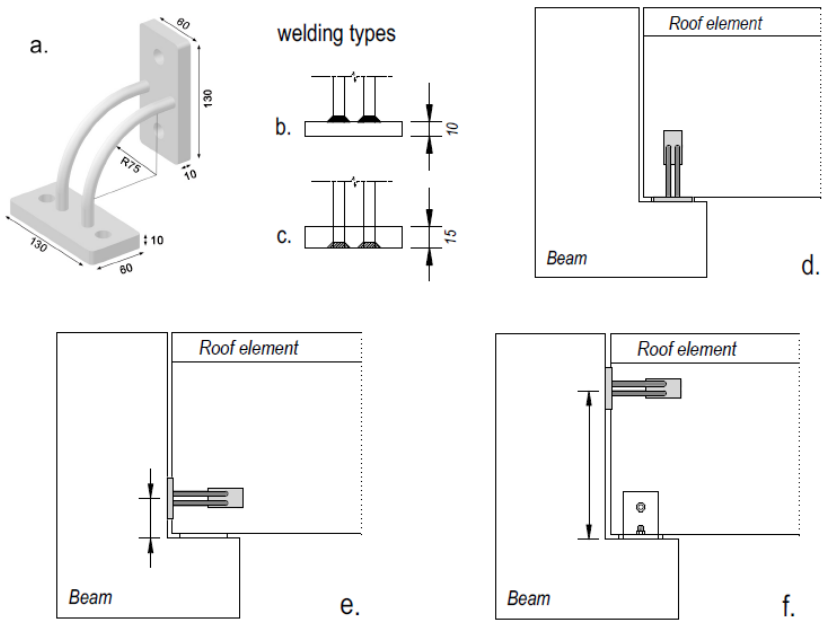

Figure 2-3 Arch shaped roof-to-beam connection and possible installation configurations (Belleri et al. 2014)

In Belleri and Riva (2012), the authors show a possible retrofitting solution for column-to-foundation connections in mat foundations. It consists in the realization of grouted corrugated steel sleeves: the cyclic behavior of the grouted corrugated steel sleeve connections in investigated in the mentioned paper, through cyclic shear tests

considering different connection details. In Figure 2-4 two of the test specimens are represented, both with four grouted sleeves: the specimen GS4 had a 90° hooks at the reinforcing bar end, whereas the specimen GS4B presents straight reinforcing bars.

The test results pointed out that the routed sleeve connections provide confinement, inhibit buckling of the longitudinal reinforcement and increase the strength of the grout. This results in localized damage at the column base avoiding inelastic mechanisms in the footing.

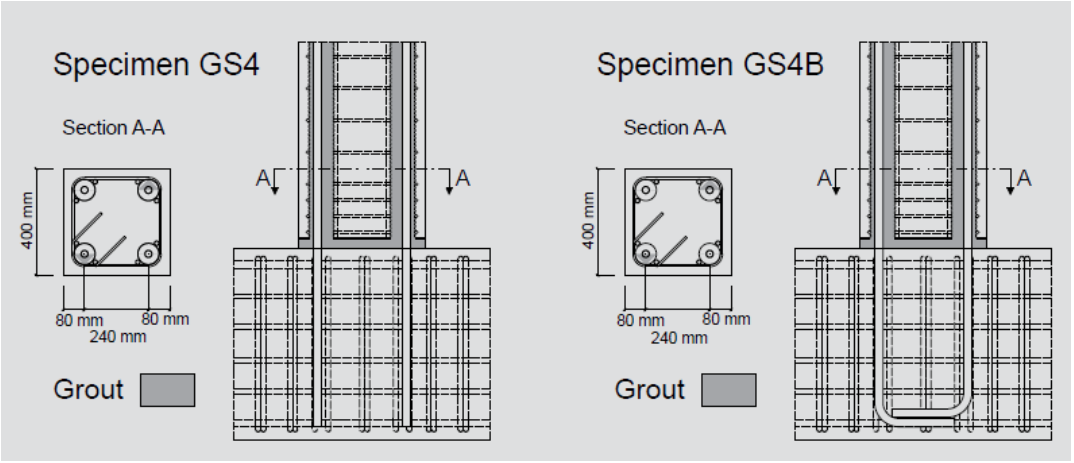

Figure 2-4 Details for column-to-foundation connections retrofitted with grouted corrugated steel sleeve connections (Belleri and Riva 2012)

Concerning the external cladding panel-to-structure connections, the European SAFECLADDING project has been developed in order both to assess the safety of the existing connections and to define innovative systems for new and retrofitted structures. In the frame of this project some researches were developed in order to define new retrofitting systems (Biondini et al. 2013).

In Dal Lago (2015) three innovative dissipative cladding connections have been presented, designed and experimentally characterized in order to define the optimal technological features for the single device. They are friction based (Figure 2-5(a)), multiple slit (Figure 2-5(b)) and folded plate (Figure 2-5(c)) devices.

The friction based devices provide a quasi rigid-plastic behavior to which a very large energy dissipation is associated, with a typical friction type hysteresis. The connection provided with brass sheets exhibited a very large cyclic reliability, to which corresponds the possibility of re-use after many large amplitude cycles. Some uncertainties are associated with the definition of the slip load threshold due to the friction mechanism.

The multiple slit devices provide large elastic stiffness and a hardening behavior due to the diffusion of plasticity along the rectangular section of each elementary beam and to the material hardening. Despite the large relative displacement capacity of the device,

the maximum displacement attained is relatively low, due to the small dimensions that are needed in order to apply the device between cladding panels.

The folded plate devices provide an in-plane flexible behavior with large displacement capacity, which corresponds to good energy dissipation. The mechanical behavior of the single device is largely influenced by the out-of-plane mechanism but the structural global response could be optimized using a proper installation scheme.

Numerical and parametrical analyses demonstrate also the influence of the dissipative connections on the global behavior of the whole structure.

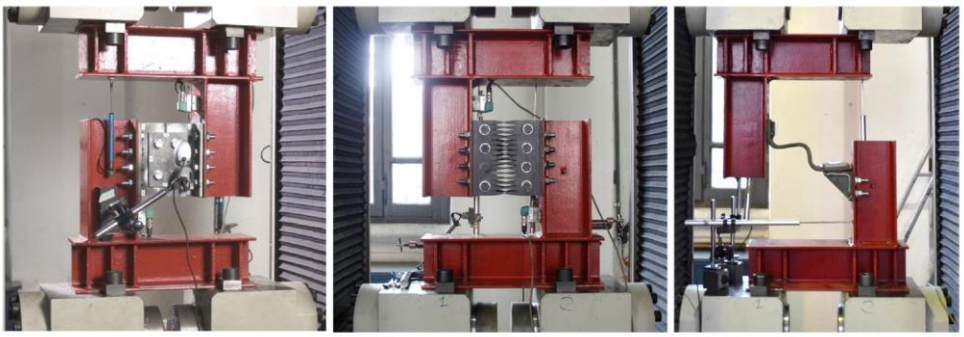

Figure 2-5 Innovative dissipative connections for cladding panels in precast structures (Dal Lago 2015)

In Latour and Rizzano (2015) a retrofitting solution for external vertical cladding panels is proposed. It consists of a dual system, composed by the external walls and the internal columns, working in parallel (Figure 2-6(a)). The connection between the cladding panels and the internal structure is performed by means of hysteretic dampers, namely XL-Stub, obtained from steel flange plates which follow the basic principle of the ADAS devices (Added Stiffness And Damping): the X-shape of the steel plate, which reproduce the diagram of the bending moment arising under tension loads, leads to the plasticization of all the plate sections with a high dissipative capacity due to the deformation demand distributed along the whole plate (Figure 2-6(b)).

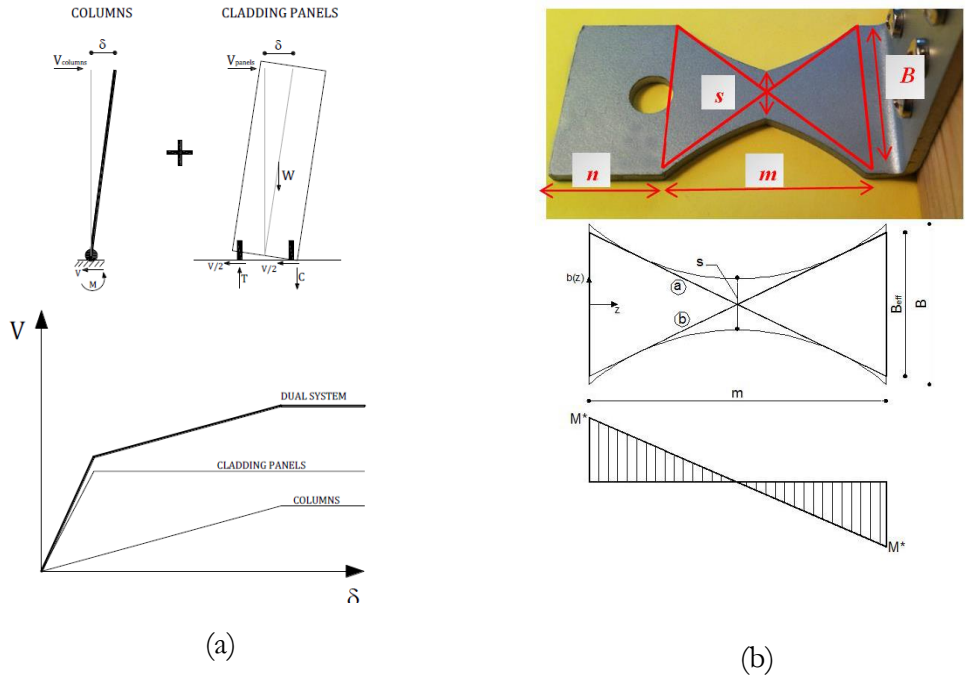

Figure 2-6 XL-Stub connection for precast cladding panels (Latour and Rizzano 2015)

2.2.3.1 Beam-to-column connection seismic retrofitting solutions

In this work, retrofitting solutions for the beam-to-column connections are mainly discussed: in the following, a brief literature review is presented in order to describe the recent applications for this kind of structural connection.

The applied solutions include mechanical devices, which offer different type of energy dissipation in order to improve the local and global structural seismic response.

In Yildirim et al. (2015) the seismic retrofit of a typical one-story industrial precast concrete building located in Turkey is performed. The existing building is not well-engineered and is expected to have very poor performances if exposed to seismic events. The selected retrofitting technique should guarantee that the building would not be vacated during the application. It consists in applying rotational friction dampers with an effective configuration defined after iterative trial-and-error linear studies. Non-linear time-history analyses are performed to verify the exhibited cyclic response.

In particular the dampers are placed at the beam-to-column dowel connections in the direction of the main frame (Figure 2-7(a)). In the orthogonal direction, steel compression members are designed in order to provide load transfer between frames (Figure 2-7(b)).

The performance of the applied retrofitting solution is studied in terms of global response, i.e. the interstory drift exhibited by the structure, the base shear force and the obtained damping ratios. It is pointed out that friction dampers, applied together with

some steel members, reduce the seismic demand of the main structure so that performance goals of ASCE 41-06 and of Turkish Earthquake Code 2007 can be satisfied. Further noticeable advantages are the easy and rapid installation procedure.

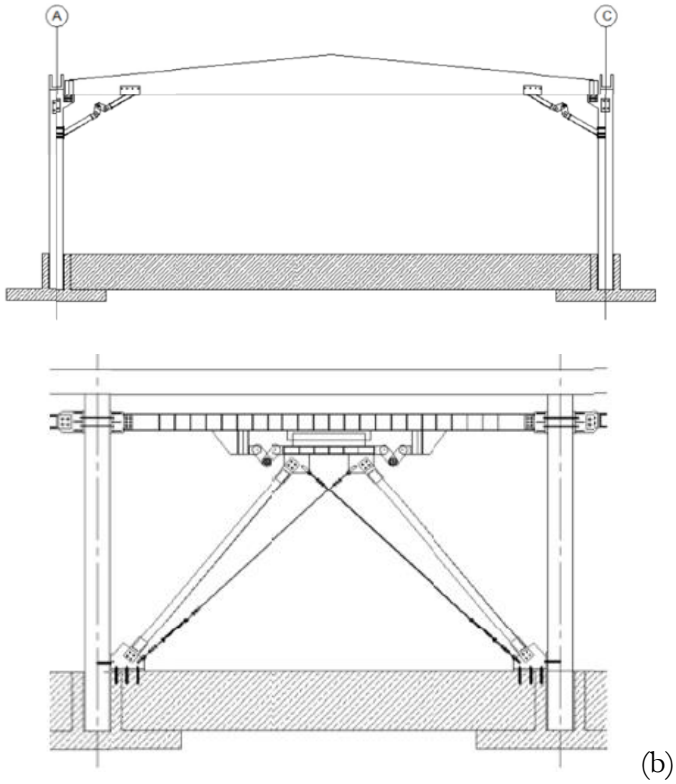

Figure 2-7 Application of friction dampers and steel members to precast structures (Yildirim et al. 2015)

Also in Martinelli and Mulas (2010), the use of friction dampers for the seismic retrofit of a one-story prototype precast building is considered, because of the advantage to have reduced dimensions and low costs for the devices application, together with a good energy dissipation providing ductility to the hinged connections.

The selection of the damper device is based on two requirements: adopting a device of small dimensions and enhancing a significant structural damping. The proposed device consists of two UPN200 channel sections assembled to form a wide flange section. It is connected to the column and the beam through a bolted connection to avoid the introduction of additional moments both in the beam and in the column. The dissipating mechanism consists of annular brass plates inserted between a steel plate and the channel profile, bolted together by a high strength bolt. The rotational strength is controlled by the bolt tension and it is provided by the friction developed between brass and steel. Different material can be adopted instead of brass (Figure 2-8).

The device efficiency is analyzed by comparing the seismic response of the bare and the retrofitted frame, by means of non-linear dynamic analyses. The numerical results pointed out an increase of the shear force in the zones where the device is inserted. On the other hand, the reduction of the maximum top displacement and of the column base bending moment, as well as the increase of hysteretic energy dissipation are demonstrated.

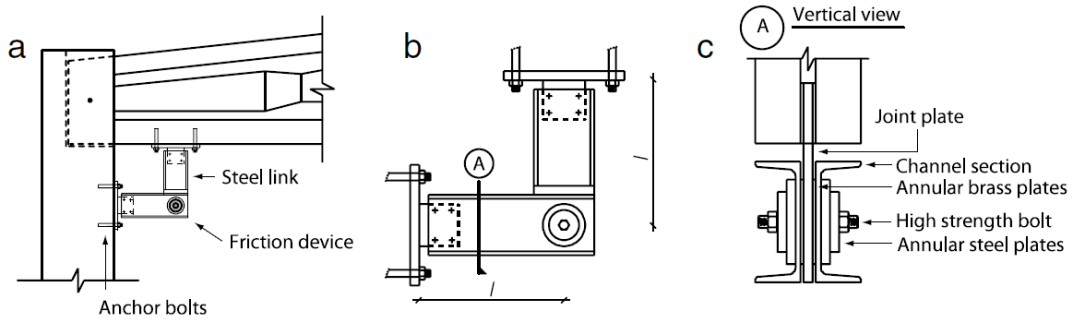

Figure 2-8 Beam-to-column connection friction dampers (Martinelli and Mulas 2010)

In some applications (da Fonseca et al. 2011) beam-to-column connection of precast concrete frame are strengthened by near surface mounted carbon fiber reinforced polymers strips (NSM CFRP strips). The performance of the considered system is investigated through quasi-static tests which pointed out an increase in the connection stiffness and in the flexural strength, reducing the midspan beam deflection. Brittle failures are recorded with the splitting of the beam edge, due to the low distance between the concrete edge and the strips. Finally, the authors indicate that particular critical an be the limited length available for the embedding of the strips on the column surface.

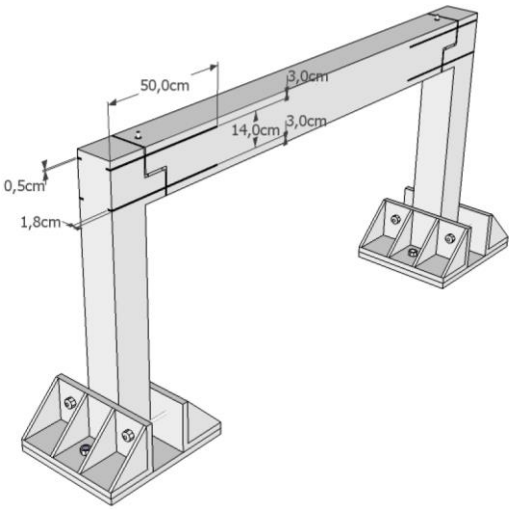

Figure 2-9 Precast beam-to-column connections retrofitted by NSM CFRP strips (da Fonseca et al. 2011)

Chapter 3

THE CASE STUDY: AN EXISTING INDUSTRIAL PRECAST ONE-STORY BUILDING

3.1 Introduction

On May 2012 two earthquakes hit Emilia-Romagna region (Northern Italy) and a huge number of existing precast RC one-story buildings was severely damaged. In some previous seismic events, the seismic vulnerability of precast RC buildings was already demonstrated, such as during Kocaeli earthquake (Turkey, 1999) (Saatcioglu et al. 2001) and L'Aquila earthquake (Italy, 2009) (Faggiano et al. 2009; Toniolo and Colombo 2012). However, in Emilia-Romagna the large number of damaged structures underlined the relevance of the seismic safety of this structural typology. In this part of the country, most of the precast structures hosted industrial and commercial activities and their collapse/damage was one of the main causes of the huge economic losses (Magliulo et al. 2014). In order to reduce the economic impact, hence, the retrofitting of these structures was one of the most important activities during the emergency phase, aimed at restoring the activities/production within short time period.

From a scientific point of view, the widespread damage caused the availability of a huge number of data and field observations about the seismic response of precast RC structures, built in Northern Italy in the second half of the twentieth century and in the first years of the twenty-first century. The first evidence of the field surveys pointed out the presence of common deficiencies, mainly related to the connection systems. Several collapses occurred because of the failure of the connections between the structural elements: several horizontal elements (e.g. roof elements and beams) experienced significant relative displacements with respect to the supporting ones (e.g. beams and columns), collapsing due to the loss of the support. Some studies have been already performed in order to assess the vulnerability of these structures (Psycharis et al. 2006; Toniolo 2013) and some papers investigated the seismic response through both

extensive photographic reports of the recorded damage in the hit region and descriptions of the main features of the analyzed structural typology. In these works, the authors drawn some main conclusions on the seismic safety of precast structures through simplified consideration about the seismic demand. For instance, in (Magliulo et al. 2014) the common failure of the friction beam-to-column connections (without mechanical devices, i.e. relying only upon the friction resistance between the connected elements) was justified by comparing the shear resistance of the connection with the elastic spectral accelerations of the first seismic event (May 20th).

In (Magliulo et al. 2008) the authors assessed the seismic safety of some existing precast RC buildings, typically employed in Europe. The vulnerability of the existing friction beam-to-column connections was demonstrated through nonlinear static and dynamic analyses. The adopted models of the precast RC structures did not take into account the friction resistance of the connections: the safety was verified by comparing a posteriori the shear seismic demand on the connections, modelled as pinned, and their friction resistance. In (Casotto et al. 2015) a seismic fragility model for Italian RC precast buildings was obtained through several nonlinear analyses on different typologies of buildings. The nonlinear models consisted of columns and beams and the beam-to-column connections were assumed as hinges. The collapse limit state due to the loss of support of the beam was verified a-posteriori by adopting two approaches: 1) the shear demand in at least one column exceeding the connection capacity; 2) the sliding displacement (Newmark sliding block analysis) of the beam exceeding its support length.

It is worth noting that several experimental studies were developed in the last decades in order to define the best models for precast RC structures. For instance, some tests investigated the inelastic behavior of structural elements (Fischinger et al. 2008) and some other studies developed models of the connection systems (i.e. designed according to modern building codes), such as between structural elements (Kremmyda et al. 2014; Magliulo et al. 2014) and between structural and nonstructural components (Biondini et al. 2013). However, these investigations are mainly referred to new buildings, designed for seismic actions according to modern codes. Some investigations were also performed concerning the seismic safety of high-rack structures (Petrovcic and Kilar 2012), typically employed in industrial buildings; these elements can influence the seismic response of the whole building and their failure can significantly increase the economic impact of the earthquake due to the contents losses. Concerning existing structures, several work were developed in order to define reliable and efficient retrofitting solutions for elements and connection systems (Belleri et al. 2014; Belleri et al. 2015).

In the following, the structural behavior of a precast RC building with friction connections, hit by the Emilia-Romagna earthquakes in 2012, is evaluated.

3.2 Description of the structure as-built

The reference building is an existing industrial precast structure built in Mirandola (Emilia Romagna, Italy, Figure 3-1), in1990, which shows the typical features and issues of most of the Italian precast buildings. The design of the load-bearing structure was performed according to the Italian building Code in force at that time (LS 1060, DM 30/05/1972, DM 3/12/1987) without any specific details for seismic design (according to LS 64), since the current seismic zonation did not include the Emilia region in the classified seismic-prone areas (Figure 3-2).

Figure 3-1 Geographical position of the reference building

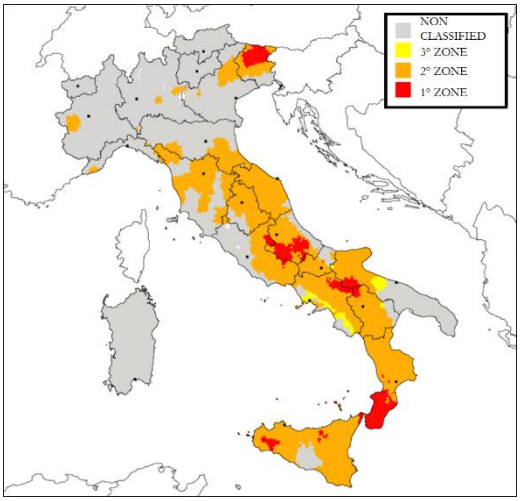

Figure 3-2 Seismic zonation in force in 1984

The one story building presents a very regular structural plan with respect to the main axes (Figure 3-3), consisting of six bays in the x direction (span length equal to 20m) and five bays in the y direction (span length equal to 10m).

The main structure consists of single precast RC columns 7.85m high, fixed at the base with isolated socket foundations. In the following, the internal columns are labelled as "type A", the columns of the external frames along the global x axis are labelled as "type B", the columns of the external frames along the global y label are labelled "type C" and the corner columns are labelled as "type D". Type A and C columns present a rectangular cross section of 50x40cm, with the higher dimension along the x axis; Type B and D columns present a square cross section of 50x50cm (Figure 3-4). All the columns present the same longitudinal steel reinforcement, consisting of 4 ϕ16 and 4

ϕ18, and the same transversal steel reinforcement, consisting of horizontal stirrups ϕ6, 20mm spaced.

The principal beams have I-shaped cross sections with a bottom and top base of 36cm. They have variable thickness and height: in order to obtain the best performance for shear and flexural behavior, they show at the ends the maximum thickness (24cm) and the minimum height (75cm), whereas in the middle span they show the minimum thickness (8cm) and the maximum height (175cm), so that the top surface shows an inclination of 10% (Figure 3-4).

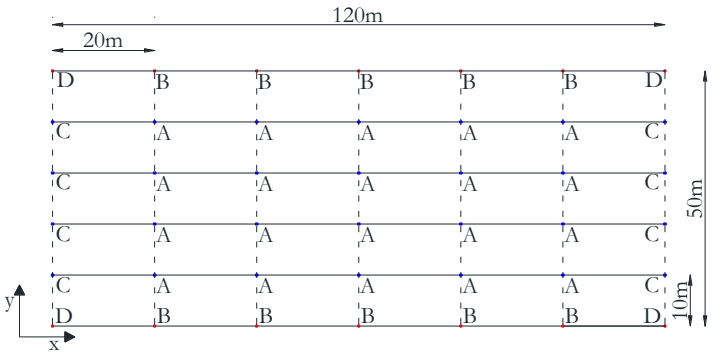

Figure 3-3 Plan view of the reference industrial precast building

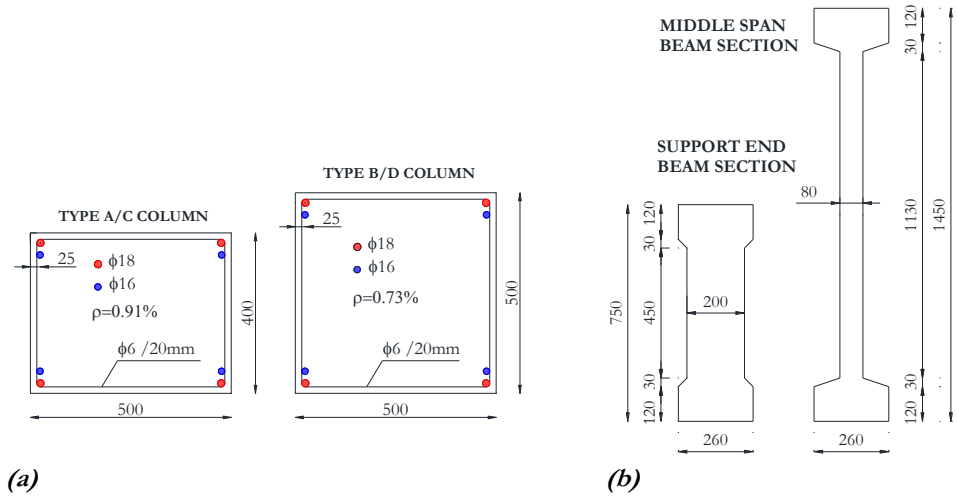

Figure 3-4 Columns and beam cross section

The principal beams connect the columns in the x direction through friction connections, using neoprene pads, without any mechanical device against shear loads. Neoprene pads arranged on the top of each column have dimensions of 23x26x1cm (Figure 3-5(a)). Girders with U-shaped cross sections (40x60cm) connect the columns

in the y direction, through bolted steel angles with a very low rotational strength around the girder transversal axis. Figure 3-5(a) shows the geometrical configuration of a typical beam-to-column friction connection of the building (column type B).

The roof elements consist of π-shaped and T-shaped precast elements, arranged in the y direction and simply supported by the principal beams for a length of 13cm (Figure 3-5(b)). For each bay, there are three groups of roof elements placed side by side (2 π-shaped -4 T-shaped-2 π-shaped), spaced with transparent elements which allow enlightenment.

The cladding elements consist of vertical panels, 8.90m high, connected to the external principal beams, in the x direction, or to the external girders, in the y direction. On both the external bays along the x direction, there are four portals consisting of vertical pillars and horizontal lintels.

Table 3-1 shows in the first column the number of elements for each member typology, the mean value of the mass for each element (m), the total mass for each member typology (m_{TOT}), the total mass at the roof level (considering the halved mass for columns and vertical panels) (M_{roof}), the total roof weight (w_{roof}).

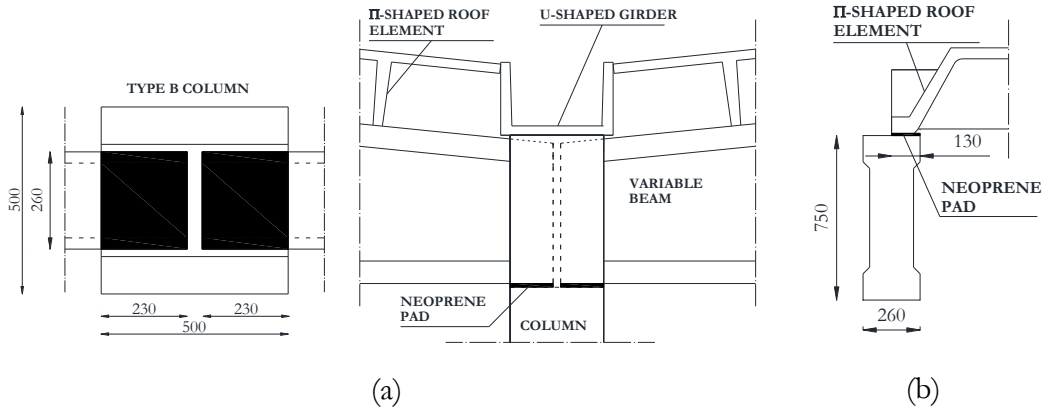

Figure 3-5 Friction beam-to-column (a) and roof-to-beam (b) connection

Table 3-1 - Mass values for members

	n. of elements [-]	m [t]	m_{TOT} [t]	M_{roof} [t]	w_{roof} kN/m²
Columns	42	4.60	193.20		
Beams	36	9.63	346.68		
Girders	35	2.56	89.60	1925.44	3.15
Roof elements	288	3.22	927.36		

Cladding panels	136	6.10	829.60
Portals	8	6.30	50.40

For all the structural elements, the adopted concrete has a characteristic cubic compressive strength of 50MPa. Longitudinal and transversal reinforcement steel has a characteristic yielding strength of 440MPa.

3.3 Structural model

3.3.1 *Structural elements and gravity loads*

The non-linear model of the existing structure is performed through the OpenSees code (Center 2007). Columns, principal beams, girders and roof elements are modeled as *elasticBeamColumn* elements, represented through their longitudinal axis, with nodal masses applied at the ends. Cladding panels are neglected in terms of lateral stiffness and they are considered in the model only in terms of additional masses and gravity loads, applied to the structural elements along the perimeter (i.e. to the girders, in the y direction, and to the principal beams, in the x direction).

Geometrical eccentricities in the connections between the longitudinal axis of the structural elements (principal beams and columns, roof elements and principal beams, girders and columns) are modeled through horizontal and vertical rigid links, with a very high flexural shear and torsional stiffness.

Gravity loads are applied as nodal forces in each connection (roof-to-beam, beam-to-column and girder-to-column): cladding panels weigh is applied as gravity nodal force in the perimetral connections. In Table 3-2, N_{roof} represents the gravity nodal force accounting for roof elements weight; N_{beam} represents the gravity nodal force accounting for main beam and horizontal lintels weight; N_{col} represents the gravity nodal force accounting for columns and pillars weight; N_{gird} represents the gravity nodal force accounting for girders weight; N_{pan} represents the gravity nodal force accounting for cladding panels weight; N_{tot} is the total gravity nodal force applied in each connection.

Table 3-2 Gravity nodal forces applied in the structural connections

		N_{roof} [kN]	N_{beam} [kN]	N_{col} [kN]	N_{gir} [kN]	N_{pan} [kN]	N_{tot} [kN]
roof-to-beam	-	18.6	-	-	-	-	18.6
	Type A	-	62.4	-	-	-	62.4
beam-to.column	Type B	-	31.2	-	-	119.7	150.9
	Type C	-	62.4	-	-	-	62.4

girder-to-column	Type D	-	31.2	-	-	-	31.2
	Type A	-	-	29.8	27.8	-	57.6
	Type B	-	-	14.9	13.9	-	28.8
	Type C	-	-	14.9	13.9	119.7	148.5
	Type D	-	-	7.4	6.9	59.9	74.2
column base	Type A						480.00
	Type B						479.4
	Type C						359.7
	Type D						179.8

3.3.2 *Structural connections*

The girder-to-column connections are modeled as perfect cylindrical hinge connections, which allow only flexural rotations of the girders (around the global x axis).

The friction roof-to-beam and beam-to-column connections are modeled through a zero length *flatSliderBearing element* (McKenna and Fenves 2013) which connects the slider element (i.e. the beam, for roof-to-beam connections, and the column, for beam-to-column connections) to the sliding element (i.e. the roof elements, for roof-to-beam connections, and the beam, for beam-to-column connections). The bearing elements accounts for three possible degrees of freedom, i.e. vertical displacements, horizontal displacements along the direction of the sliding elements longitudinal, flexural rotations of the sliding elements (around the global x axis, for roof-to-beam connections, and around the global y axis for the roof-to-beam connections). All the other degrees of freedom of the bearing elements are restrained, assuming high values of lateral and rotational stiffness. In particular, for both the roof elements and beams, torsional rotations are neglected and a single sliding direction is considered for numerical simplicity. This assumption does not compromise the analysis results because also in the actual seismic response, the neglected relative displacements are limited by the presence of the adjacent roof elements or by the forks at the column top end.

The mechanical properties of the bearing elements reflect the geometrical and mechanical properties of the neoprene pads used to perform the friction connections. In particular, according to Magliulo et al. (2011), the neoprene shear modulus, the Poisson's ratio and the Young's modulus are assumed equal to 1.1MPa, 0.5 and 3.3MPa, respectively, so that axial and lateral stiffness in the sliding direction (i.e. the x axis for the main beams and the y axis for the roof elements) can be evaluated (Table 3-3).

In the vertical direction, for both roof-to-beam and beam to-column connections, the bearing elements allow free uplifts (due to tensile axial loads) and compressive

displacements (due to compressive axial loads) depending on the neoprene axial stiffness.

In the horizontal directions, according to the Coulomb model, the bearing elements allow elastic displacements along the global x direction (for the beam-to-column connections) or along the global y direction (for the roof-to-beam connections), depending on the assigned lateral stiffness. When the elastic shear reaction reaches the friction strength value $R_{frict} = \mu \cdot N$ (μ is the friction coefficient (Magliulo et al. 2011) and N is the vertical load acting in the connection), plastic deformations and sliding displacements occur.

Table 3-3 Geometrical and mechanical properties for neoprene pads in friction connections

	geometry [cm]	K_a [kN/m]	K^*_l [kN/m]
beam-to-column	23x20x1	19734	6578
roof-to-beam	13x5x1	4290	1430

*the lateral stiffness refers to the sliding direction

Table 3-4 Friction strengths

		A_{neopr} [m^2]	N [kN]	σ_v N/mm^2	μ [-]	R_{attr} [kN]
Column	Type A	0.0598	211.15	3.53	0.12	24.40
	Type B	0.0598	225.28	3.77	0.11	25.82
	Type C	0.0598	211.15	3.53	0.12	24.40
	Type D	0.0598	105.58	1.77	0.13	13.85
roof-to-beam		0.0065	18	2.77	0.12	2.16

3.3.3 *Non-linear model*

A lumped plasticity approach is assumed for the structural non-linear model: *zerolength elements* (McKenna and Fenves 2013) are introduced at the column bases, for which only rotations around global x and y axes are allowed. The backbone curve of the hysteresis loops for moment-rotation deteriorating relationships is defined according to Ibarra et al. (2005), considering the mean values of the material properties, and introduced in the model through a *ModIMKPeakOriented Material* (McKenna and Fenves

2013) assigned to the corresponding degree of freedom (rotation around the global x and y axis) of the zerolength elements.

In the following, the main parameters for the plastic hinges definition are described, in terms of moment-rotation relationship. The four characteristic points of the backbone curve are:

- the cracking point (θ_{cr}, M_{cr}), which correspond to the attainment of the concrete tensile strength (f_{ctm}). Moment and rotation values are obtained on the basis of the gross section properties;
- the yielding point (θ_y, M_y), for which the yielding moment is obtained from a fiber analysis of the cross-section, corresponding to the first attainment of the concrete deformation (ε_{c1}) equal to 2‰ or the steel yielding deformation ($\varepsilon_{sy}=f_{ym}/E_s$); the yielding rotation is evaluated in Eq. 3.1 according to Ibarra et al. (2005):

$$\theta_y = \varphi_y \cdot \frac{L_s}{3} + 0.00275 + a_{sl} \cdot \frac{\varepsilon_y}{(d-d')} \cdot \frac{0.2 \cdot d_b \cdot f_y}{\sqrt{f_c}} \qquad 3.1$$

  In Eq. 3.1, ϕ_y represents the yielding curvature, L_s represents the shear span (equal to the column high for cantilever schemes), a_{sl} represent the longitudinal reinforcement ratio, ε_y represents the steel yielding deformation, d and d' represent the effective high of the cross section and the reinforcement distance respectively, d_b represents the longitudinal bar diameter, f_y represents the mean value of the steel yielding strength and f_c represents the mean value of the concrete compressive strength;
- the ultimate point (θ_u, M_u), which corresponds to the attainment of the maximum moment value, considering an hardening ratio equal to 1%; the ultimate rotation is evaluated in according to Ibarra et al. (2005):

$$\theta_u = 0.6 \cdot 0.0194\left(1+0.5a_{sl}\right)\left(0.3\right)^{\nu}\left[\frac{\max\left\{0.01;\ \omega'\right\}}{\max\left\{0.01;\ \omega\right\}} \cdot f_c\right]^{0.175} \left(\frac{L_S}{h}\right)^{0.4} 25^{\left[\frac{a\rho_w f_{yw}}{f_c}\right]}$$

  In Eq. 3.2, ν represents the normalized axial force, ω' and ω represent the tensile and compressive mechanical ratio, h represents the cross section high. Due to the very low transversal reinforcement, the transversal reinforcement ratio (ρ_w) is assumed to be equal to zero and the last term of the equation Eq. 3.2 is neglected.

- the last point (θ_{last}, M_{last}), which corresponds to the final state after the moment degradation up to the zero value; the last rotation value is assumed to be equal to $1.01 \cdot \theta_u$.

On the basis of the geometrical features of the cross sections and on the basis of the axial force acting at the column bases (Table 3-2) different envelops for the plastic hinges can be obtained for different column types and around both directions (x and y).

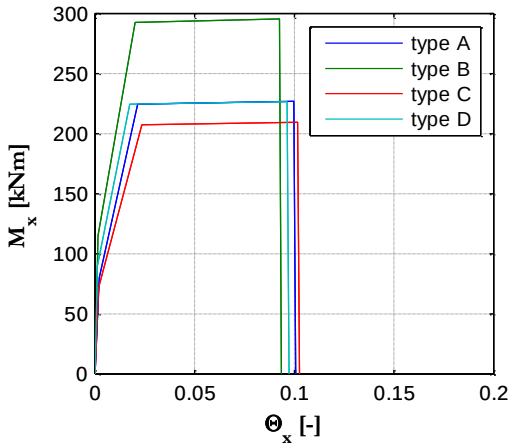

Figure 3-6 Moment-rotation envelops for plastic hinges around global x axis

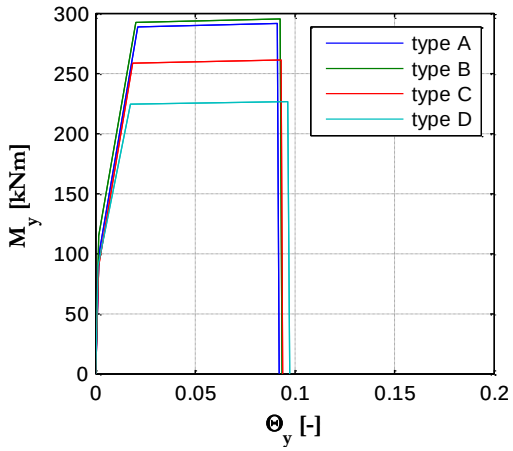

Figure 3-7 Moment-rotation envelops for plastic hinges around global y axis

3.3.4 *Modal properties*

In the analysis, a classical Rayleigh damping is assumed to model the inherent damping of the structural elements, considering the damping matrix proportional to the mass and stiffness ones. The damping ratio is considered equal to 5%.

The first and third periods of vibration correspond to translational modes along the y axis and x axis, respectively, and are equal to 1.58sec and 1.30sec, respectively. The second period of vibration is equal to 1.46sec and corresponds to a torsional mode.

3.4 Dynamic analyses

The seismic assessment of the precast structure is performed through non-linear dynamic analyses.

The considered input motion is the acceleration time-history recorded in the Mirandola station (Modena, Emilia region) during the second main shock of the Emilia earthquake (May, 29th 2012). Station details (Table 3-5), event details (Table 3-6) and the input motion records refer to the Italian Accelerometric Archive (Luzi et al. 2008).

Table 3-5 Station details

Station name	Mirandola (MRN)
Network	IT - Italian Strong Motion Network (DPC)
Address	Via Napoli, 16 - Mirandola (MO), Italy
Lat.	44.87823
Long.	11.06174
V_{s30} [m/sec]	208
Site Class [EC8]	C
Topografy	T1

Table 3-6 Event details

Event id	IT-2012-0011
Name	EMILIA_2ND_SHOCK
Date	29/05/2012 07:00
Lat.	44.84°
Long.	11.07°
Depth [km]	8.07
M_0 [dyn/cm]	1.07E+25
M_W	6.0

In the following, Figure 3-8 shows the acceleration time history for the horizontal components, along East direction (MRN-E) and North direction (MRN-N), of the input motion; Figure 3-9 shows the acceleration time history of the vertical component (MRN-V). In Figure 3-10, the acceleration response spectra are represented for the three input components: the horizontal components along the East and North direction show a peak ground acceleration equal to 0.22g and 0.29g, respectively; the vertical component shows a peak ground acceleration equal to 0.86g. In order to show the frequency content of the input motion, the Fourier spectra are represented in Figure 3-11: the graphs show the maximum Fourier amplitude for the East, North and vertical component at 2.18Hz, 1.52Hz and 15.47Hz, respectively.

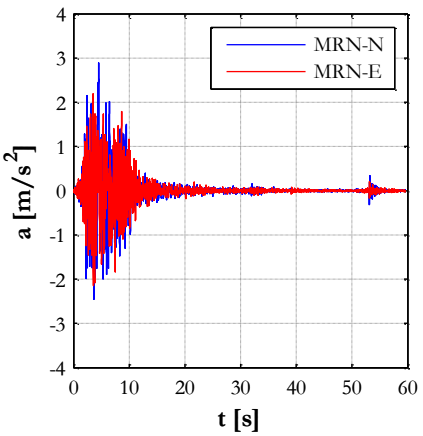

Figure 3-8 Acceleration time histories for the horizontal components of the input motion (MRN - IT-2012-0011)

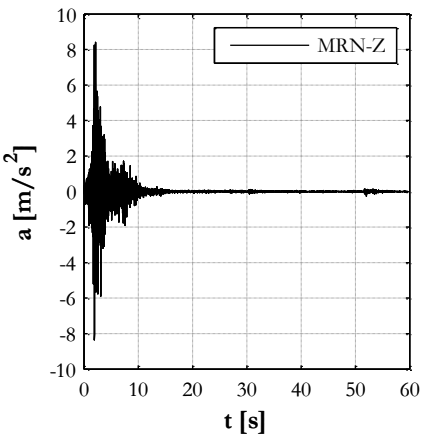

Figure 3-9 Acceleration time history for the vertical component of the input motion (MRN - IT-2012-0011)

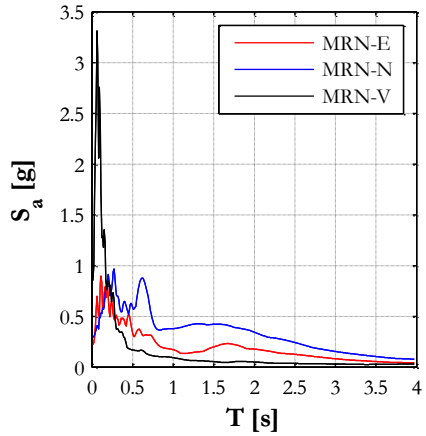

Figure 3-10 Acceleration response spectra for the three components of the input motion (MRN - IT-2012-0011)

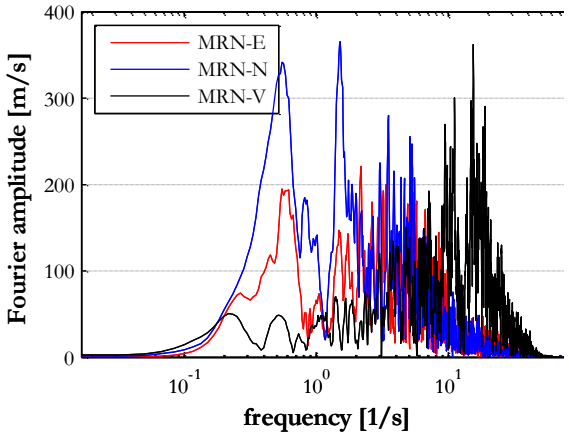

Figure 3-11 Fourier spectra for the three components of the input motion (MRN - IT-2012-0011)

For further investigations, dynamic analyses are also performed using a set of ground motion records, selected according to the Eurocode spectral compatibility using REXEL (Iervolino et al. 2010). In particular:

- the number of the considered accelerograms is higher than 3. In fact, seven events are selected (Table 3-7). For each event, the three available acceleration components can be considered (Figure 3-12, Figure 3-13 and Figure 3-14) and the spectral compatibility is verified for the horizontal component with the maximum peak ground acceleration, i.e. the x component (Figure 3-15);
- the mean of the zero period spectral response acceleration values (calculated from the individual time histories considered for the spectral compatibility, i.e. the x components of the input motion) is higher than the value of $a_g \cdot S$, i.e. the peak ground acceleration, for the site in question;
- in the range of periods between $0.2 \cdot T_1$ and $2 \cdot T_1$ (where T_1 is the fundamental period of the structure in the direction where the accelerogram will be applied) no value of the mean 5% damping elastic spectrum (blue line in Figure 3-15), calculated from all time histories, is less than 90% of the corresponding value of the 5% damping elastic response spectrum (black solid line in Figure 3-15).

Also for the selected records, the frequency content of each input motion can be represented through Fourier spectra: shows the Fourier spectra for the horizontal component (along the x direction) of the input motions; the black solid vertical line represents the fundamental frequency of the reference building.

Table 3-7 Records information for the spectral compatibility

ID	Earthquake Name	Date	Mw	Epic. Dist. [km]	PGA_ X [m/s²]	PGA_ Y [m/s²]	PGV_ X [m/s]	PGV_ Y [m/s]
333	Alkion	24/02/81	6.6	20	2.2566	3.0363	0.2234	0.2262
592	Umbria Marche	26/09/97	6	5	1.951	2.1834	0.1735	0.1399
5488	Chenoua	29/10/89	5.9	29	2.8302	2.2604	0.1311	0.1312
5653	NE of Banja Luka	13/08/81	5.7	7	4.3397	3.9657	0.2633	0.1648
581	Komilion	25/02/94	5.4	16	1.7162	1.9593	0.1283	0.1441
42	Ionian	04/11/73	5.8	15	5.1459	2.4983	0.57	0.255
879	Dinar	01/10/95	6.4	8	2.6739	3.1306	0.2937	0.4059
mean:			6.0	14.3	2.9876	2.7191	0.2548	0.2096

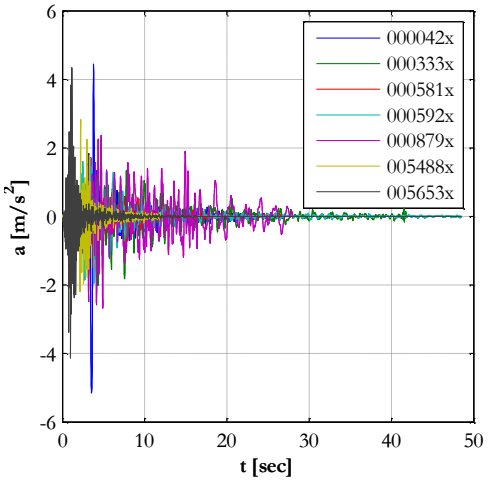

Figure 3-12 Horizontal acceleration time history for the selected input records (x component)

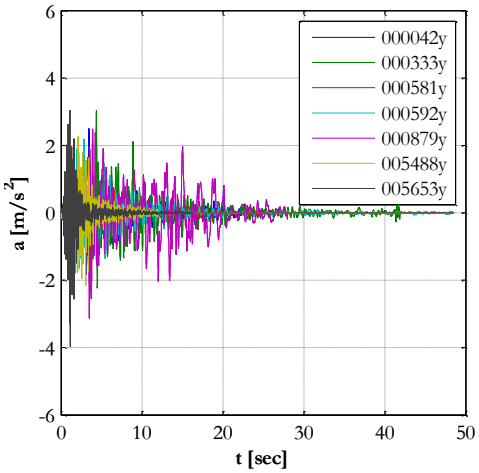

Figure 3-13 Horizontal acceleration time history for the selected input records (y component)

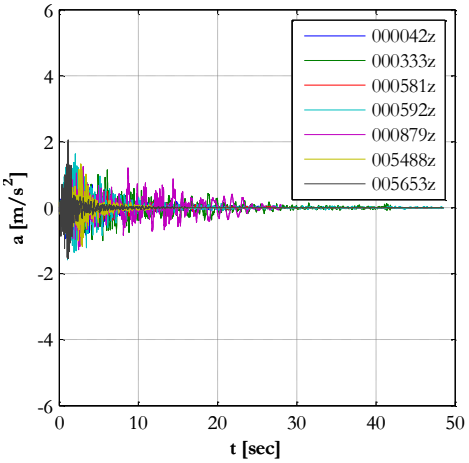

Figure 3-14 Vertical acceleration time history for the selected input records (z component)

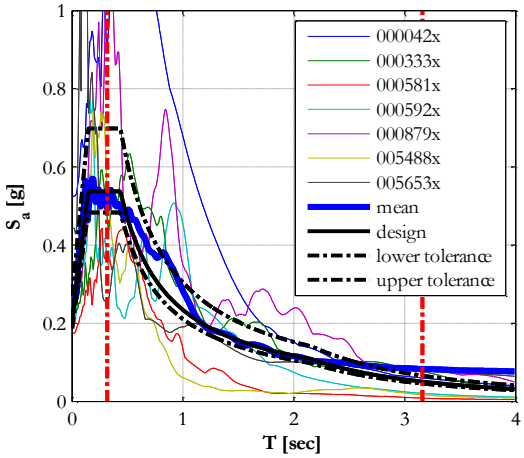

Figure 3-15 Spectral compatibility for the horizontal component (x direction) of the input records

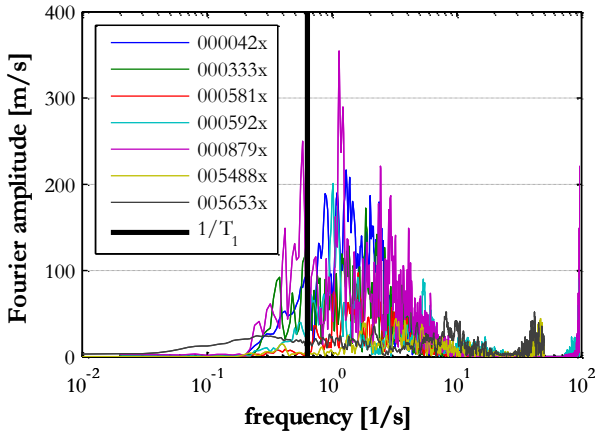

Figure 3-16 Fourier spectra for the horizontal component (along the x direction) of the selected records

3.5 Assessment procedure for the existing structure

In order to assess the seismic performance of the existing reference building, non-linear dynamic analyses are performed before the implementation of the retrofitting options, using the input ground motion recorded in Mirandola on May 29th 2012 described in the previous section. In the first phase of the structural assessment, only horizontal components are considered simultaneously for the analyses (Figure 3-8). In particular, the North component is applied in the direction of the main beams (i.e. the global x direction, see Figure 3-3) and the East component is applied in the orthogonal direction (i.e. the global y direction, see Figure 3-3).

The local and global expected response is described through different parameters related to the structural and non-structural damage. Moreover, the condition of the structure "as-built" leads to the estimation of the possible target performances to obtain after the seismic retrofit.

3.5.1 *Local response of the friction connections*

A high source of seismic vulnerability for the reference building consists in the occurrence of sliding displacements in the friction connections, i.e. roof-to-beam and beam-to-column connections, which can lead to unseating phenomena due to limited supporting lengths.

In the following, Figure 3-17 represents the shear force (F) versus the sliding displacement of a roof element with respect to the supporting main beam (Δ), in the global y direction (no sliding displacements are allowed in the x direction, according to the structural model described in Section 3.3). It can be seen that the shear force reaches the maximum value, which represents the friction strength obtained considering the

axial force on the roof-to beam connection and the corresponding friction coefficient. However, it can be recognized that the sliding displacements are very small and far from the unseating values (13cm).

Figure 3-18 represent the shear force (F) versus the sliding displacement (Δ) of the main beams with respect to the supporting columns (type A, type B, type C and type D, respectively) in the global x direction (no sliding displacements are allowed in the y direction, according to the structural model described in Section 3.3). It can be seen that the shear force reaches the maximum value, which represents the friction strength obtained considering the axial force on the beam-to-column connections and the corresponding friction coefficient. However, it can be recognized that the sliding displacements are lower than the unseating values (23cm): in the figure, the dashed red line corresponds to the available support length.

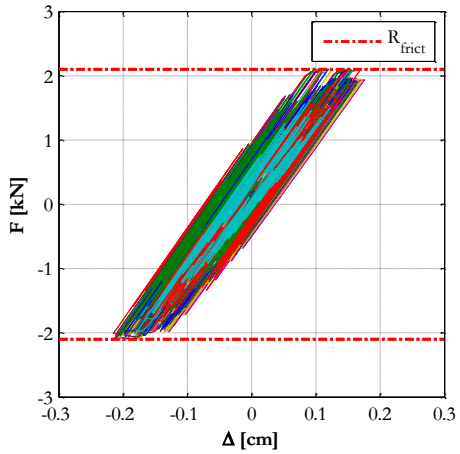

Figure 3-17 Friction force-sliding displacements for roof-to-beam connections

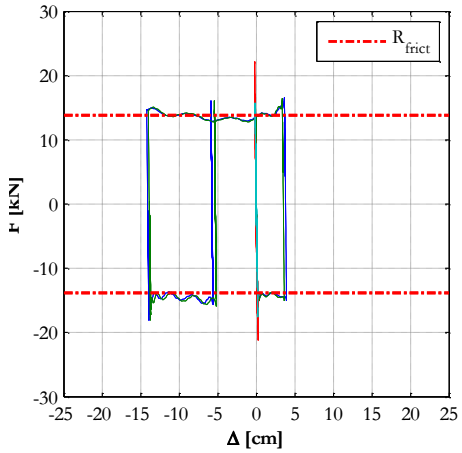

Figure 3-18 Friction force-sliding displacements for beam-to-column connections (type D)

In Figure 3-19 a schematic plan view of the roof is represented. The beam to column and the roof-to-beam connections are represented with colored circles: the green circles correspond to "safe" connections, for which the maximum relative displacements are lower or equal to $1.5\Delta_{unseat}$; the yellow circles correspond to "critical" connections, for which the maximum relative displacements are higher than $1.5\Delta_{unseat}$ and lower than Δ_{unseat}; the red circles correspond "failed" connections for which the maximum relative displacements are equal or higher than Δ_{unseat}.

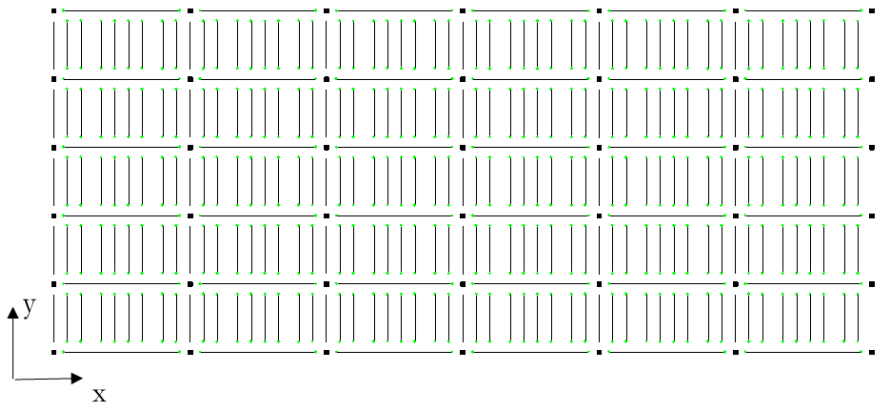

Figure 3-19 Friction connections assessment

3.5.2 *Non-structural damage*

According to the modern performance-based methodology, it is known that the seismic performance of buildings is highly influenced by the seismic response of nonstructural components. In fact, the improper seismic design of nonstructural components and of mutual connections with the main structure can lead to early failures, without any source of structural ductility.

The extensive damage and serviceability interruption may induce high costs in terms of casualties and injuries, due to nonstructural collapses, but also in terms of repair costs. Especially for industrial facilities, the study of nonstructural components seismic response is of high interest considering their large presence and the possible consequences and impact on the structural performance.

Nonstructural components include interior components (e.g. partitions and ceilings), exterior components (e.g. building facades) and building services components (e.g. mechanical-electrical components, storage racks, heavy furniture), which can be attached to single or multiple points of the main structure. The seismic assessment of these components could be related to different floor and ground motion parameters. For example, considering a suspending ceiling (Figure 3-20), the initial damage is due to the separation of the ceiling from the wall supports resulting from the inertial forces and from the peak response floor acceleration. After the separation, the damage of the suspending ceiling is related to the pounding against next objects: this phenomenon depends on the peak response floor velocity. Finally, as the ceiling is subjected to significant drift, the deformation of the fire-sprinklers and air ducts (or any other component connected to the ceiling) is related to the peak response floor displacement.

For these reason, in the following, the seismic performance of the existing reference building, is described in terms of lateral drift, floor acceleration and relative velocity.

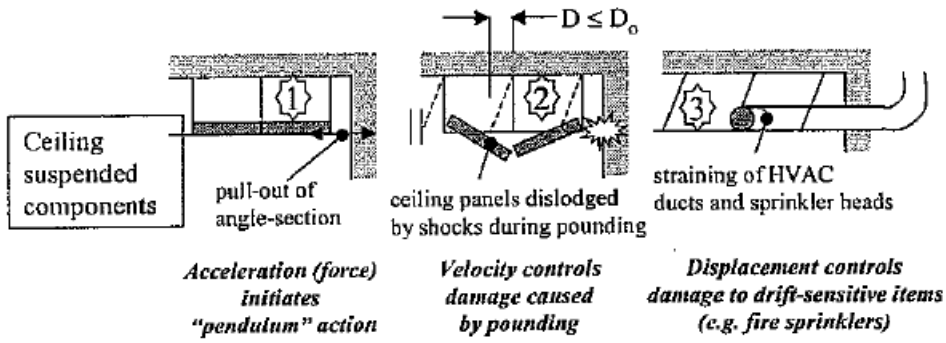

Figure 3-20 Non-structural damage during seismic input motion (courtesy of (Lam and Gad 2002))

3.5.2.1 Lateral drift

According to the Italian building code (D. M. 14/01/2008 2008) and to the Eurocodes (CEN 2005) nonstructural components damage and the temporary serviceability interruption should be avoided limiting the interstory drifts, i.e. the interstory displacement divided by the interstory height. The maximum tolerable value depends on the importance class of the building. For the reference building, i.e. industrial building with normal crowding and without any dangerous activity or material, with cladding panels designed so that their deformations (or of the mutual connections with the main structure) do not lead to any damage, the interstory drift should be lower than 1%.

In the following, show the time histories for interstory drifts of the columns type A (internal columns), type B (external columns on the longer side of the structural plan), type C (external columns on the shorter side of the structural plan) and type D (corner columns), respectively. Red dashed lines in the figures represent the code limitation for the reference building.

It can be observed that, for all the columns, the interstory drifts largely overpass the code limit value and that high residual drifts can be recognized at the end of the seismic event.

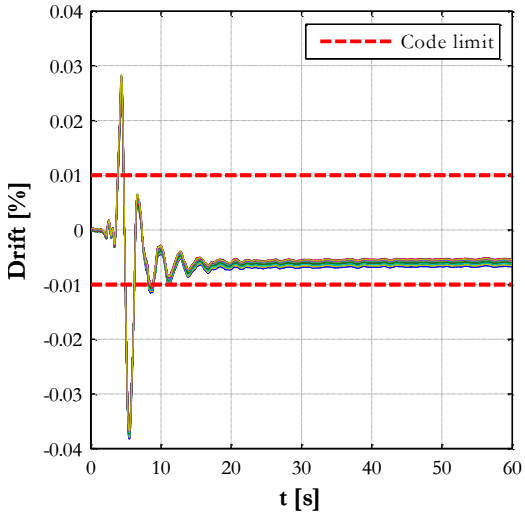

Figure 3-21 Interstory drifts for columns type A

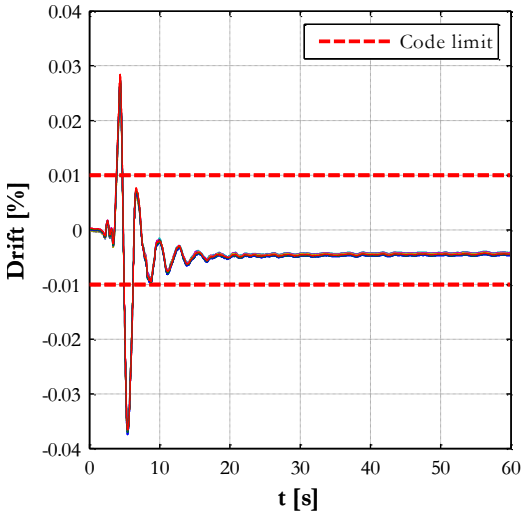

Figure 3-22 Interstory drifts for columns type B

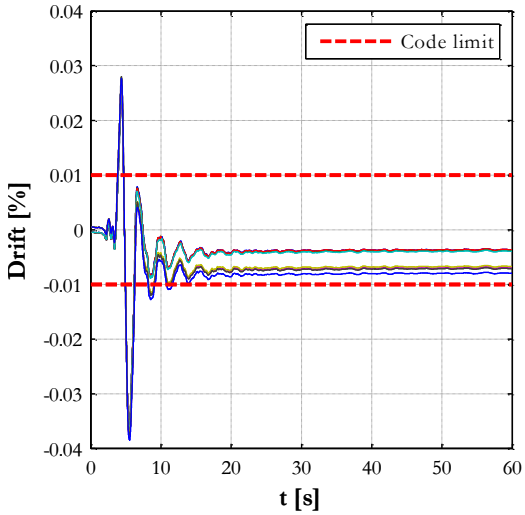

Figure 3-23 Interstory drifts for columns type C

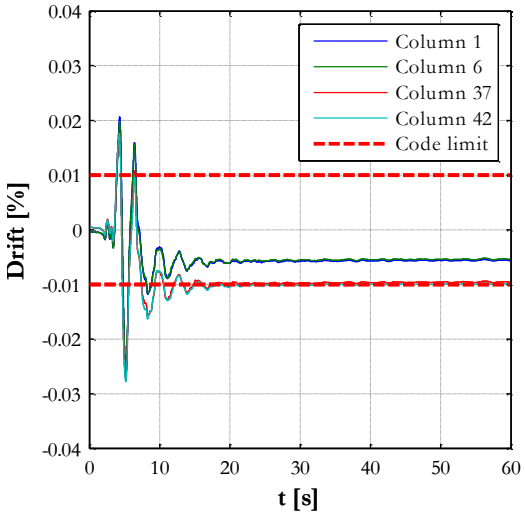

Figure 3-24 Interstory drifts for columns type D

3.5.3 *Plastic hinges*

Considering the adopted lumped plasticity approach (Figure 3-6 and Figure 3-7), the non-linear behavior of the reference building can be investigated observing the moment-rotation diagrams at the column base, which represent the cyclic response of the plastic hinges.

In the following, the moment-rotation diagrams around x and y axes are represented. It can be observed that, for all the columns, plastic hinges around the global x axis do not reach the yielding rotation. On the contrary, for all the columns, plastic hinges

around the global y axis overpass the yielding rotation but are still far from the ultimate value.

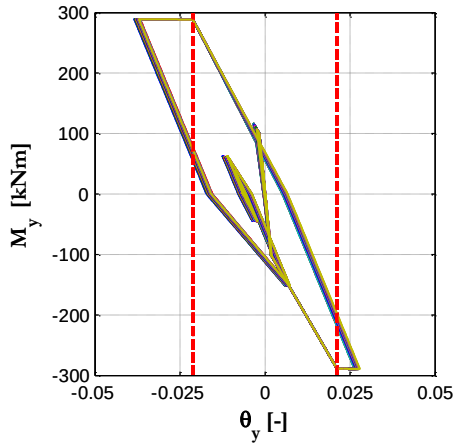

Figure 3-25 Moment-rotation diagrams for type A column around y axis

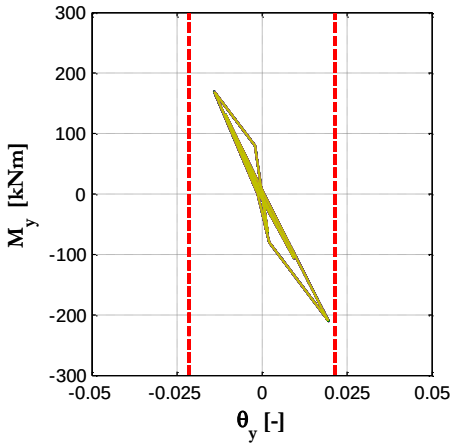

Figure 3-26 Moment-rotation diagrams for type A column around x axis

3.5.4 *Energy balance*

As a part of the evaluation, an energy balance analysis is performed (Eq. 3.3) aiming at estimate how the structure is storing or dissipating the input energy from the ground motion though time. In this way, it is possible to determine the amount of energy that the earthquake is soliciting from the structure, and how it is able (or unable) to manage it.

The different energy quantities can be defined by integrating the equation of motion of an inelastic system (Chopra 1995) so that the input energy due to the earthquake excitation (ground acceleration dependent) is balanced by the output energy terms related to inertial forces (system acceleration dependent), viscous forces (system velocity dependent) and deforming forces (system displacement dependent).

$$E_I = E_K + E_D + E_S \qquad 3.3$$

Each energy term can be calculated, using the numerical results of the dynamic analyses, through the following relationships:

- input energy (E_I): it is related to the total energy perceived from the ground motion and it is obtained as:

$$E_I(t) = \int_0^u m \cdot \ddot{u}_g(t) \cdot du \qquad 3.4$$

The term above is calculated as the sum of the input energy for all the structural elements, considering the nodal displacements (du) and the corresponding masses (Table 3-1).

- kinetic energy (E_K): it is related to the motion of the mass of the structure and its components. It is a conservative component, completely returned to the system at the end of the earthquake motion:

$$E_K(t) = \int_0^u m \cdot \ddot{u}(t) \cdot du \tag{3.5}$$

The term above is calculated as the sum of the kinetic energy for all the structural elements, considering the nodal acceleration (ü), the nodal displacements (du) and the corresponding masses (Table 3-1);

- viscous damping energy (E_D): it represents the energy dissipated by the inherent damping of the structural and non-structural elements and it is obtained as:

$$E_D(t) = \int_0^u f_D(t) \cdot du \tag{3.6}$$

The term above is calculated as the sum of the inherent viscous energy for all the structural elements, considering the nodal Rayleigh forces (f_D) and the nodal displacements (du);

- deforming energy (E_S): it represents the sum of the recoverable strain energy (E_{el}), the hysteretic damping energy dissipated by inelastic deformations in the plastic hinges (E_h) and the energy dissipated by the frictional mechanisms occurred in the structural connections (E_f).

The recoverable strain energy, which is elastically stored in the structural elements through their mechanical deformations and returned to the system, can be calculated as:

$$E_{el}(t) = \frac{[f_{el}(t)]^2}{2k} \tag{3.7}$$

in which f_{el} represent the elastic forces and k represents the initial lateral stiffness. For the reference structural system, the lateral stiffness depends only on the columns stiffness. For this reason, the term of Eq. 3.7 represents the sum of the ratio between the shear force at the column base and the flexural initial stiffness, for all the columns.

The hysteretic damping energy is dissipated by the structural elements through the yielding of the component's materials, due to permanent deformations and damage of the structure. For the reference structural model, the non-linear behavior of the whole structure is represented by the plastic hinges at the columns base (lumped plasticity). For this reason, the hysteretic damping energy corresponds to the area under the moment-rotation diagrams, which represent the response of the plastic hinges:

$$E_h = \int_0^\theta M(t) \cdot d\theta \tag{3.8}$$

Finally, the frictional energy is the dissipated energy due to relative displacements between structural elements (i.e. between main beams and columns). It is obtained as the sum of the area under the shear force (f_s) -sliding displacements (s) diagrams in all the friction connections:

$$E_f = \int_0^s f_s \cdot ds \qquad 3.9$$

In Figure 3-27 and Figure 3-28 the energy terms versus time are represented, along the x and y direction respectively. It can be worthy observed that the energy contents are different for the two considered directions. In particular, even if the structure exhibits a lower initial lateral stiffness along the y direction (only due to the flexural initial stiffness of columns, considering the static structural scheme) with respect to the x direction, during the earthquake, plastic hinges form in the x direction so that the lateral deformability and the related energy content increase. This consideration is confirmed by the evidence that for the energy balance in the global x direction, the energy content related to the hysteretic structural response (E_h) represents more than 50% of the input energy.

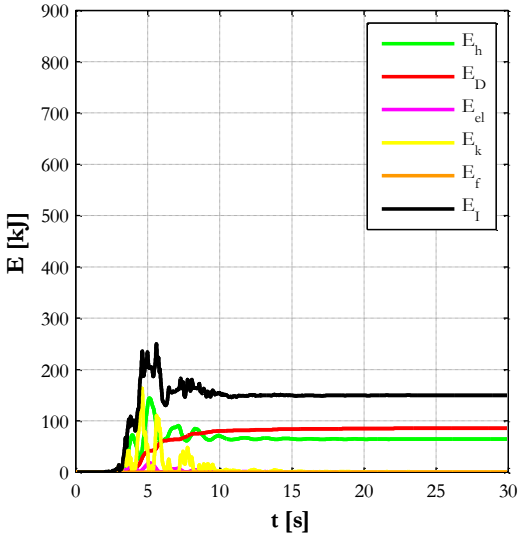

Figure 3-27 Energy balance representation along the global y direction

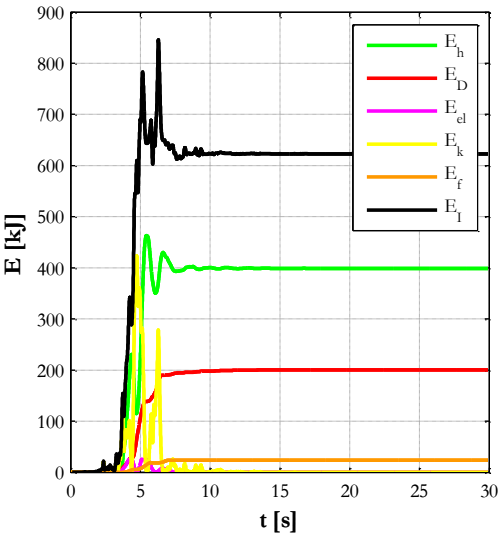

Figure 3-28 Energy balance representation along the global x direction

Chapter 4

SEISMIC RETROFIT SOLUTION USING HYSTERETIC DEVICES

4.1 The SicurLink™ system

In this section, a retrofitting system for precast connections is described, consisting of a three-hinged steel device obtained by two steel profiles connected to the concrete elements through horizontal steel dowels. The working principles are described in details in the following. Concerning the possible geometrical configurations, it can be performed in a lateral configuration if the dowels are applied at the external surface of the concrete elements; a bottom configuration if the dowel are connected to the concrete elements by means of steel flanges at the internal surfaces of the concrete elements; the mixed configuration considers connection both on the internal surface and on the external ones (Figure 4-1, Figure 4-2 and Figure 4-3).

Figure 4-1 SicurLink™: lateral configuration

Figure 4-2 SicurLink™: bottom configuration

Figure 4-3 SicurLink™: mixed configuration

The system was applied to a damaged dowel beam-to-column connection and two shear cyclic tests were performed on two different configurations in order to define the seismic performance. The experimental results demonstrated the capacity of the new connection system; moreover, the comparison with the cyclic behavior of the standard dowel connection shows the more efficient seismic performance of the three-hinged steel device in terms of both shear strength and energy dissipation.

4.2 Experimental investigations

4.2.1 *The damaged beam-to-column connection*

The reference connection is a dowel beam-to-column connection, typically used in precast structures (Kremmyda et al. 2014; Zoubek et al. 2015).This connection was tested under cyclic shear loads up to collapse before the installation of the retrofitting system. A more accurate description of both testing protocol and results of the cyclic test on the dowel connection is reported in Magliulo et al. (2015); in the following a brief summary is presented.

The specimen is showed in Figure 4-4: it consists of a horizontal beam, connected to the North (left side in Figure 4-4(a) and Figure 4-4(b)) column by a dowel connection and simply supported on the South column (right side in Figure 4-4(a) and Figure 4-4(b)). Figure 4-5 shows the cross section dimensions and the reinforcement details for both columns and beam, designed according to European provisions (CEN 2004; CEN 2005). In order to have an uniform distribution of normal stresses on the column, a neoprene pad (15cmx60cmx1cm) was placed on the dowels side (left side in Figure 4-4(a) and Figure 4-4(b)), designed according to the CNR provisions (CNR 10018 1999). On the South side of the specimen (right side in Figure 4-4(a) and Figure 4-4(b)) two teflon sheets avoided undesirable frictional strength between beam and column.

The concrete of the structural elements (beam and columns) had a characteristic cubic compressive stress equal to 55MPa (i.e. design class equal to C45/55) and the adopted threaded steel bars (B450C) have a mean strength at yielding, f_y, equal to 473MPa.

The specimen was tested under cyclic loads along the beam axis direction (Figure 4-6). During the shear test, several cracks occurred in the concrete covers of the column up to the complete spalling of the frontal cover at the end of the test. Figure 4-7 shows the final configuration of the damage pattern on the lateral surfaces of beam and column. The recorded failure mechanism was caused by two main reasons: 1) the small concrete cover of the steel dowels with respect to the dowel diameter (Vintzeleou and Tassios 1986; Zoubek et al. 2013) and; 2) the reduced confinement of the concrete because of the large depth of the transversal reinforcement in the column (Magliulo et al. 2014).

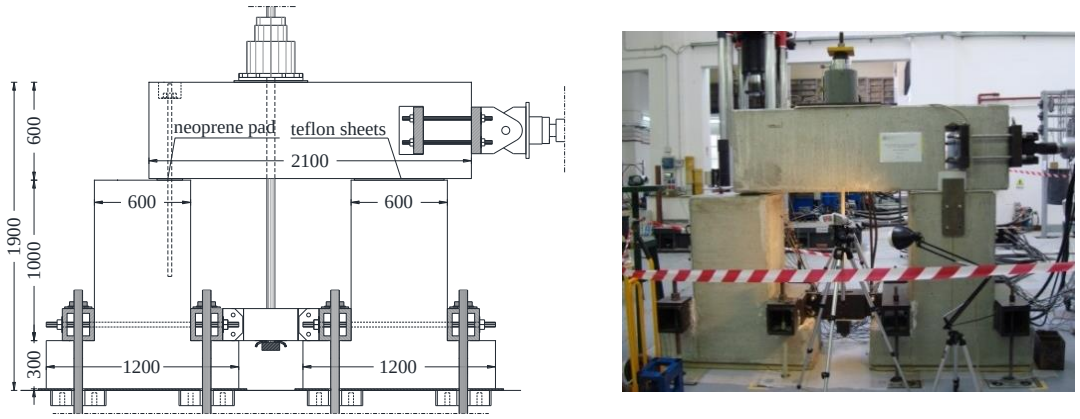

(a) (b)

Figure 4-4 Setup of the cyclic shear test on the dowel connection: (a) specimen dimensions (in mm), (b) specimen arrangement

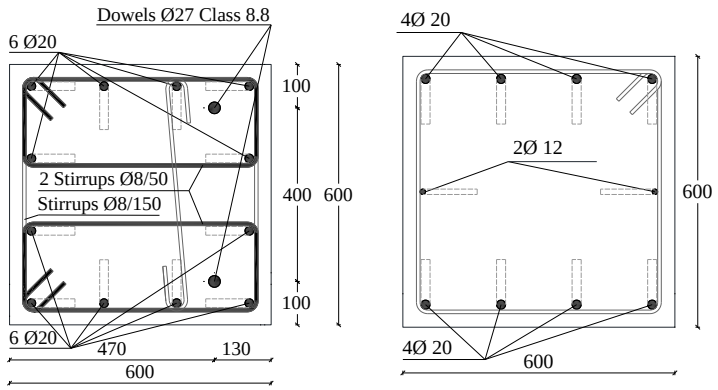

(a) (b)

Figure 4-5 Reinforcement details: (a) column; (b) beam (dimensions are expressed in mm)

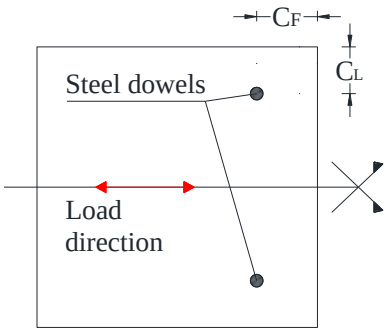

Figure 4-6 Frontal cover (CF) and lateral cover (CL) in the column

(a) (b)

Figure 4-7 Final damage pattern of the tested dowel connection: (a) West and (b) East view

The connection response is described in Figure 4-8 in terms of force-displacement curve of the whole cyclic test (solid gray line). In this figure, the negative values of both forces and displacements correspond to pulling loads (i.e. horizontal loads against the column frontal cover, CF in Figure 4-6), while the positive values of both forces and displacements correspond to pushing loads (i.e. the horizontal loads are applied against the column core).

For pushing loads, the connection exhibits higher shear strength and more limited stiffness degradation than in the case of pulling loads. In particular, for pulling loads a significant strength degradation occurs after the attainment of the maximum shear strength (176.57kN), corresponding to the occurrence of the first crack in the column concrete cover (red point in Figure 4-8). The black curve in Figure 4-8 represents the force-displacement curve up to the 6th step of the loading history, which corresponds to the 20% of shear strength reduction. Such a strength reduction can be assumed as the connection collapse; indeed, after this step the negative values of the force-displacement curve are mainly related to the steel dowel behavior.

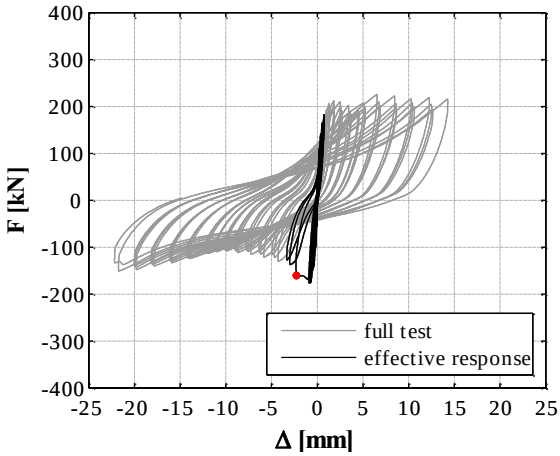

Figure 4-8 Force-displacement curve of the whole cyclic test (gray curve) and up the 6th step (black curve)

4.2.2 *The retrofitting system*

After the cyclic shear test, the described beam-to-column connection was retrofitted through a three-hinged steel system, which is a connection system patented by Capozzi and Magliulo (2012) and Magliulo et al. (2014). This system can be used in different structural applications, as for the retrofitting of connections between structural elements, either damaged after seismic events or deficient in terms of seismic response. It has been already applied in some industrial buildings in Italy as retrofitting device for beam-to-column connections. This three-hinged steel device can be also adopted in new precast buildings for both structural and nonstructural elements. In the case of nonstructural elements, for instance, it can be used for the connection of the cladding panels to the structure, since it can allow the high seismic drift of the structure, reducing/removing its interaction with the cladding panels (Magliulo et al. 2015).

In this work the three-hinged steel connection was tested as a retrofitting system of the damaged beam-to-column connection described in the previous section. In this kind of application, it consists of two inclined steel profiles anchored to the concrete elements through horizontal steel dowels. The seismic response is investigated through cyclic shear tests; in particular, two cyclic shear tests were performed without (test 1) and with (test 2) a rubber sheath around the horizontal dowel in the beam.

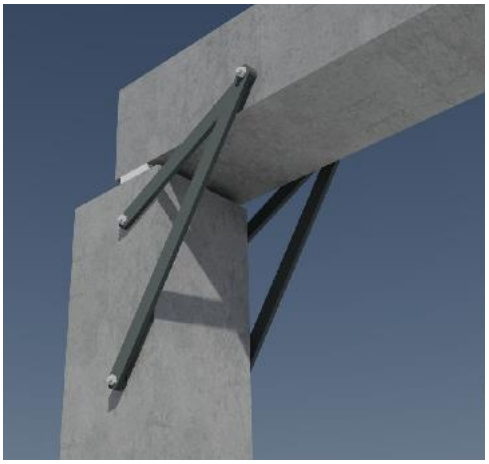

Figure 4-9 Three-hinged steel system for beam-to-column connections

The proposed retrofitting solution is based on two main mechanical principles: the three hinged arch and the dowel effect. According to the former mechanism, the total seismic force applied to the beam is transferred to a couple of hinges on the column through two steel profiles. If the steel profiles have a planar configuration, they carry neither flexural nor shear stresses and can be designed only for axial loads. According to the dowel effect, these axial loads are transferred to the steel dowels.

The presented system has several advantages with respect to other mechanical devices, commonly applied for the seismic retrofitting of precast structures. It is characterized by a fast installation and it can be easily removed/reinstalled after damage. It can be adopted in several different geometrical configurations, also in order to not interfere with the steel reinforcement in existing structural elements. Moreover, this system does not modify the inertial forces during seismic events.

4.2.3 *Design of the three-hinged steel connection system*

The design of the retrofitting system was performed according to the Italian seismic code [21] (very similar to Eurocode 8 (CEN 2005)) and Eurocode 3 provisions (CEN 2005). The design shear force (Fed=142kN) was evaluated by assuming an Italian high seismicity zone (ag=0.35g) and a soil type B. Since two connection systems were applied at the two sides of the beam (Figure 4-9), each of them was designed for a halved shear force.

The main geometrical characteristics of the installed retrofitting system are summarized in Figure 4-10. For the sake of clarity, some definitions are necessary: i) the node at the beam side is defined as "node 2"; ii) "node 1" and "node 3" are the lower and the upper node at the column side, respectively; iii) the steel profile from node 1 to

node 2 is referred to as "profile 1" and iv) the steel profile from node 2 to node 3 is the "profile 2".

The three dowels for the steel profiles anchorage are threaded bars with a diameter of 30mm and with a characteristic yielding strength of 640N/mm2 (Class 8.8). Table 1 shows their main features obtained from two tensile tests: effective cross section area (Ares), equivalent diameter (ϕeq), mean yielding strength (fym), mean Young Modulus (Em), mean yielding strain (εym). The dowels were designed according to the provisions for pin connections and their maximum shear strength was also evaluated according to the provisions by CNR 10025.

The design of the two steel profiles (fyk,profile=275N/mm2, Ey,profile=210000N/mm2) was performed according to the geometrical requirements of Eurocode 3 for pin ended members and their buckling failure was also prevented according to Eurocode 3. Figure 4-10 shows the geometrical features of the two steel profiles, as the hole diameter (Φ) and the radius of the profile ends (R). The profile 1 has a greater thickness at the node 1 in order to allow a planar configuration.

The damaged neoprene pad between beam and column was replaced; it was designed according to the CNR provisions, resulting of the same dimensions of the replaced pad (15cmx60cmx1cm).

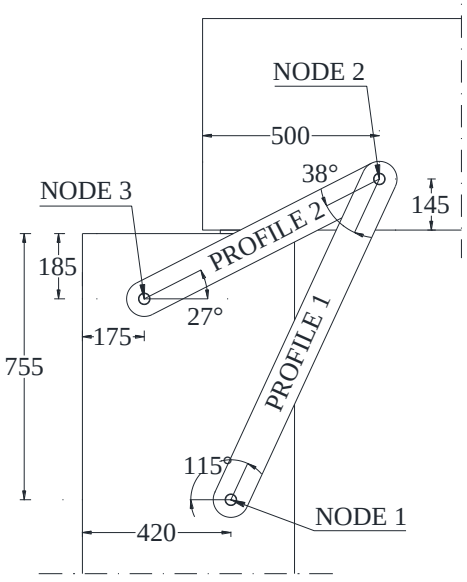

Figure 4-10 Connection system configuration (dimensions are expressed in mm)

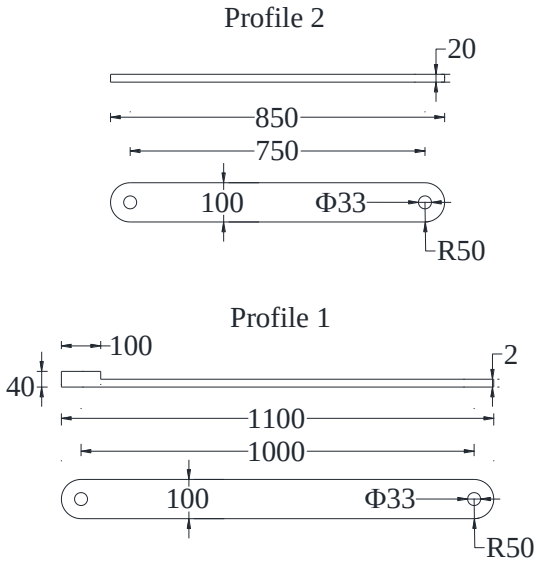

Figure 4-11 Geometrical configuration of the steel profiles (dimensions are expressed in mm)

Table 4-1 Geometrical and mechanical properties of the 30mm diameter steel dowels

A_{res}	ϕ_{eq}	f_{ym}	E_m	ε_{ym}
mm^2	mm	N/mm^2	N/mm^2	[-]
560	26.7	685	176660	0.003878

4.2.4 *Installation of the three-hinged steel connection system*

The retrofitting system installation steps are described in the following (Fig. 9).

a. The first step aims at repairing the concrete elements to be connected, significantly damaged after the cyclic test. At this aim, the existing steel dowels were cut and the beam was removed from the setup. The cracked concrete was completely removed and the concrete and steel surfaces were accurately cleaned. The concrete elements were repaired through shrinkage compensated grout with high mechanical performances (Figure 4-12a), i.e. characteristic compressive strength equal to 60N/mm2 and to 75N/mm2 after 7 and 28 days, respectively. The grout was easily cast in situ because of its fluidity and good adhesion to both concrete and steel surfaces.

b. The preliminary identification of the steel reinforcement in the concrete elements was performed on both the beam and the column in order to choose the location of the holes without interfering with the existing steel elements (Figure 4-12b).

c. The anchorage holes for the steel dowels were created in the concrete elements (Figure 4-12c).

d. The system components, i.e. the dowels and the two profiles, were installed (Figure 4-12d). In the test 2 the rubber sheath was also inserted in the holes.

e. The connection between the dowels and the concrete elements was provided by filling the holes with high strength grout. In order to guarantee the grout filling, the drilled hole diameter is 2cm greater than the dowel diameter (Figure 4-12e).

f. The connection was completed by tightening the nuts and the washers between the dowels and the profiles. In this phase, a preliminary pre-stressing of the bars could be applied in order to guarantee a higher energy dissipation due to the friction. For the tested specimen, prestressing forces were not provided.

(a) (b) (c) (d) (e)

Figure 4-12 Installation phases: (a) restoration of the damaged concrete; (b) reported location of the reinforcement bars; (c) anchorage holes; (d) installation of steel profiles and dowels; (e) cast in situ of high strength grout

4.2.5 *Cyclic shear test on the retrofitted connection: test 1*

Two cyclic shear tests were performed on the beam-to-column connection, retrofitted with the three-hinged steel system (Figure 4-13). The difference between the two performed tests is the presence of a rubber sheath in the concrete holes around the steel dowels. In this section the results of the first test (test 1) are described, i.e. the test without the rubber sheath.

During the test both vertical and horizontal loads were applied to the specimen. The vertical load is provided by a vertical jack with a rate of 3kN/s up to the maximum value of 450kN, which remains constant during the application of the cyclic horizontal load. The vertical jack is restrained to a prestressed metallic bar, that crosses the RC beam through a special hole; a sleigh anchorage system is placed at the other side of the metallic prestressed bar, in order to avoid undesirable restraining effects (Figure 4-13). Since in the real applications the gravity loads are applied to the structure before the

installation of the retrofitting system, in the performed test the vertical load was applied before tightening the connection device through nuts and washers.

The horizontal load simulated the seismic forces and it was provided along the beam longitudinal axis through a hydraulic actuator controlling the displacements. Figure 4-14 shows the protocol displacements recorded by the actuator load cell; in this figure the horizontal displacements from North to South, pulling the dowels against the column frontal cover (from left to right in Figure 4-13), are assumed negative and the horizontal displacements in the opposite direction assume positive values (from right to left in Figure 4-13)). The adopted loading protocol was the same of the cyclic test on the dowel connection (Magliulo et al. 2015): it consisted of 17 displacement steps and, for each step, three complete cycles (negative and positive semi-cycles) were performed. From the first step to the 12th step, the load was applied with a rate of 0.02mm/s and from the 13th step to the test end the load rate was equal to 0.04mm/s. The maximum horizontal load, recorded by the actuator cell at the end of the test, was equal to 312.98kN.

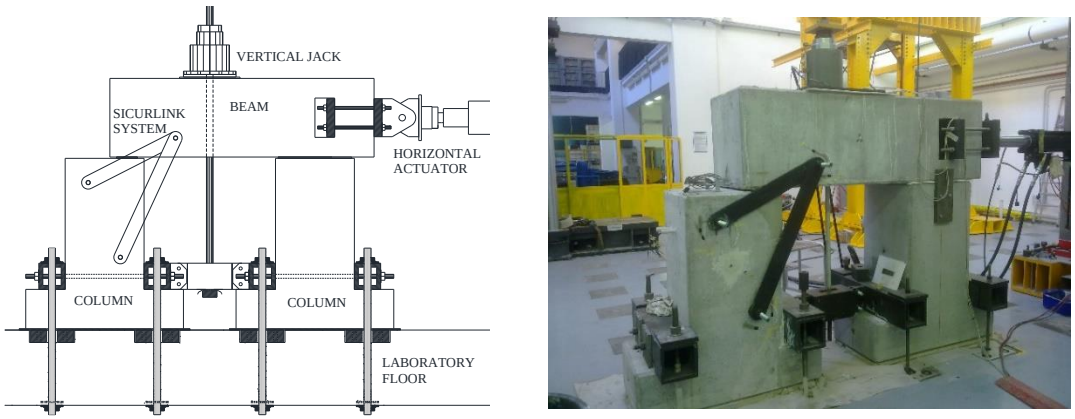

Figure 4-13 Setup of the cyclic test on the retrofitted connection

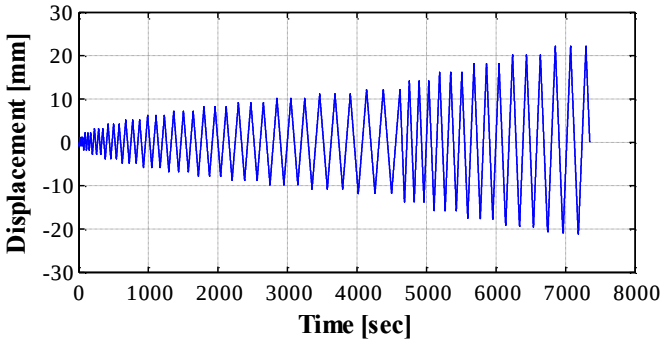

Figure 4-14 Loading protocol of the cyclic shear test on the retrofitted beam-to-column connection

The seismic response of the connection during the test was recorded through several instruments.

- The applied vertical and horizontal loads were recorded by two load cells.
- Two LVDTs were installed between the column top horizontal section and the beam end vertical surface in order to record both the beam-to-column relative displacements and the possible beam rotations (L1 and L2 in Figure 4-15).
- The strains in the steel profiles were recorded by two strain gauges (length=6mm) installed on the profile thickness (P1 and P2 in Figure 4-16).
- The concrete strains around the horizontal steel dowels were recorded on one side of the specimen through uniaxial strain gauges (length=60mm), installed on the beam and column surfaces (Fig. 14). At each node of the retrofitting system, the uniaxial strain gauges were placed orthogonally with respect to the steel profile axis: C1-I and C1-II (Fig. 14a) represent the first and the second strain gauge of the column (C), orthogonal to the direction of the profile 1 (1), around the node 1; B1-I and B1-II (Fig. 14b) represent the first and the second strain gauge of the beam (B), in the direction of the profile 1 (1), around the node 2; B2-I and B2-II (Figure 4-17b) represent the first and the second strain gauge of the beam (B), orthogonal to the direction of the steel profile 2 (2), around the node 2; C2-I and C2-II (Figure 4-17c) represent the two strain gauges of the column (C), orthogonal to the direction of the profile 2 (2), around the node 3.
- Uniaxial strain gauges were placed on the horizontal steel dowels and they were embedded in the concrete grout in order to record the axial strains (D1 at the node 1, D2 at the node 2 and D3 at the node 3).

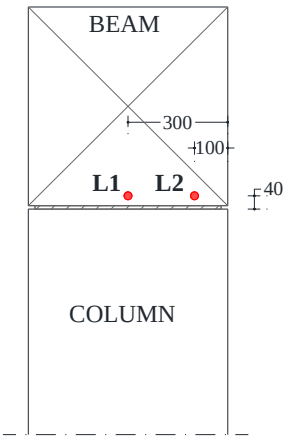

Figure 4-15. Geometrical layout of the LVDTs at the beam end (dimensions are expressed in mm)

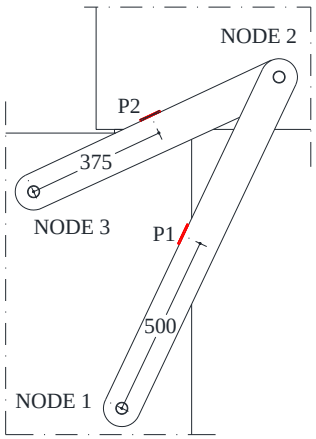

Figure 4-16. Geometrical layout of the strain gauges on the steel profiles (dimensions are expressed in mm)

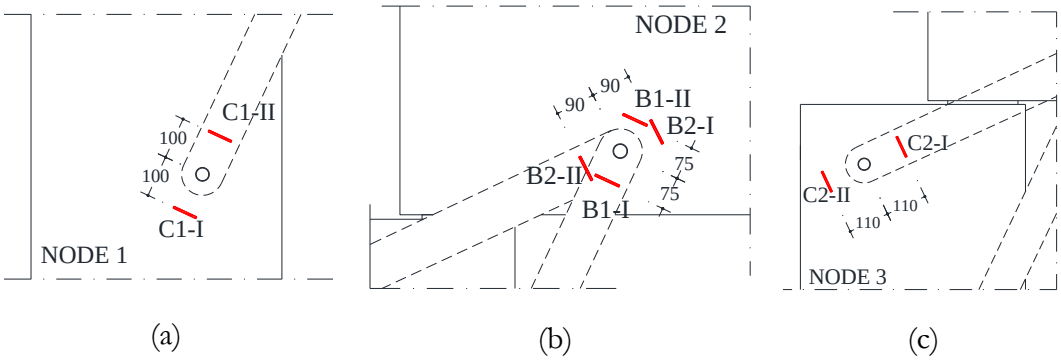

Figure 4-17 Geometrical layout of the strain gauges on concrete surfaces: (a) Node 1, (b) Node 2, (c) Node 3 of the retrofitting system (dimensions are expressed in mm)

Fig. 15 shows the cracking pattern on both the sides of the beam (node 2) at the end of the test. Most of the cracks were recorded in the direction of the profile 2 as well as in the orthogonal one because of the high compressive and tensile axial forces in this profile during the cyclic test. The concrete cracks propagated up to the bottom of the beam (Figure 4-19).

Figure 4-18 shows the final state of the column: few cracks, with limited length and width, were recorded.

(a)

(b)

Figure 4-18 Cracking pattern around the node 1 after the test 1: (a) West and (b) East side

Figure 4-19 Cracking pattern on the bottom surface of the beam (test 1)

Figure 4-20 Cracking pattern around the node 3 (test 1)

The records of the strain gauges can describe the development of the damage during the test. Fig. 18 and Fig. 19 show the ratio between the recorded strain values (ε) of the concrete and the limit concrete tensile strain (εt=0.01%), i.e. the strain which corresponds to the attainment of the concrete tensile strength (fctm). The strain gauge records at the node 1 (C1-I and C1-II in Figure 4-25) and at the node 3 (C2-I and C2-II in Fig. 19) justify the low damage recorded in the column. On the contrary, the strains in the beam reached the limit value εt: the strain gauges B1-II (blue line in Figure 4-25) and B1-I (red line in Figure 4-25) recorded the limit value at 2211sec (first cycle of the 9th step) and at 3984sec (third cycle of the 11th step), respectively. These records are confirmed by the specimen inspection during the test: at these times the first crack occurred along the profile 1 (Figure 4-23) at the two sides of the node 2. At the node 2, the strain gauges B2-II (blue line in Fig. 19) and B2-I (red line in Figure 4-22) achieved the concrete limit tensile strain at 2846sec (first cycle of the 10th step) and 3353sec

(third cycle of the 10th step), respectively: these times corresponded to the occurrence of the first crack along the profile 2 at the two sides of the node 2 (Figure 4-24).

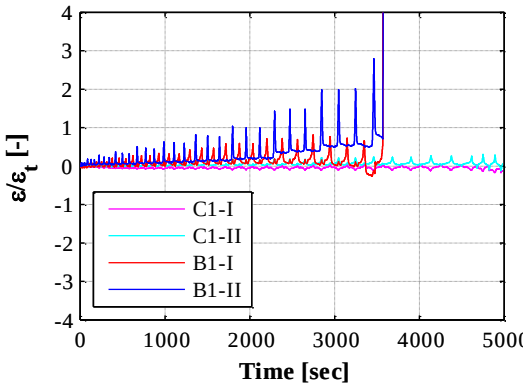

Figure 4-21 Records of the strain gauges orthogonal to the profile 1 (test 1)

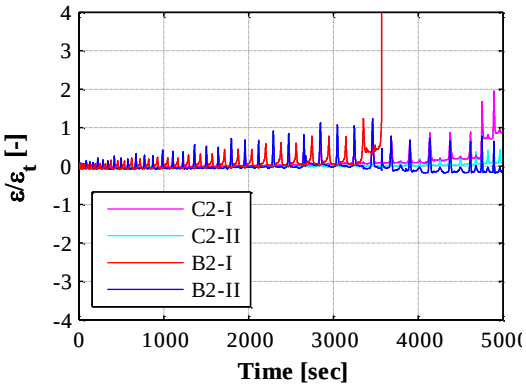

Figure 4-22 Records of the strain gauges orthogonal to profile 2 (test 1)

Figure 4-23 First crack at the node 2 along the profile 1 (test 1)

Figure 4-24 First crack at the node 2 along the profile 2 (test 1)

Figure 4-25 shows the ratio between the axial strains ε of the strain gauges on the steel profiles (P1 and P2) of the West side and the yielding value εy,profile of the adopted steel. Due to the geometrical configuration, the strain values of the profile 2 (red line in Figure 4-25) were higher than those of the profile 1 (blue line in Figure 4-25). However, both the profiles did not reach the yielding limit up to the end of the test: the strain values were quite smaller than the yielding strain. The same considerations can be stated for the East side of the retrofitted specimen (Figure 4-26). The strain gauges records on the steel profiles (Figure 4-25 and Figure 4-26) also show a fairly symmetric behavior of the connection: the differences between the two sides of the system are caused by constructive imperfections.

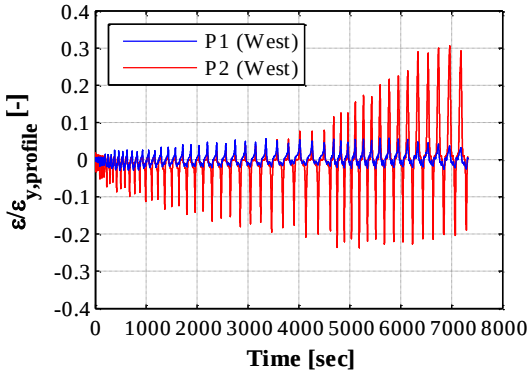

Figure 4-25 Records of the strain gauges on the steel profiles on the West side (test 1)

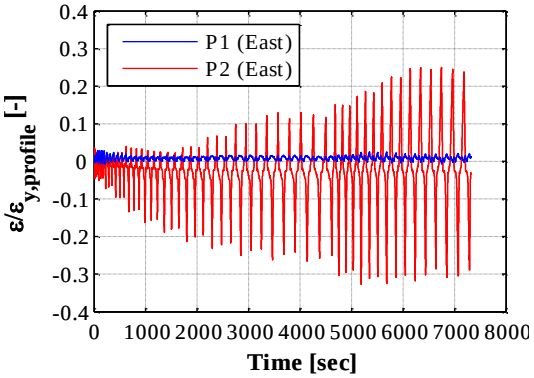

Figure 4-26 Records of the strain gauges on the steel profiles on the East side (test 1)

Fig. 24 shows the ratio between the axial strains ε of the dowels in the column (D1 and D3) and their limit yielding value, εy,dowel. The values recorded by the strain gauge D3 (red line in Figure 4-27), which reached the yielding value at 4755sec, were higher than the strains recorded by D1 (blue line in Figure 4-27). This result confirms the high force level in the profile 2 during the cyclic test. The records of the strain gauge on the dowel in the beam are not showed, because it failed at the beginning of the test due to the significant concrete damage in the node 2.

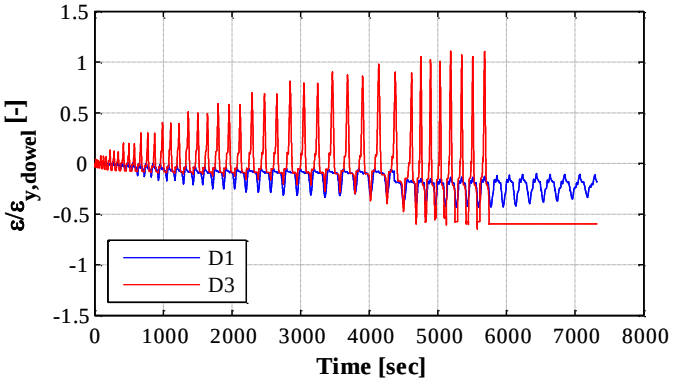

Figure 4-27 Records of the strain gauges on the horizontal steel dowels in the column (test 1)

In Fig. 25 the behavior of the retrofitted connection is shown in terms of force-displacement curve, i.e. the shear forces and the relative displacements between beam and column (gray line). The horizontal displacements are evaluated as the mean value of the LVDT records at the beam end (L1 and L2 in Figure 4-25) and the shear forces are assumed as the records of the load cell of the actuator. The negative values of forces and displacements correspond to pulling loads, i.e. horizontal loads against the column frontal cover. The connection behavior is not symmetric in the two loading directions because of an irregular distribution of the local stresses in the concrete. This evidence

can be justified by installation defects of the horizontal dowels and it is also demonstrated by the different crack patterns in the two loading directions. In particular, in the case of pushing loads (positive values), a lower damage of the concrete corresponds to a higher initial stiffness and to smaller relative displacements than in the case of pulling loads. Concerning the pulling loads (negative values), the force-displacement curve shows a clear pinching effect up to a relative horizontal displacement equal to 7mm, due to the concrete damage around the horizontal dowels.

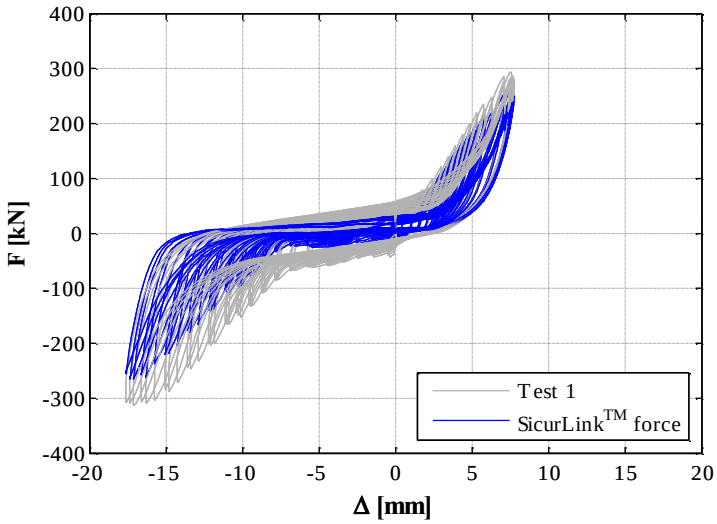

Figure 4-28 Force-displacement curve for the cyclic shear test 1on the retrofitted specimen

The gray curve in Fig. 25 includes different forces: the shear force absorbed by the three-hinged connection system, the frictional forces between concrete and neoprene and the undesired frictional forces due to the setup components (e.g. teflon sheet). Since the goal of the experimental test is the study of the behavior of the retrofitted beam-to-column connection, the frictional forces of the setup should be depurated. At this purpose, the three-hinged connection system and the neoprene associated forces were separately evaluated. Concerning the three-hinged connection system, the corresponding forces were evaluated with the records of the strain gauges installed on the steel profiles, shown in Figure 4-25 and Figure 4-26. Since the steel profiles exhibited an elastic behavior during the entire test, the axial forces in the profile can be easily evaluated by using their mechanical properties (Ey,profile) and their geometrical features (thickness and width). The horizontal components of these axial forces correspond to the shear forces in the three-hinged steel system on each side of the beam-to-column connection. Figure 4-28 shows the overall shear force (blue line) absorbed by the West and East connection profiles, during the test.

The maximum recorded shear force (see gray curve) for positive loading semi-cycles was equal to 293.58kN (first cycle of the 14th step) and the corresponding shear force in the retrofitting system (blue curve) was equal to 258.19kN. The difference between these values can be assumed as the neoprene associated forces, which are elastic, plastic and neoprene-concrete friction forces; consequently the other setup frictional forces can be neglected. The maximum recorded shear force (see gray curve) in the negative loading semi-cycles was equal to 312.98kN (first cycle of the 17th step) and the corresponding retrofitting system shear internal force (blue curve) was equal to 264.59kN: also in this direction the other setup frictional forces can be neglected. As a consequence, the total shear force (gray curve in Figure 4-28) can be considered as the effective connection response.

4.2.6 *Cyclic shear test on the retrofitted connection: test 2*

Another cyclic shear test (test 2) was performed on a retrofitted connection, which originally was a dowel connection tested under monotonic horizontal loads as described in Magliulo et al. [32] The retrofitting system had the same geometrical and mechanical features and its installation steps were the same described for test 1; however, in this case a rubber sheath was inserted around the horizontal steel dowel in the beam. This element was added to the system in order to improve the connection performance by avoiding/reducing the high local stresses in the concrete around the steel dowels, recorded in the test 1. Moreover, the rubber sheath can also allow connection deformations, as the ones due to the thermal actions. In particular, the thickness of the rubber was designed in order to avoid earlier loading actions on the retrofitting system: the rubber sheath should allow the displacements due to the applied vertical loads, which induce both beam rotations and neoprene pad deformation. With reference to a simply supported precast beam, the vertical displacement at the node 2 location was evaluated by assuming typical values of beam length, inertia moment and applied permanent and live loads. According to these evaluations, a 2mm rubber sheath was adopted by also taking into account the axial deformability of the neoprene pad.

The same loading protocol of the test 1 was adopted in the test 2, for both vertical and horizontal loads.

During the cyclic test, the connection response was recorded by several instruments. The layout of some instruments was changed with respect to the test 1 in order to improve the records quality. Figure 4-29 shows the location of the two LVDTs at the beam end, which recorded the horizontal beam-to-column relative displacements and the possible horizontal rotations of the beam. Figure 4-30 shows the strain gauges placed along the two steel profiles and Figure 4-31 shows the location of the strain gauges on the beam and column surfaces, which recorded the concrete strains around

the horizontal steel dowels. Other strain gauges (length=60mm) were also introduced in order to record the concrete cover strains at each node: CC1 at the node 1 column concrete cover, CC3 at the node 3 column concrete cover and BC2 at the node 2 beam concrete cover (Fig. 28).

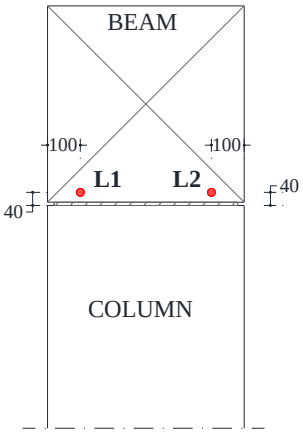

Figure 4-29 Geometrical layout of the LVDTs at the beam end in the test 2 (dimensions are expressed in mm)

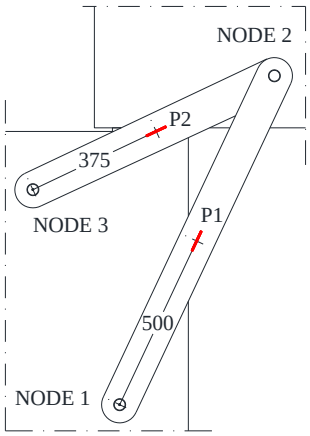

Figure 4-30 Geometrical layout of the strain gauges on the steel profiles in the test 2 (dimensions are expressed in mm)

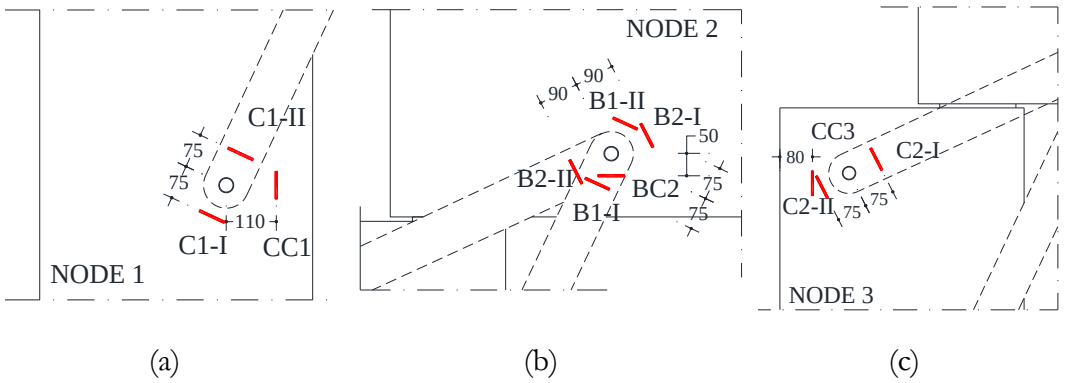

Figure 4-31 Geometrical layout of the strain gauges on the concrete surface (test 2): (a) node 1, (b) node 2, (c) node 3 (dimensions are expressed in mm)

At the end of the test, the rubber sheath around the steel dowel in the beam (node 2) was significantly damaged (Figure 4-32) and the surrounding grout crushed. Moreover, the neoprene pad showed large deformations due to the high compressive loads (Figure 4-33). Several inclined cracks appeared in the concrete around the node 2 at both the sides of the specimen (Figure 4-34). However, in this test the thickness and the length of the crack were smaller than in the test 1 because the rubber reduced the damage in the surrounding concrete.

Figure 4-32 Rubber sheath deformation (test 2)

Figure 4-33 Neoprene pad deformation (test 2)

(a) (b)

Figure 4-34 Cracks pattern at the node 2 at the end of the test 2: (a) West and (b) East view

The records of the strain gauges on the concrete elements are showed in the following in terms of ratio between the recorded strain values (ε) and the limit concrete tensile strain (εt=0.01%). Figure 4-35 shows the records in the strain gauges orthogonal to the profile 1 (C1-II in the column for the node 1 and B1-II in the beam for the node 2): only the records referring to the beam node (blue line in Figure 4-35) reached the limit concrete tensile strain at 2844sec (first cycle of the 10th step), i.e. later than in the case of the test 1. Both the strain gauges orthogonal to the profile 2 (C2-I in the column for the node 3 and B2-I in the beam for the node 2) reached the limit concrete tensile strain (Figure 4-36) almost simultaneously (during the first cycle of 13th step): in node 3 at 4753sec and in node 2 at 4824sec. These results justify the observed concrete damage of the beam around the node 2 and they are also confirmed by the records of the strain gauges at the concrete cover of the beam (BC2 in Figure 4-37) and of the column (CC1 and CC3 in Figure 4-37).

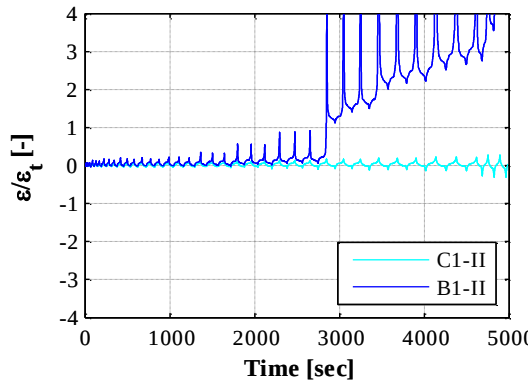

Figure 4-35 Records of the strain gauges orthogonal to the profile 1 (test 2)

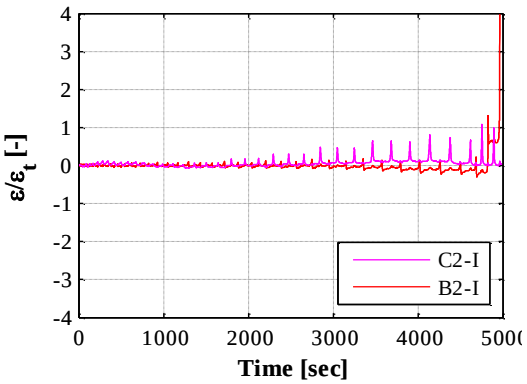

Figure 4-36 Records of the strain gauges orthogonal to the profile 2 (test 2)

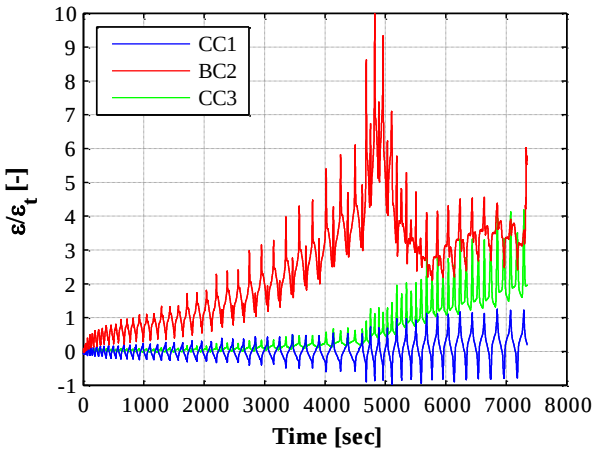

Figure 4-37 Records of the strain gauges at the concrete cover (test 2)

The axial strains of the horizontal dowels in the column (D1 at node 1 and D3 at node 3) did not reach the yielding value of the threaded bars (Figure 4-38).

The records of the strain gauges on the steel profiles again show the high axial forces in the profile 2 (Figure 4-39); however, neither of the two profiles reached the yielding strength. The axial deformations trend of the two steel profiles, as in the case of the test 1, confirms the effectiveness of three hinged arch mechanism, since the two profiles work in tension and in compression, alternatively.

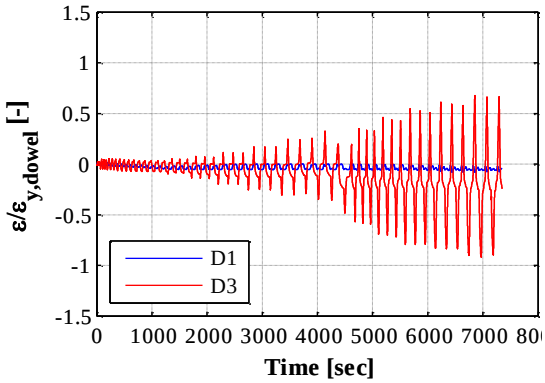

Figure 4-38 Records of the strain gauges on the horizontal steel dowels (test 2)

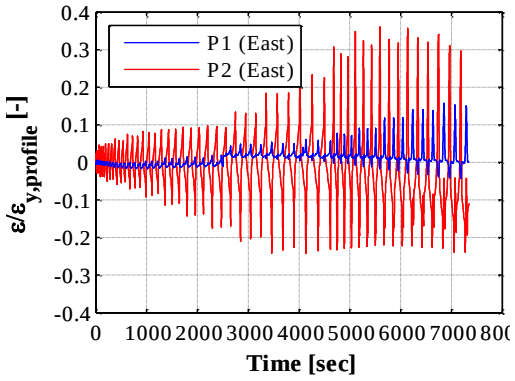

Figure 4-39 Records of the strain gauges on the steel profiles (East side, test 2)

In Fig. 37, the behavior of the connection during the test 2 is shown in terms of horizontal forces and relative displacements. The horizontal displacements are the mean values of the LVDT records at the beam end and the shear force values are the load cell records of the horizontal actuator. The specimen showed a quite symmetrical behavior up to the end of the test. The recorded total shear strength accounts for the retrofitting system strength, the neoprene elastic and plastic internal forces, the neoprene-concrete frictional strength, and the other setup resistances; however, as in the case of the test 1, the setup resistances can be neglected and the total shear strength (red curve in Figure 4-40) can be assumed as the effective retrofitted connection response. The maximum value of the retrofitting system shear force occurred under pulling loads (negative values) and it is equal to 284.54kN.

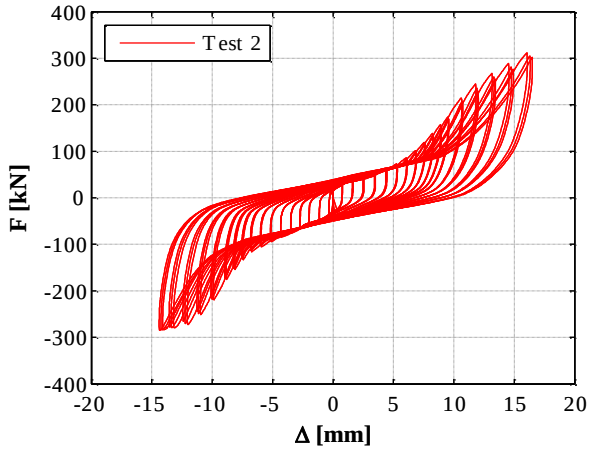

Figure 4-40 Force-displacement curve of the cyclic shear test on the retrofitted connection (test 2)

4.2.7 *Comparison between dowel and retrofitted connection*

This section aims at comparing the cyclic behavior of the dowel beam-to-column connection with the two tested retrofitted connections in terms of both global behavior and dissipated energy.

Figure 4-41 shows the envelopes of the force-displacement curves of the three investigated cyclic tests. As already written, for all the investigated tests the load protocol consisted of increasing displacement steps and, for each step, three complete cycles (negative and positive semi-cycles) were performed. Since, at each step, the maximum value of the shear force was reached at the first cycle, the envelope takes into account only the first cycle of each step. Moreover, in Fig. 38 the envelope of the shear test on the dowel connection (black curve) is showed up to the 20% strength degradation, assumed as the attainment of the connection failure.

The comparison demonstrates that the dowel connection (black curve in Figure 4-41) shows higher initial stiffness with respect to the retrofitted connections; however, it has lower shear strength in both the considered load directions. Moreover, the seismic behavior of the dowel connection is strongly not symmetric in the two loading directions: for pulling loads a sudden decrease of strength and stiffness was recorded. This evidence is justified by the failure mechanism that occurred for pulling loads (force negative values) with the spalling of the lateral concrete cover in the column.

The first tested retrofitted connection (blue curve in Figure 4-41) shows higher shear strength with respect to the dowel connection in both the directions. Moreover, the more symmetric behavior demonstrates the efficiency of the retrofitting system. However, it is worth to underline that also this connection shows larger relative displacements for pulling loads (force negative values) with respect to pushing loads;

this is related to the larger damage observed around the horizontal steel dowels when the load is applied in the former direction.

The second retrofitted connection (red curve in Figure 4-41) shows the best seismic performance, with high shear strength values and a very symmetric response. The rubber sheath around the horizontal dowel in the beam led to a lower stiffness in test 2 than in test 1 for pushing loads (force positive values) because of its deformability; on the contrary, for pulling loads the behaviors are more similar, because of the significant concrete damage around the beam dowel in test 1.

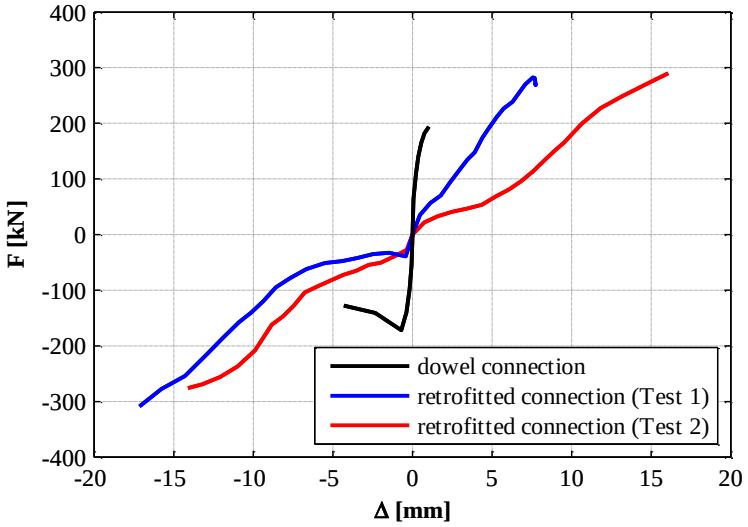

Figure 4-41 Force-displacement envelopes of the tests on the dowel beam-to column connection (black curve) and on the two retrofitted connections, i.e. without (blue curve) and with (red curve) the rubber sheath around the horizontal dowel

Fig. 39 shows the dissipated energy at each negative semi-cycle, corresponding to pulling loads, for the three investigated tests: the dowel connection (black bars), the retrofitted connection without the rubber sheath (blue bars) and the retrofitted connection with the rubber sheath (red bars). The dissipated energy of the dowel connection is plotted only for the first six steps, i.e. until the assumed failure of the connection. Up to the fourth step of the test on the dowel connection (i.e. the step which corresponds to the first crack formation), its dissipated energy was strongly lower than the dissipated energy in the retrofitted solutions because of the high initial stiffness. After the first concrete cracking, the dissipated energies in the dowel connection and in the retrofitted solutions were quite similar, because of the increased deformability of the dowel connection due to the concrete damage. The dissipated energy in the two retrofitted connections increased up to the end of the shear tests; moreover, the rubber sheath around the horizontal dowel in the beam provided higher values of dissipated energy in test 2 with respect to test 1.

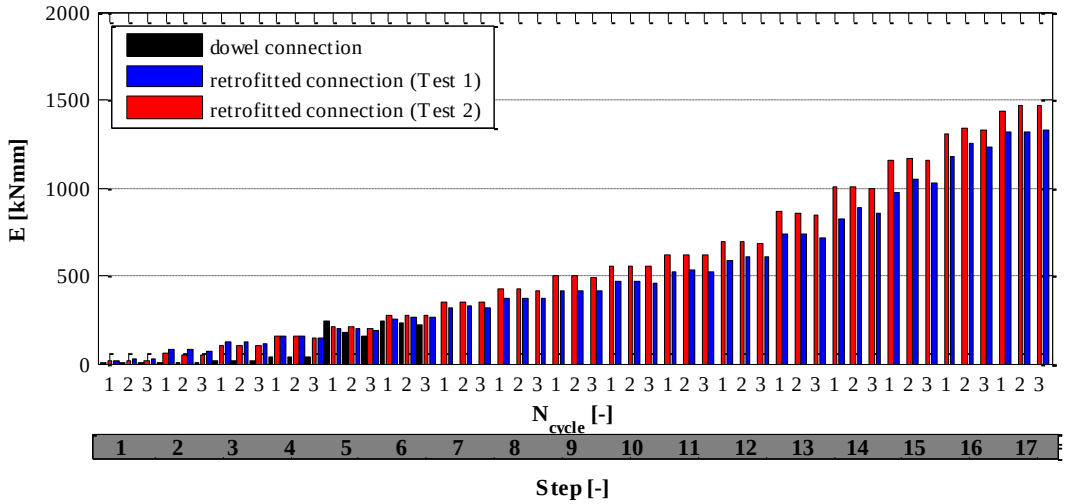

Figure 4-42 Dissipated energy during the negative semi-cycles of the shear tests on the dowel beam-to column connection (black bars) and on the two retrofitted connections, without (blue bars) and with (red bars) the rubber sheath

Figure 4-43 shows the dissipated energy at each positive semi-cycle (corresponding to pushing loads) for the three investigated shear tests. The comments concerning the dissipated energy of the negative semi-cycles are confirmed.

As in the pulling direction, at each step, the dissipated energy during the first semi cycle is generally lightly greater than the dissipated energy during the second and the third ones.

The dissipated energy of the dowel connection is always much lower than the one recorded in the retrofitted solutions, because of its large stiffness.

Furthermore, the dissipated energy values of the test 2 retrofitted solution are significantly higher than the values of the test 1 retrofitted solution and this difference is also higher than in the case of pulling loads. This is due to the lower damage recorded in test 1 related to the pushing loads.

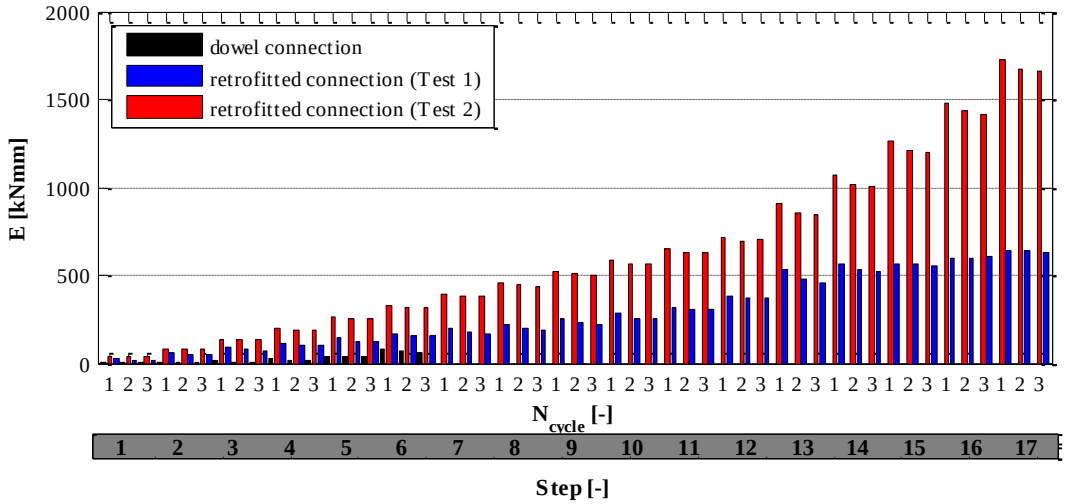

Figure 4-43 Dissipated energy during the positive semi-cycles of the shear tests on the dowel beam-to column connection (black bars) and on the two retrofitted connections, without (blue bars) and with (red bars) the rubber sheath

4.2.8 *Final remarks*

In this paper, a retrofitting solution for RC precast beam-to-column connections is presented. An experimental campaign was performed in order to evaluated the seismic performance of this system through cyclic shear tests.

The reference specimen is a dowel beam-to-column connection, typically adopted in one-story RC precast structures. This connection was tested in a previous experimental campaign under cyclic shear loads up to the failure of the lateral concrete cover in the column, which caused the failure of the connection. The damaged specimen was retrofitted by a three-hinged steel connection system. Two different configurations of this system were tested, i.e. without and with a rubber sheath around the dowel in the beam. For both the systems, the global behavior in terms of force-displacement curve was investigated and the damage patterns after the tests were described through both visual inspections and instrumentation records.

The experimental results allowed to draw the following conclusions.

- Both the configurations of the retrofitting system showed a good behavior under cyclic horizontal forces. In the retrofitted connection system, the horizontal shear force was mostly sustained by the three hinged arch mechanism, ensured by the two steel profiles pinned to the horizontal dowels.
- The retrofitted connections showed larger shear strength as well as larger dissipated energy values than the standard dowel connection. For loads against the column core (positive direction), the maximum shear force was recorded in the configuration with the rubber sheath (test 2). It increased of 50% with respect to the

dowel connection and of 3% with respect to the configuration without the rubber (test 1). For loads against the column cover (negative direction), the maximum shear force recorded in the test 2 increased of 60% with respect to the dowel connection.

- The initial stiffness of the retrofitted connections was significantly lower than the stiffness of the dowel connection. For the negative direction, the stiffness recorded in the two described tests was almost constant and it was about 10 times lower than the stiffness of the dowel connection. For the positive direction, the stiffness recorded in test 2 was about two times lower than the stiffness recorded in test 1 and about 30 times lower than the stiffness of the dowel connection.
- In both the tests on the retrofitting system, no significant damage was recorded in the concrete. The large concrete covers of the horizontal dowels prevented brittle failures in the connected elements: the concrete damage was not severe up to the end of the test. However, the retrofitted connection without the rubber sheath showed a larger damage around the beam dowel than the system with the rubber.

4.3 Numerical investigations

In this section, the seismic performance of the SicurLink™ system, as well as the seismic performance of the whole retrofitted building, are described in detail, considering the structural model described in section 3.3, in which the retrofitting system is applied only at the beam-to-column connections.

The seismic performance of the retrofitting system is investigated through numerical analyses on a single frame of the reference building. In particular, FIGURE shows the considered frame, i.e. an external frame along the x global direction. FIGURE show a schematic representation of the structural elements, the structural eccentricities, the concentrated masses, and the applied gravity loads. The gravity load on the columns (N_{col}) takes into account the gravity load coming from the adjacent spans. The symbols refer to Table 3-1 and Table 3-2.

For the definition of the non-linear model (column plastic hinges and frictional connections), the properties of column type B should be taken into account (Figure 3-7 and Table 3-4)

According to the above defined frame model, the fundamental period of the existing frame, associated to the translational mode along the x axis, is equal to 1sec.

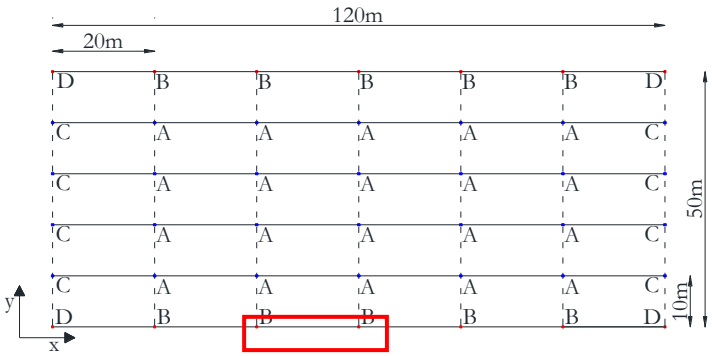

4.3.1 *The retrofitted frame model*

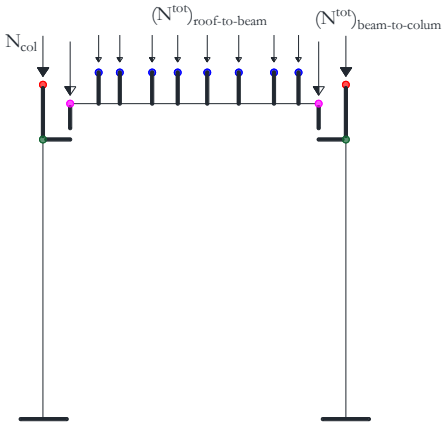

The beam-to-column connections of the existing frame are retrofitted applying the SicurLink™ system, in a bottom configuration (Figure 4-44), type "short" (Section 4.1). Hence, the retrofitting system of each connection consists of two steel profiles, both connected to the beam in the same point and connected to the column at two different heights. The steel profiles are connected to the concrete elements through horizontal steel dowels, passing through steel plates and fixed by nuts and washers. The steel plates are bolted to the internal side of column and the lower side of the beam.

The two steel profiles present a width equal to 10cm and a thickness of 2cm, so that the transversal area is equal to 20cm^2. For the assumed configuration, the lower and upper profiles are 100cm and 60cm long, respectively.

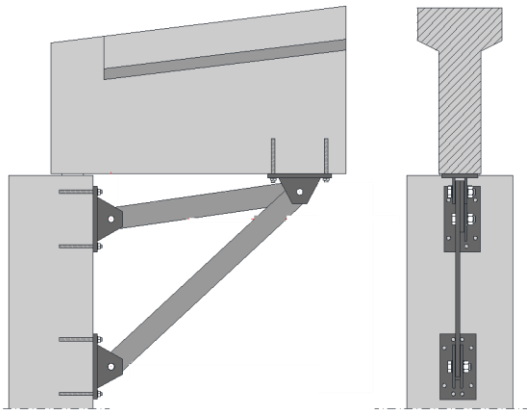

Figure 4-44 SicurLink™ system: bottom configuration

Since the retrofitting system performs a three-hinges arc configuration and the steel profiles work in turn as struts and ties, absorbing only axial loads, the retrofitted connection is modeled in OpenSees adding (to the existing friction connection model, Section 3.3.2) rigid blocks and *truss elements* in order to represent the geometrical eccentricities and the steel profiles, respectively. The mechanical and geometrical properties of the truss elements reproduce the properties of the steel components, i.e. the transversal area, the profile length and the constitutional law of the profile material.

The constitutional low, which reproduces the mechanical properties of the profiles, is obtained combining in series an elastic perfect plastic material (which represents the steel behavior) and a gap material (which models the presence of the rubber sheath covering the horizontal dowels), assigned in the axial direction of the steel profiles. For this reason, in the OpenSees model, a *uniaxialMaterial ElasticPPGap* is assigned to the truss elements, in which the initial deformation gap, the initial stiffness and the yielding force should be defined (Figure 4-45).

The deformation gap considers the rubber sheath properties, with a very low stiffness and a thickness of 4mm. The rubber sheath is assumed to be placed around both the dowels at the steel profiles ends, so that up to 8mm in compression and 8mm in traction, no reaction forces should be accounted in the steel profiles.

The elastic part of the constitutional law exhibits an initial stiffness EA/L, where E is the steel Young modulus, A is the steel profile transversal area and L is the steel profile length. The elastic behavior is limited in compression by maximum compressive axial force (C_{max} in Figure 4-45), which is the lowest value between the dowel shear strength and the critical axial load, which induces buckling for the steel profiles (Table 4-2). In tension, the elastic behavior is limited by the maximum tensile force (T_{max} in Figure 4-45), which is the lowest value between the horizontal dowel shear strength and the yielding force for the steel profiles (Table 4-2).

In compression, the plastic behavior is not performed since both the shear failure of the dowel and the buckling of the steel profiles do not offer any significant ductile deformation. For this reason, if failure occurs in compression, the corresponding steel profile is removed from the model during the analysis using the *remove element* command in OpenSees.

In tension, the plastic behavior is performed only if the yielding force for the steel profile is reached first with respect to the shear failure of the dowel. Otherwise, the corresponding profile is removed from the model during the analysis using the *remove element* command in OpenSees.

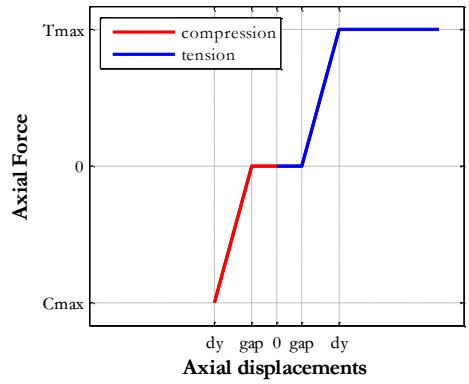

Figure 4-45 UniaxialMaterial ElasticPP Gap

Table 4-2 Maximum value of the axial force in the steel profiles

	Upper profile (L_2)		Lower profile (L_1)	
	T_{max} [kN]	C_{max} [kN]	T_{max} [kN]	C_{max} [kN]
Profile failure	900.00	122.17	900.00	43.98
Dowel failure	215.42	215.42	215.42	215.42

The dynamic non-linear analyses on the single frame are performed considering the only horizontal component of the earthquake, in the x direction.

In the following, the seismic behavior of the retrofitting system is described through the numerical results of the dynamic analysis performed on the reference frame, using the North component of the Emilia earthquake (29/05/2012), recorded in Mirandola (Section 3.4).

4.3.2 *Connection system*

During the analysis, the lower profiles of both the retrofitted connections and the upper profile on the right retrofitted connection reached the maximum value of the axial force so that they are progressively removed from the model. This results in the fact that all the steel profiles fail in the early stage of the analysis and they do not reach the plastic deformations range, exhibiting an elastic behavior up to the failure (Figure 4-46 and Figure 4-47).

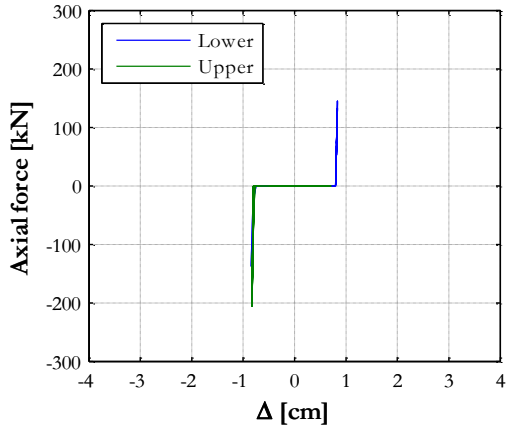

Figure 4-46 Axial force versus axial deformation for the retrofitting system on the left connection

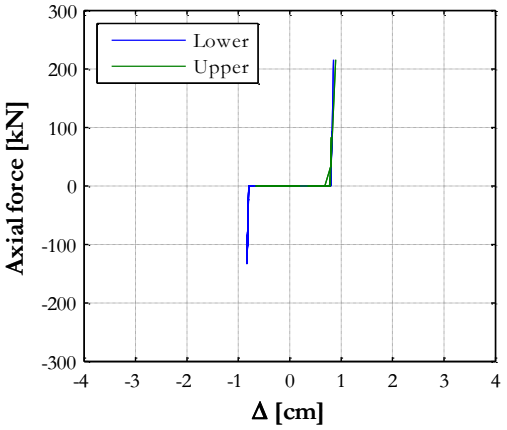

Figure 4-47 Axial force versus axial deformation for the retrofitting system on the left connection

4.3.3 *Friction connections*

The retrofitting device offers shear strength against the horizontal seismic loads and provides mechanical restrains for relative horizontal displacements in the friction beam-to-column connections.

Figure 4-48 and Figure 4-49 show the shear force F versus the relative displacements Δ between the main beam and the column, on both the sides of the frame (the red solid line corresponds to the right connection, the blue solid line corresponds to the left connection), for the existing frame and the retrofitted one, respectively. It is worth noticing that in the first case, the friction connections exhibits large sliding displacements so that unseating fenomena can occur with respect to the available support length (dashed line in Figure 4-48 and Figure 4-49). In the latter case, thanks to the presence of the steel devices, which offer high shear stiffness, very small relative displacements can be observed, mainly due to the initial gap and to the elastic behavior of the steel profiles. However, the shear force increases due to the fact that, if one of the steel profile which composes each retrofitting systems reaches the maximum axial force and fails, the three-hinge arc mechanism does not work and localized forces occur in the beam and the column. These forces produce beam rotations, which lead to higher axial forces on the friction connection and to corresponding higher frictional strength.

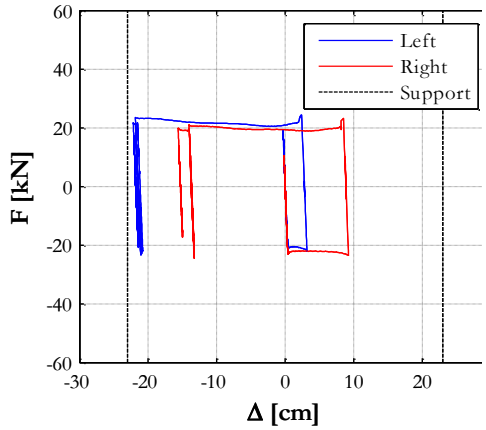

Figure 4-48 Shear force versus relative displacement for the beam-to-column friction connection of the existing frame

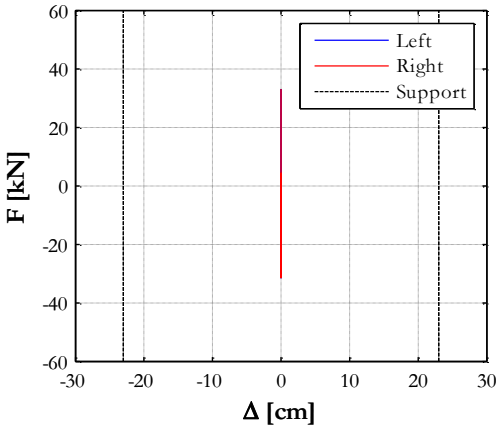

Figure 4-49 Shear force versus relative displacement for the beam-to-column friction connection of the retrofitted frame

4.3.4 *Plastic hinges*

The non-linear behavior of the reference frame can be investigated observing the moment-rotation diagrams at the column base. Figure 4-50 and Figure 4-51 show the cyclic response of the plastic hinges for the existing frame and the retrofitted one, respectively. It can be observed that the rotation at the column bases overpasses the yielding value both in the existing and the retrofitted frame, with a high plastic deformations in the latter case. Moreover, the plastic hinges at the right and left column, in the retrofitted frame, show different cyclic responses due to the fact that the progressively failure of the steel profiles leads to non-symmetric structural scheme.

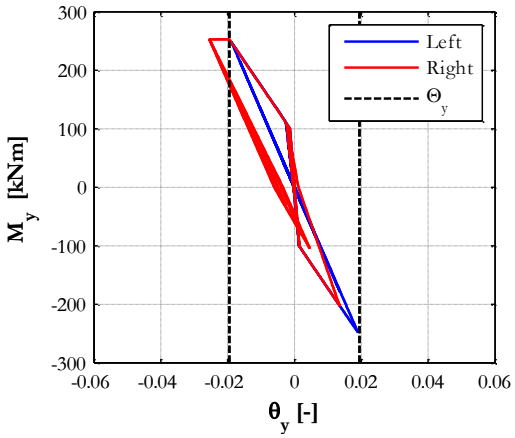

Figure 4-50 Moment-rotation diagram for column plastic hinges of the existing frame

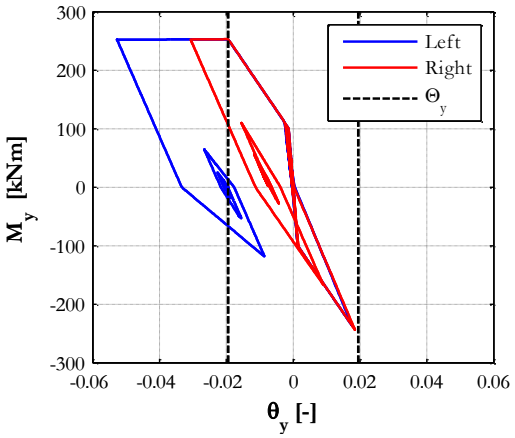

Figure 4-51 Moment-rotation diagram for column plastic hinges of the retroffitted frame

4.3.5 *Lateral drifts*

In order to assess the non-structural damage, the later drift is controlled. Figure 4-52 shows the later drifts for the column on the left side (blue solid line) and on the right side (red solid line) of the existing frame. Figure 4-53 refers to the retrofitted one. It can be observed that in both the cases the lateral drift overpasses the Code limit value (1%) and that in the retrofitted frame, the structural asymmetries due to the progressive failure of the steel profiles leads to different values of lateral drift. The plastic deformations at the column bases result in residual drifts at the end of the input motion.

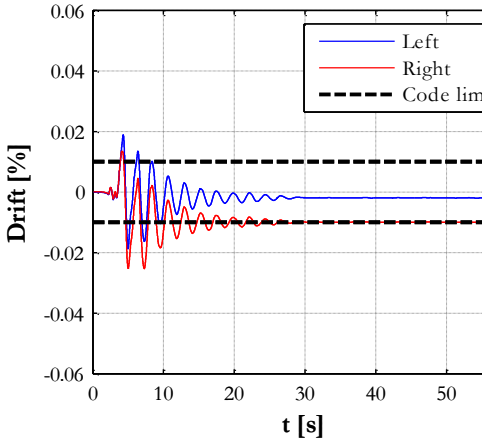

Figure 4-52 Lateral drifts for the existing frame

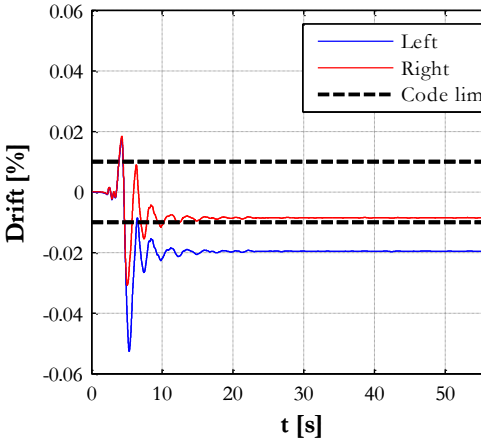

Figure 4-53 Lateral drifts for the retrofitted frame

4.3.6 *Energy balance*

The global behavior of the reference frame can be described by the energy balance, verified during the analysis. First, it should be observed that, even if the retrofitted frame exhibits the same initial period of the existing frame (T=1sec), during the analysis the increased stiffness, related to the presence of the retrofitting system, leads to lower periods which reflect into higher accelerations and inertial forces. For this reason, the input energy for the retrofitted frame is higher that the input energy for the existing frame.

Moreover, due to the high plastic deformations, the hysteretic energy for the retrofitted frame increases and for the retrofitted frame overpasses the 50% of the input energy.

The energy content related to the frictional behavior, which is about the 50%of the input energy for the existing frame, strongly decreases for the retrofitted one and it is about the 20% of the input energy.

The viscous energy related to the inherent damping is not influenced by the presence of the retrofitting system.

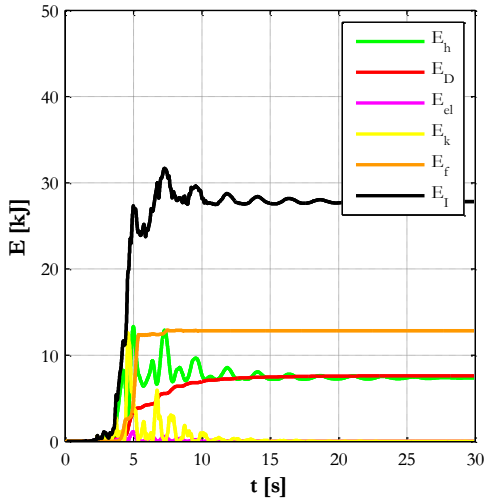

Figure 4-54 Energy balance for the existing frame

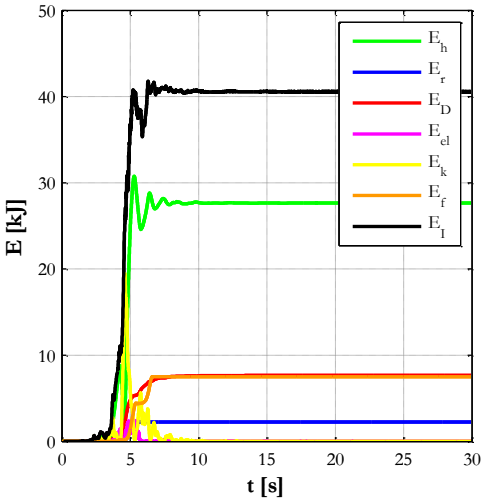

Figure 4-55 Energy balance for the retrofitted frame

4.3.7 *Hysteretic damper*

In order to improve the seismic behavior of the retrofitting system, it should be avoid that the steel profiles or the horizontal dowels reach a brittle failure before the plastic behavior is developed (Figure 4-45). The best performance could be obtained if the plastic deformations in the retrofitting system avoid structural damage, i.e. yielding rotation at the column base.

For this reason, it could be assumed that the maximum shear force in the connection should be lower than the shear force corresponding to the yielding rotation of the column base (Eq. 4.1), so that the activation of the connection system occurs before the column damage. A reduction factor equal to 0.8 is also adopted.

After that, based on the geometrical configuration, the maximum axial force in the steel profiles can be obtained (Figure 4-56, Eqs. 4.2 and 4.3). For each profile, the axial force can assume tensile or compressive values: in the following table, figure and equations the label N represent the axial force modulus, the labels T and C represent the tensile ad the compressive value, respectively.

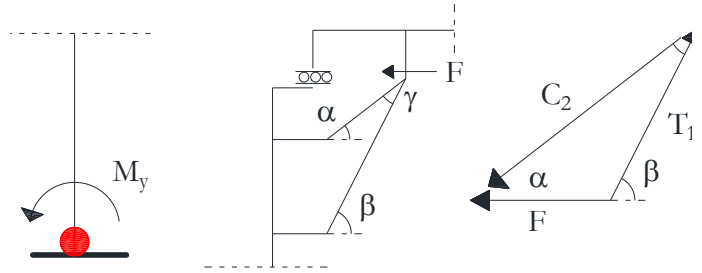

α	[°]	25
β	[°]	57
γ	[°]	32
M_y	[kNm]	253
F	[kN]	25.60
N_2	[kN]	40.14
N_1	[kN]	19.96

Figure 4-56 Design parameters for beam-to-column connection (type B)

$$F = 0.8 \cdot M_y / H_{col} \tag{4.1}$$

$$T_1 = F \cdot \frac{\sin\alpha}{\sin\gamma} = -C_1 \tag{4.2}$$

$$C_2 = F \cdot \frac{\sin\beta}{\sin\gamma} = -T_2 \tag{4.3}$$

In the following, the results of the dynamic analysis for the retrofitted frame with the dissipative connection are presented. It can be observed that the steel profiles exhibit plastic deformations in tension as well as in compression (Figure 4-57 and Figure 4-58). Also in this case, the relative beam-to-column displacements are restrained, but the shear force is now limited (Figure 4-59). However, due to the limited relative displacements, the steel profiles exhibit only low plastic deformations, with few hysteretic cycles. For this reason, the retrofitting system damage is not enough to avoid the formation of the column plastic hinges, which still show rotation higher than the yielding value (Figure 4-60). However, in this case, the presence of an effective beam-to-column connection leads to a symmetric structural response, which results in equal moment-rotation diagrams for both the plastic hinges and equal lateral drifts for both the columns (Figure 4-61).

Concerning the global behavior, Figure 4-62 shows the energy balance during the analysis: it is worth noticing that the presence of dissipative connection systems avoids increase of lateral stiffness without reduction of stiffness so that the input energy is the same with respect to the input energy in the existing frame, without beam-to-column connection systems. However, the low frictional displacements lead to very low friction energy and the energy damping is only related to the plastic deformations in the plastic hinges with higher structural damage with respect to the existing frame.

It should be observed that even if a lower maximum axial force in the steel profiles are assigned, it is not possible to avoid structural damage. This is due to the fact that in order to activate the connection system before the activation of the column plastic hinges, the maximum shear force in the connection should be lower that the shear force

which corresponds to the column yielding moment. However, if the connection shear force is lower than the frictional strength, the beam-to-column connection do not exhibits relative displacements which activate the dissipative device.

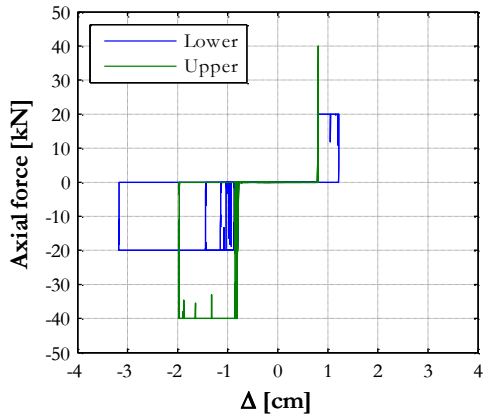

Figure 4-57 Axial force versus axial deformation for the dissipative retrofitting system on the left connection

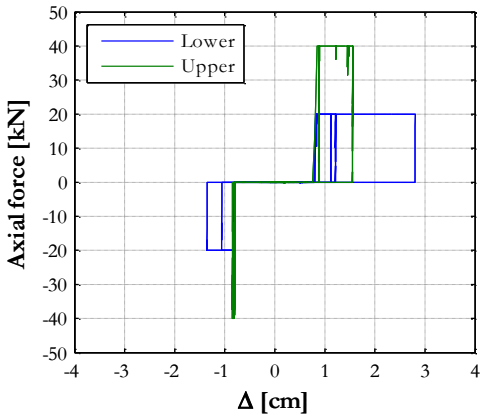

Figure 4-58 Axial force versus axial deformation for the dissipative retrofitting system on the right connection

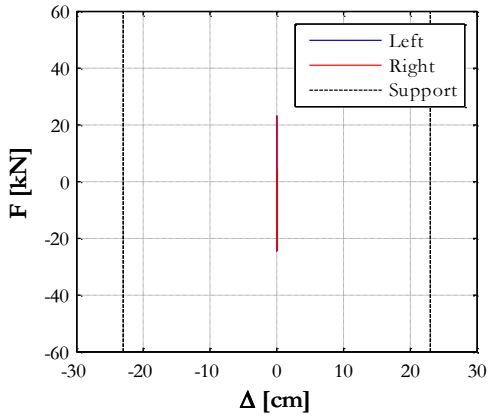

Figure 4-59 Shear force versus relative displacement for the beam-to-column friction connection of the dissipative retrofitted frame

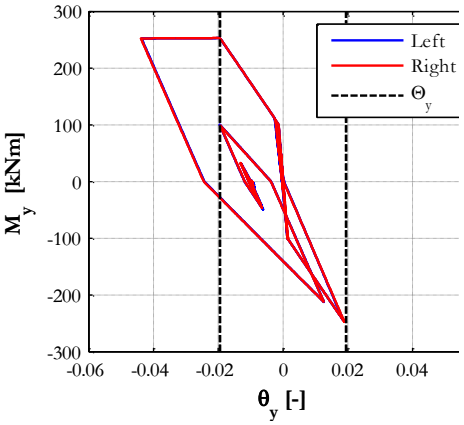

Figure 4-60 Moment-rotation diagram for column plastic hinges of the dissipative retroffitted frame

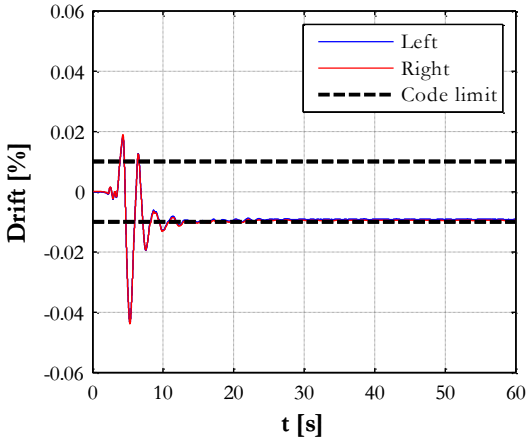

Figure 4-61 Lateral drifts for the dissipative retrofitted frame

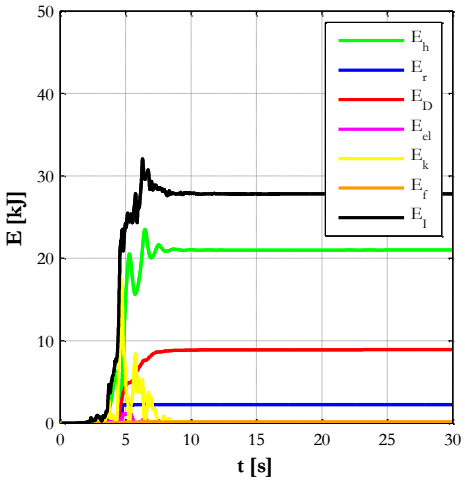

Figure 4-62 Energy balance for the dissipative retrofitted frame

Chapter 5

SEISMIC RETROFIT SOLUTION USING VISCOUS DEVICES

In this section, the seismic retrofit of the reference building using viscous dampers is presented. The considered devices aim at reducing the dynamic response of the structural system during an earthquake. It is assumed to apply the viscous devices to the precast beam-to-column connections.

5.1 Viscous dampers description

The viscous dampers consist in mechanical devices that take advantage of the material aptitude in absorbing and damping external forces. They were largely applied from nineties in civil and mechanical engineering structures in order to reduce vibrations, e.g. vibrations due to wind. Only in the last decades, they were also used for seismic applications, in order to reduce the dynamic response of structures during earthquakes.

The most common adopted technology consists of fluid dampers: a steel cylinder incorporates a stainless steel piston with a bronze orifice head. The internal section of the cylinder could be divided in two different chambers filled with compressible silicone oil. During the piston movement, flow characteristics can be altered, depending on the fluid relative velocity, because of specially shaped orifices on the piston head. The force produced by the damper is generated by the pressure differential across the piston head.

They present both many advantages and critical issues to be faced in structural applications.

They do not change the dynamic properties of the main structure; however, they reduce both displacements and accelerations during earthquakes so that the base shear and the interstory shear decrease as well as the inertia forces. The high damping levels, which can be reached due to their application, can lead to low stresses and deflection in the main structure.

They can be designed with different geometries and installed with different layouts so that they can produce different level of maximum force and relative displacement in

the device. They are usually installed in a structure as diagonal braces or as part of a base isolation system.

They exhibit stable and predictable performance at any temperature, low maintenance costs and long life. However, the production and installation costs could be higher with respect to alternative retrofitting systems.

In the design process, it is difficult to predict the force level that the device could exhibit during the earthquake and then the forces transmitted to the structure.

5.2 Viscous damper model

The dynamic characteristics of a viscous damper depend on the properties of the viscous fluid and on the geometry and materials of the device. For these reasons, the viscous dampers exhibit viscoelastic behavior that incorporates both elastic and viscous frequency dependent characteristics and the hysteretic response can be modeled using a Maxwell model (Makris and Constantinou 1991) which considers springs and dashpots connected in series (Figure 5-1).

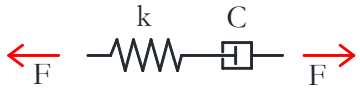

Figure 5-1 The Maxwell model

It consists of Hookean springs, which take into account the instantaneous device deformations, related to the mechanical energy reversibly stored as strain energy. The constitutive low of the Hookean springs is described by:

$$F = k \cdot \Delta \qquad 5.1$$

in which the elastic axial stresses and forces are proportional to the axial deformations and displacements by the Young modulus E (of the considered material for the device) and to the axial stiffness, respectively.

The entropic uncoiling process of the fluid can be modeled by a Newtonian dashpot, in which axial stresses and forces are proportional to the stress rate and velocity, respectively:

$$F = C \cdot v^{\alpha} \qquad 5.2$$

in which C (in N·s/m) represent the viscous parameters and α is the viscous damper exponent (Figure 5-2). When α=1, the device acts as a linear viscous damper; when α >1 the device acts as a shock transmitting or a lock-up unit which develops high forces for high velocities due to the hardening relationship between F and v; when α <1 the

device acts as a non-linear viscous damper which produces a force reduction at high velocities due to a softening relationship between F and v.

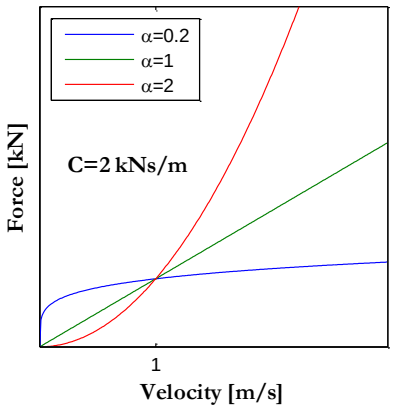

Figure 5-2 Force-velocity relationship for different viscous exponents

In a series connection such as the Maxwell model considers (Figure 5-1), the force on each element is the same and equal to the imposed force (Eq. 5.3), while the total deformation is the sum of the deformation in each element (Eq. 5.4).

$$F = F_s + F_d \tag{5.3}$$

$$\Delta = \Delta_s + \Delta_d \tag{5.4}$$

In order to introduce the viscous dampers in the OpenSees model of the reference building, to perform a seismic retrofitting system of the beam-to-column connections, the truss elements used to model the steel profiles of the three-hinge arc system (Section 3.3.2) are replaced with a *twoNodeLink* element (McKenna and Fenves 2013). This object is defined by two nodes *i* and *j*: if the element has a non-zero length (distance between the two nodes), the local x axis corresponds to the *i-j* direction. An orientation vector should be assigned in order to define the local y axis components in the global coordinates. For the reference model the local x-y plane corresponds to the global z-x plane (Figure 3-3).

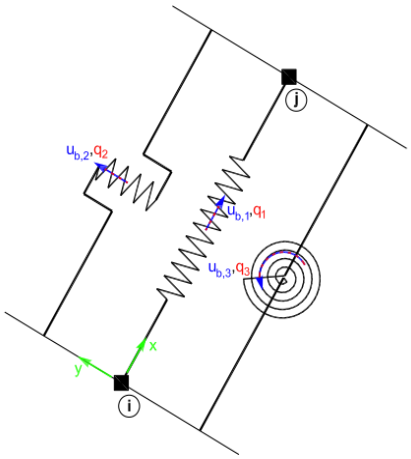

Figure 5-3 TwoNodeLink element

In particular, for the considered geometry (Figure 5-4), in which the lower profile has an inclination angle β=57° and the upper one has an inclination angle α=25°, the orientation vectors for the local x and y axes of the lower profile (x_{p1} and y_{p1}) and of the upper one (x_{p2} and y_{p2}) can be defined as follows, providing for each vector the three components with respect to the global axes (Table 5-1):

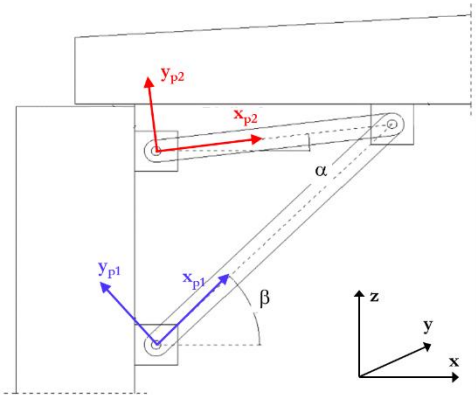

Figure 5-4 Geometrical arrangement of the retrofitting system

Table 5-1 Orientation vectors for the two node elements

	x_p			y_p		
Profile 1	0.5	0.0	0.8	-0.8	0.0	0.5
Profile 2	0.9	0.0	0.4	-0.4	0.0	0.9

The two node element can have six degrees of freedom and, for this reason, six *UniaxialMaterials* (McKenna and Fenves 2013) should be associated in each direction, in order to define the constitutive law for translations along the local x, y and z axes and rotations about local x, y and z axes.

In particular, it is assumed that the viscous damper is activated only in the connection device axial direction (local x axis) so that:

- the uniaxial material assigned to model the translations along the local x axis performs the Maxwell model;

- the uniaxial material assigned to model the rotations about the local z axis allows free rotations (relative hinge restrain in the global z-x plane). This condition can be obtained using an *Elastic UniaxialMaterial*, with a very low initial stiffness;
- the uniaxial materials assigned in all the remaining directions block the corresponding degrees of freedom. This condition can be obtained using an *Elastic UniaxialMaterial* with a very high initial stiffness.

The uniaxial material which performs the Maxwell model and simulates the hysteretic response of a nonlinear viscous damper is the ViscousDamper material (McKenna and Fenves 2013). The required input parameters are: the elastic stiffness (K) of the linear spring (to model the axial flexibility of the viscous damper related to the brace and damper elastic deformations), the viscous parameter (C) of the damper and the viscous damper exponent (α). In the following, the viscous exponent is assumed to be equal to 1 (linear viscous damper).

5.3 Numerical investigations

5.3.1 *Viscous damper parameters*

In order to define the optimal values for the elastic stiffness and the viscous parameter, parametric studies are conducted varying both the damper stiffness K and the viscous parameter C.

Dynamic analyses are performed on the single frame model, defined in 4.3.1, for which each beam-to-column connection is retrofitted with two viscous dampers (placed in the same position of the steel profiles used in the hysteretic connection), so that the three hinge arc configuration is still present.

The dynamic non-linear analyses on the single frame are performed considering the only horizontal component of the earthquake in the x direction.

In the following, the seismic behavior of the retrofitting system is described through the numerical results of the dynamic analysis performed on the reference frame, using the North component of the Emilia earthquake (29/05/2012), recorded in Mirandola (Section 3.4).

Different values for K and C are assumed: in the following, the numerical results refer to the nine couples of values presented in Table 5-2.

Table 5-2 Assumed values for the viscous stiffness K and the viscous parameter

	C_1 [kNs/mm]		**C_2 [kNs/mm]**		**C_3 [kNs/mm]**	
K_1 [kN/mm]	10	1	10	2	10	5
K_2 [kN/mm]	50	1	50	2	50	5

K_3 [kN/mm]	500	1	500	2	500	5

Figure 5-5 shows the axial force-axial displacement in a single device, i.e. the lower profile of the left side of the frame, recorded for each value of C, varying the value of K. Table 5-3 and Table 5-4 show the maximum force and the maximum displacement recorded for each value of C, varying the value of K. It is worthy notice that:

- for each value of the viscous parameter C, increasing the elastic stiffness, the hysteresis cycles increase their slope. This evidence is clearer for higher values of C;
- different values of C and K do not significantly affect the maximum axial displacement recorded in the device. The maximum axial displacement is only affected by the damper configuration since for the upper damper (Table 5-5) lower displacements are recorded. This evidence is of high interest because it implies that the viscous damper can be designed for different values of K and C, in order to have different dynamic responses in terms of damped energy (dependent on the area enclosed by the hysteresis cycles) and arranged so that the relative displacements between the beam and the column are kept under control in order to guarantee that they always are lower than the values which correspond to unseating phenomena;
- on the contrary both the increase of K and the increase of C result in an increase of maximum axial force in the device. In particular, the axial force in the device appears to be strongly dependent on the value of K and this dependence is more noticeable for higher values of C.

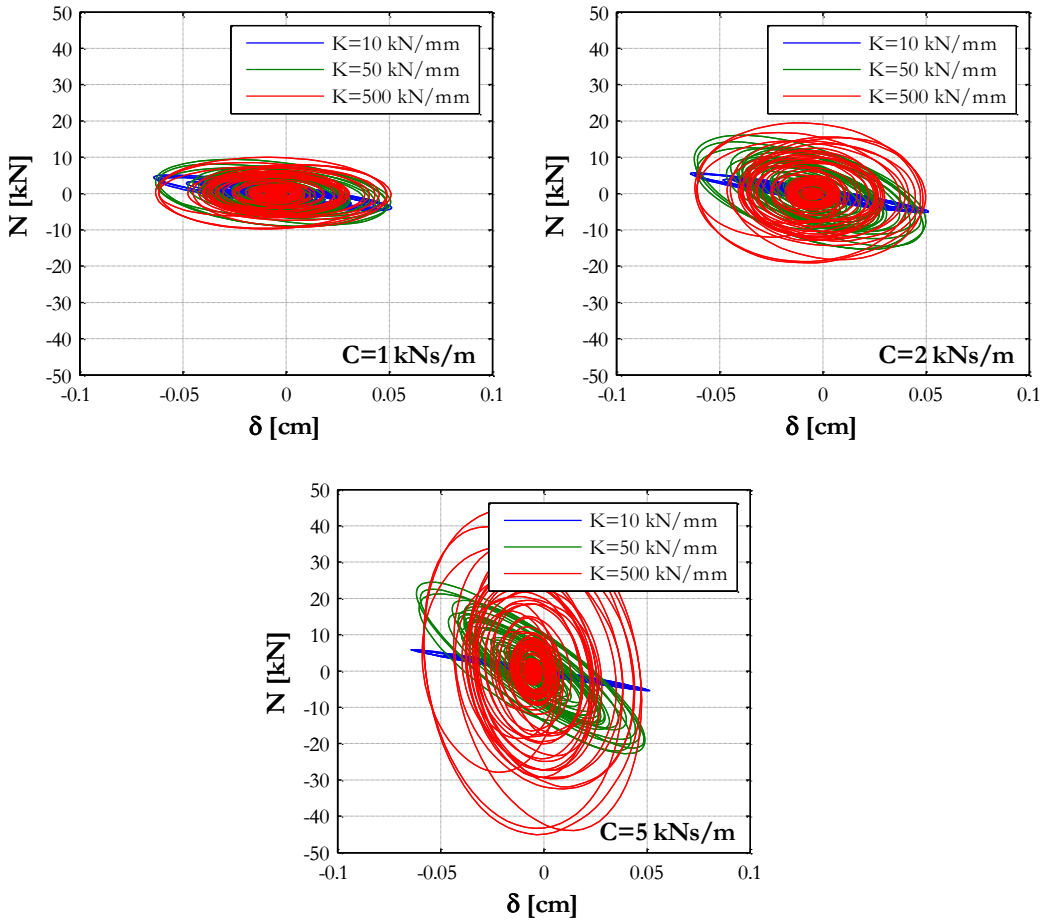

Figure 5-5 Hysteretic response for the viscous damper, varying the elastic stiffness (K) and the viscous parameter (C)

Table 5-3 Maximum axial displacement in the viscous damper (lower profile, left side), varying K and C

Max Displ. [cm]	C_1 [kNs/mm]	C_2 [kNs/mm]	C_3 [kNs/mm]
K_1 [kN/mm]	0.0512	0.0512	0.0512
K_2 [kN/mm]	0.0507	0.0499	0.0490
K_3 [kN/mm]	0.0508	0.0498	0.0474

Table 5-4 Maximum axial force in the viscous damper (lower profile, left side), varying K and C

Max Force [kN]	C_1 [kNs/mm]	C_2 [kNs/mm]	C_3 [kNs/mm]
K_1 [kN/mm]	5.11	5.71	5.91
K_2 [kN/mm]	9.38	16.06	24.47

K_3 [kN/mm]	9.97	19.42	44.79

Table 5-5 Maximum axial displacement in the viscous damper (upper profile, left side), varying K and C

Max Displ. [cm]	**C_1 [kNs/mm]**	**C_2 [kNs/mm]**	**C_3 [kNs/mm]**
K_1 [kN/mm]	0.029	0.029	0.029
K_2 [kN/mm]	0.028	0.028	0.027
K_3 [kN/mm]	0.028	0.028	0.026

Table 5-6 Maximum axial force in the viscous damper (upper profile, left side), varying K and C

Max Force [kN]	**C_1 [kNs/mm]**	**C_2 [kNs/mm]**	**C_3 [kNs/mm]**
K_1 [kN/mm]	2.88	3.21	3.32
K_2 [kN/mm]	5.28	9.03	13.76
K_3 [kN/mm]	5.61	10.93	25.20

The seismic performance of the viscous dampers is strictly connected to their damping capacity which could be measured through the damped energy during the hysteresis loops. In Figure 5-6 each bar represents the cumulated energy dissipated by the lower and the upper device, on both connection of the reference frame, at the end of the input seismic motion. It is confirmed once again that for lower values of C, the seismic performance is slightly improved for different values of the elastic stiffness; whereas, for high values of the viscous parameter C, the seismic performance is more influenced by the elastic stiffness and for higher values of K the viscous damper increase significantly the dissipated energy during the input motion.

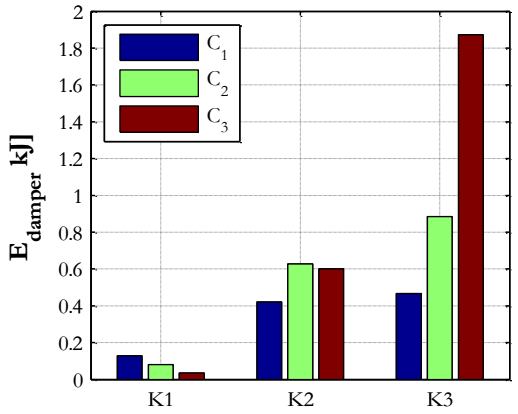

Figure 5-6 Dissipated energy by the viscous dampers on both the connections of the reference frame

An important issue to check during the application of a retrofitting solution is the variation of the dynamic properties of the retrofitted structures due to the presence of external dampers which may results in a variation of the fundamental period. The presence of external devices, could lead to higher lateral stiffness and lower fundamental periods. This could result in higher inertial force, due to the seismic input motion, with higher input energy for the structure. Then, if this input energy is not efficiently dissipated by the external dampers, it could result in higher structural damage.

For the selected retrofitting solution, it is pointed out that the structural vibration period is affected by the presence of the viscous dampers but it is not influenced by the viscous damper properties (Table 5-2). In fact, for all the dampers properties, the fundamental period of the retrofitted frame is equal to 0.89sec, lower than the fundamental period of the bare frame, equal to 1sec. However, this does not affect significantly the cumulated input energy at the end of the input motion (Figure 5-7).

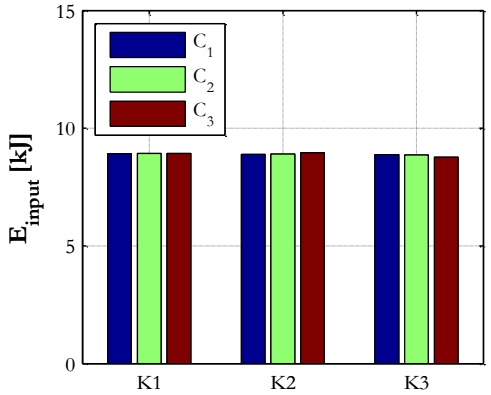

Figure 5-7 Input energy for the considered viscous damper properties

In Figure 5-8 to Figure 5-10 the seismic performance of the retrofitted frame is described in terms of the energy content absorbed by the plastic hinges at the column base (E_{hyst}), the energy content absorbed by the external dampers (E_{damper}) and the energy content absorbed by the inherent structural damping ($E_{in.damp}$). In the figures the values of each energy content is a percentage of the input energy (E_{input}). It could be pointed out that, even if the dissipated energy by the external dampers is quite low, the dissipated energy by the column plastic hinges is decreased with respect to the bare frame due to an overall global response of the structure. The presence of viscous dampers, moreover, decreases the inherent viscous damping of the structure: more the external dampers dissipate (Figure 5-9), more the inherent damping reduces (Figure 5-10).

The overall good behavior is confirmed by a good local response in terms of moment-rotation diagrams and in terms of lateral drifts: Figure 5-11 and Figure 5-12 show the moment-rotation envelopes and the drifts versus time for the column on the left side of the frame, considering the viscous damper parameter C=5kNs/mm. It is worthy noticeable that the column rotations, after overpassing the cracking value, do not reach yielding. As well, the drift values are much lower than the code limit equal to 1%.

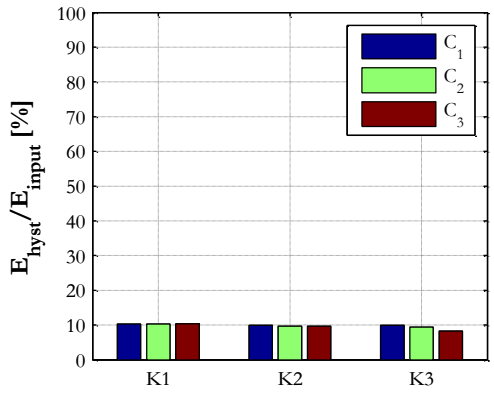

Figure 5-8 Dissipated energy by the column plastic hinge with respect to the input energy

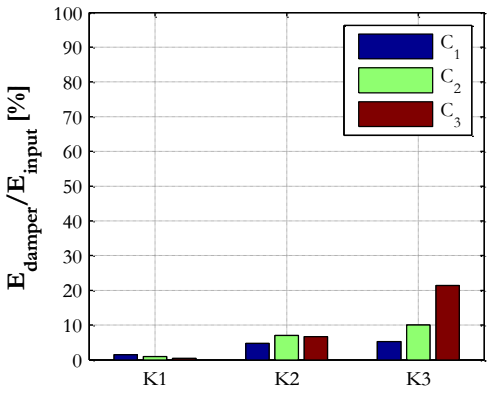

Figure 5-9 Dissipated energy by the external dampers with respect to the input energy

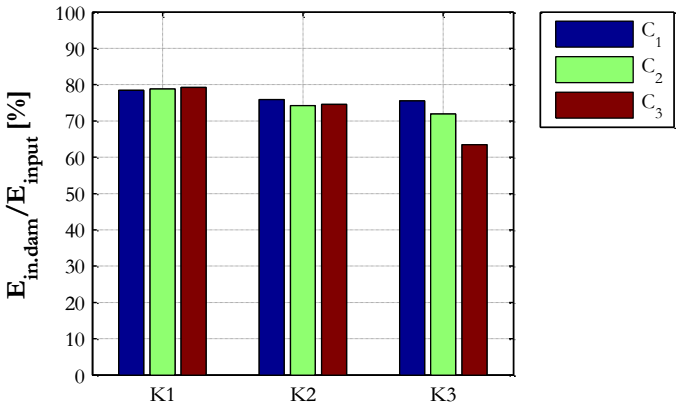

Figure 5-10 Dissipated energy by the inherent damping with respect to the input energy

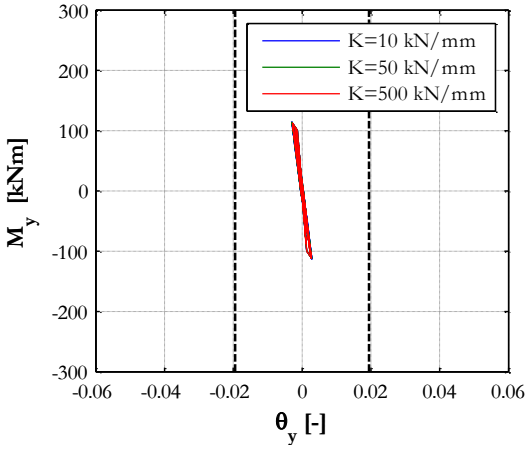

Figure 5-11 Moment-rotation envelopes for the left column of the retrofitted frame (C=5kNs/mm)

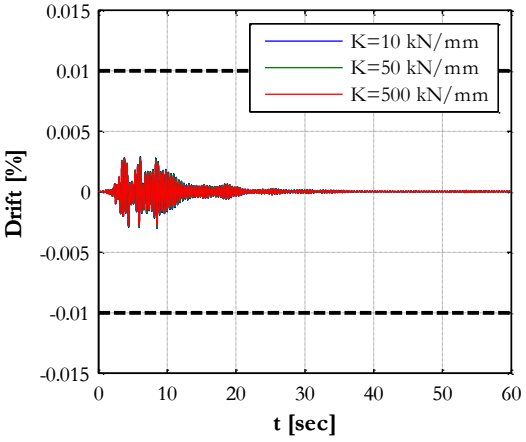

Figure 5-12 Drifts time-series for the left column of the retrofitted frame (C=5kNs/mm)

5.3.2 *Frequency content dependence*

According to the previous analysis results, in order to investigate further issues related to the application of the viscous dampers, the values of elastic stiffness K and of the viscous parameter C are chosen equal to 500kN/mm and 2kNs/mm, respectively.

In the following, in order to verify the dependence on the frequency content of the input motion, the seismic performance of the viscous devices and of the main structure are investigated applying the set of accelerograms defined in Section 3.4. In fact, for the selected accelerograms, different Fourier amplitudes correspond to the fundamental period of the bare frame (Figure 5-13). Given the damper properties, as specified before,

the natural frequency of the external damper is fixed and its response could be influenced by resonance phenomena. In Figure 5-14 also the Fourier spectrum of the Mirandola input motion is represented in order to compare the frequency contents.

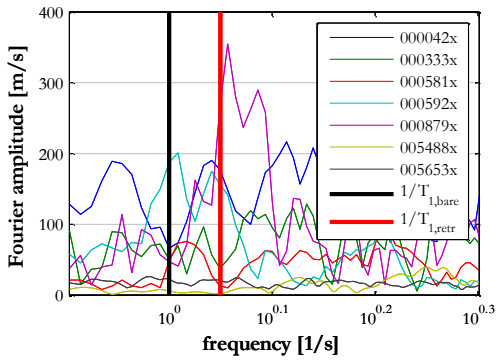

Figure 5-13 Fourier amplitudes corresponding to the fundamental period of the bare and retrofitted frame, for the selected accelerograms

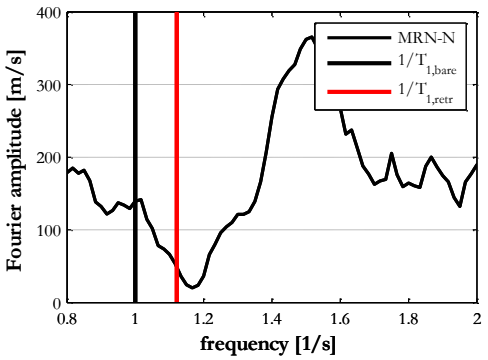

Figure 5-14 Fourier amplitudes corresponding to the fundamental period of the bare and retrofitted frame, for the MRN accelerogram

In Figure 5-15 it can be pointed out that if higher Fourier amplitude are recorded in correspondence of the fundamental period of the retrofitted frame, the viscous dampers show a better performance in terms of damping capacity. It should be notice, however, that for the same device properties used considering the Mirandola input (Figure 5-5), for the selected accelerograms with higher Fourier amplitude higher axial displacements and higher axial forces are recorded.

This consideration should be taken into account during the design process in order to control the maximum force transmitted to the main structure during the earthquake.

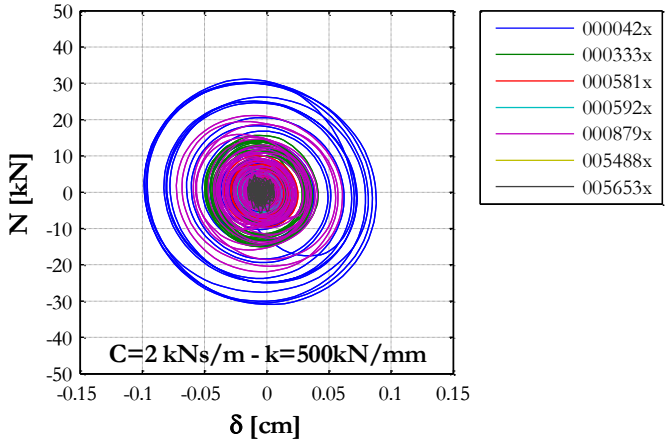

Figure 5-15 Hysteretic response for the lower viscous damper of the left beam-to-column connection, varying the input motion

5.3.3 *Friction coefficient dependence*

As observed in Section 4.3.7, for external dampers displacements dependent the seismic performance of the dampers as well as of the retrofitted structure could be influenced by the possibility that relative displacements between beam and column can occur.

In the seismic retrofitting of friction connections in existing structures it is very difficult to design an hysteretic device (which can properly activate and dissipate) because the evaluation of the friction coefficient is non-reliable due to material deterioration or to the presence of vertical seismic excitations.

For this reason, the application of external devices based on relative velocities can avoid this problem. In order to verify the effectiveness of viscous dampers applied to friction beam-to-column connections, dynamic analyses are performed using the Mirandola input presented in the previous sections, varying the value of the friction coefficient which characterizes the sliding surfaces.

Five different values of the friction coefficient μ are applied, varying from μ=0 (which corresponds to a perfectly smooth surface) to μ=0.8 (which corresponds to a very rough surface).

However, observing the hysteresis loops in Figure 5-16, which refer to the cyclic response of the lower device applied on the beam-to-column connection on the left side of the reference frame, it can be pointed out that, for the selected device properties (C=2kNs/mm and K=500kN/mm), the viscous dampers show the same response, in terms of both maximum force and maximum displacement.

This is an important consideration to take into account during the design process and the selection of the device properties.

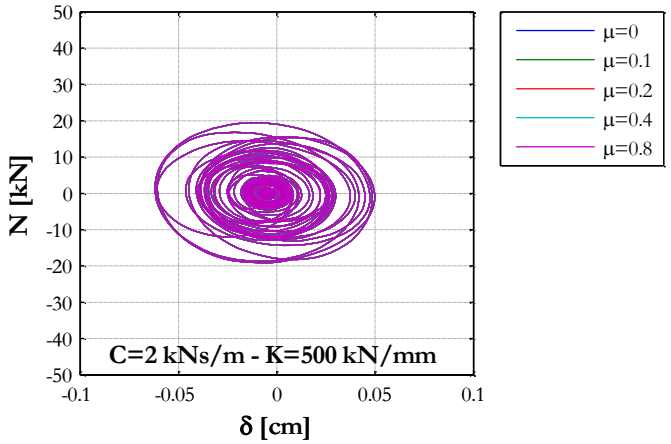

Figure 5-16 Hysteretic response for the lower viscous damper of the left beam-to-column connection, varying the friction coefficient at the beam-to-column surface

Chapter 6

FINAL REMARKS

Precast structures are largely applied in the modern building practice because of the good mechanical properties of the adopted materials and because of the quick installation procedures. However, the component members produced in the manufacturing plants are then assembled on the construction site and high sources of structural vulnerabilities can be associated to the realization of mutual connections.

In some cases, when poor construction details are provided in accordance with non-seismic or out-of-date seismic codes, structural deficiencies can also affect the main elements and especially the elements devoted to offer ductility sources, i.e. the vertical columns.

Recent seismic events, which interested industrial areas, produced large damage to the precast structures. This work focuses on typical one-story precast buildings, designed without any seismic criteria, characterized by isolated columns fixed in socket foundations and connected to the beams by friction connections. Roof elements are arranged so that no rigid diaphragm is provided and the seismic force at the roof level is transferred to the lateral resisting system by masses proportional criteria which lead to plan irregularities.

For the above considerations, it is recognized that seismic retrofitting interventions are required for the existing precast structures. However, two main issues should be faced: first, the code recommendations for seismic retrofit of the precast structures are still poor; second, the retrofit strategies typically adopted for the reinforced cast-in situ buildings are not suitable to fix the specific vulnerabilities related to the structural scheme of the precast buildings. For this reason in the Chapter 2 of this work, the principles of seismic retrofitting strategies are described and the Italian and European codes approach have been presented.

In this work, the retrofit solutions for the friction beam-to-column connections have been considered monitoring the seismic response of a real case study precast structure, located in Mirandola (Emilia Romagna region). The structural performance both of the as-built structure and of the retrofitted one is presented in terms of several parameters, which describe the local and the global seismic response. The local response has been

described through the relative displacements occurred in the friction connections and the moment-rotation envelopes of the plastic hinges at the column bases. The global response has been described through the structural dynamic properties, i.e. the vibration periods, the energy contents associated to the input motion and the lateral drifts exhibited by vertical resisting elements.

The monitoring of the above cited parameters for the existing structure, subjected to the Emilia earthquake (May, 29th 2012), demonstrated a poor seismic performance. In fact, the columns exhibited high plastic rotations, which overpassed the yielding threshold resulting in a wide structural damage. Moreover, the lateral drifts exceeded the code limit, which should prevent the non-structural damage for displacement sensitive equipment.

In this work, two different retrofit strategies are applied. The first one consists in the application of a steel device, which can provide additional shear strength to the beam-to-column connection and prevent unseating phenomena, limiting the relative beam-to-column displacement. This device can work as a rigid restrain without any damping capacity. Otherwise, it can provide energy dissipation through hysteretic mechanisms based on the attainment of a yielding threshold in the constitutive behavior of the steel members. The second one consists in the application of a viscous device, which can be activated by relative velocities and takes advantage of the material aptitude in absorbing and damping external forces. A detailed description of both the strategies has been presented in the Chapter 4 and Chapter 5, respectively. In these chapters, experimental and numerical parametric analyses and several considerations based on the results judgements are performed in order to define the optimal configuration and the mechanical properties of the retrofitting devices, which lead to good seismic performances.

The main results of this work can be summarized as follow:

- a three-hinged steel retrofit device which connects precast beams and columns and applied to the external surface of the concrete elements, is tested under quasi-static cyclic loads along the beam axis direction. The shear tests, performed on two different configurations (with and without rubber sheath around the horizontal dowels), demonstrated high strength and deformation capacity. However, the connection failure regards the concrete elements (column and beam concrete covers) since the steel elements (horizontal dowels and steel profiles) perform an elastic behavior;
- in order to investigate the seismic performance of the three-hinged steel retrofit device, non-linear dynamic analyses are performed on a single frame of the reference building in which the device is applied at the internal surfaces of the concrete elements. The analyses results demonstrate that the steel profiles reach failure for buckling or for the shear failure of the horizontal dowels. This results

in a brittle mechanism without any ductile source. The numerical model is able to perform the failure in run time of the single steel profile: the profile is removed from the structural model but this results in an asymmetric seismic response of the frame. The retrofit system does not perform any ductile deformation and the whole non-linear response is related to the structural damage recorded in the column plastic hinges;

- in order to improve the seismic performance of the retrofit system, the maximum axial force in compression and in tension is limited so that the maximum shear force in the connection should be lower that the shear force which causes the attainment of the yielding moment in the column plastic hinge. However, it is recognize that this condition is not sufficient to optimize the ductile behavior of the retrofitting system because if the connection shear force is lower than the friction strength of the beam-to-column connection, no relative displacements are performed and the hysteretic damper van not be activated;
- in order to overpass the limitation of the displacement dependent devices, a viscous damper is applied to the beam-to-column connection. This solution appears to be very convenient since it does not significantly modify the dynamic properties of the main structure and performs a high energy dissipation which results in a reduction of the lateral drifts and of the structural damage at the column base. The behavior of the viscous damper appears to be not dependent from the friction coefficient between beam and column. On the contrary it appears to depend on the frequency content of the input motion.

References

Baird, A., Palermo, A., and Pampanin, S. (2011). "Facade damage assessment of multi-storey buildings in the 2011 Christchurch earthquake." *Bulletin of the New Zealand Society for Earthquake Engineering*, 44(4), 368-376.

Belleri, A., Brunesi, E., Nascimbene, R., Pagani, M., and Riva, P. (2015). "Seismic performance of precast industrial facilities following major earthquakes in the Italian territory." *Journal of Performance of Constructed Facilities*, 29(5).

Belleri, A., and Riva, P. (2012). "Seismic performance and retrofit of precast concrete grouted sleeve connections." *PCI Journal*, 57(1), 97-109.

Belleri, A., Torquati, M., and Riva, P. (2014). "Seismic performance of ductile connections between precast beams and roof elements." *Mag Concrete Res*, 553-562.

Belleri, A., Torquati, M., and Riva, P. (2014). "Seismic performance of ductile connections between precast beams and roof elements." *Magazine of Concrete Research*, 66(11), 553-562.

Belleri, A., Torquati, M., Riva, P., and Nascimbene, R. (2015). "Vulnerability assessment and retrofit solutions of precast industrial structures." *Earthquake and Structures*, 8(3), 801-820.

Belleri, A., Torquati, M., Riva, P., and Nascimbene, R. (2015). "Vulnerability assessment and retrofit solutions of precast industrial structures." *Earthq Struct*, 8(3), 801-820.

Biondini, F., Dal Lago, B., and Toniolo, G. (2013). "Role of wall panel connections on the seismic performance of precast structures." *Bulletin of Earthquake Engineering*, 11(4), 1061-1081.

Bournas, D. A., Negro, P., and Taucer, F. F. (2013). "Performance of industrial buildings during the Emilia earthquakes in Northern Italy and recommendations for their strengthening." *Bulletin of Earthquake Engineering*, 1-22.

Capozzi, V., and Magliulo, G. (2012). "Struttura e procedimento di montaggio della stessa (in italian)."

Casotto, C., Silva, V., Crowley, H., Nascimbene, R., and Pinho, R. (2015). "Seismic fragility of Italian RC precast industrial structures." *Engineering Structures*, 94, 122-136.

CEN (2004). "Eurocode 2: design of concrete structures - Part 1-1: General rules and rules for buildings."Brussels, Belgium. .

CEN (2005). "Eurocode 3: design of steel structures - Part 1-1: General rules and rules for buildings. EN 1993-1-1."Brussels, Belgium. .

CEN (2005). "Eurocode 8: design of structures for earthquake resistance - Part 1: general rules, seismic actions and rules for buildings. EN 1998-1." Brussels, Belgium.

CEN (2005). "Eurocode 8: Design of structures for earthquake resistance - Part 3: Assessment and retrofitting of buildings." Brussels, Belgium.

Center, P. E. E. R. 2007. OpenSeesUniversity of California, Berkeley.

Chopra, A. K. (1995). *Dynamics of structures: Theory and Applications to Earthquake Engineering*, Prentice Hall, Englewood Cliffs, New Jersey, USA.

Circolare 02/02/2009 n. 617 (2009). "Istruzioni per l'applicazione delle "Nuove norme tecniche per le costruzioni" di cui al D.M. 14 gennaio 2008." M. d. I. e. d. Trasporti, ed.Gazzetta Ufficiale n. 47 del 26 febbraio 2009.

CNR 10018 (1999). "Apparecchi di appoggio per le costruzioni (in Italian)." Bollettino Ufficiale del CNR.

D. M. 14/01/2008 (2008). "NormeTecniche per le Costruzioni (in Italian) ", G.U. n. 29 4 febbraio 2008.

da Fonseca, T. d. C. S., de Almeida, S. F., and de Hanai, J. B. (2011). "Beam-to-Column Connection of a Precast Concrete Frame Strengthened by NSM CFRP Strips." *Advances in FRP Composites in Civil Engineering*, L. Ye, P. Feng, and Q. Yue, eds., Springer Berlin Heidelberg, 858-861.

Dal Lago, B. A. (2015). "Seismic performance of precast structures with dissipative cladding panel connections." *PhD dissertation, Doctoral School in Structural, Earthquake and Geotechnical Engineerign - Politecnico di Milano*, Cicle XXVI.

Faggiano, B., Iervolino, I., Magliulo, G., Manfredi, G., and Vanzi, I. (2009). "Post-event analysis of industrial structures behavior during L'Aquila earthquake." *Progettazione sismica* 3, 203-208.

Fardis, M., Liosatou, E., and Kosmopoulos, A. (2015). "Analysis of first building retrofitted to EN-Eurocode 8 versus performance under near-design-level earthquake." *Bulletin of Earthquake Engineering*, 13(9), 2567-2590.

FEMA, P. (2000). "Commentary for the Seismic Rehabilitation of Buildings." *FEMA-356, Federal Emergency Management Agency, Washington, DC*.

fib (2003). "Seismic assessment and retrofit of reinforced concrete buildings." *fib Bulletin No.24*.

Fischinger, M., Kramar, M., and Isaković, T. (2008). "Cyclic response of slender RC columns typical of precast industrial buildings." *Bulletin of Earthquake Engineering*, 6(3), 519-534.

Gruppo di Lavoro Agibilità Sismica dei Capannoni Industriali (2012). "Linee di indirizzo per interventi locali e globali su edifici industriali monopiano non progettati con criteri antisismici." http://www.reluis.it/images/stories/Linee_di_indirizzo_GDL_Capannoni.pdf.

Ibarra, L. F., Medina, R. A., and Krawinkler, H. (2005). "Hysteretic models that incorporate strength and stiffness deterioration." *Earthquake Engineering & Structural Dynamics*, 34(12), 1489-1511.

Iervolino, I., Galasso, C., and Cosenza, E. (2010). "REXEL: computer aided record selection for code-based seismic structural analysis." *Bulletin of Earthquake Engineering*, 8(2), 339-362.

Kremmyda, G., Fahjan, Y., and Tsoukantas, S. (2014). "Nonlinear FE analysis of precast RC pinned beam-to-column connections under monotonic and cyclic shear loading." *Bulletin of Earthquake Engineering*, 12(4), 1615-1638.

Lam, N., and Gad, E. "An Innovative Approach to the Seismic Assessment of Non-Structural Components in Buildings." *Proc., Procs. of the Australian Earthquake Engineering Society (AEES) Annual Seminar*.

Lampropoulos, A. P., and Dritsos, S. E. (2011). "Modeling of RC columns strengthened with RC jackets." *Earthquake Engineering & Structural Dynamics*, 40(15), 1689-1705.

Latour, M., and Rizzano, G. (2015). "The role od the connection between panels and structure on the seismic behavior of industrial building." *Conference proceedings, ANIDIS XVI - L'Aquila September 2015*.

Legge 01/08/2012 n. 122 (2012). "Conversione in legge, con modificazioni, del decreto-legge 6 giugno 2012, n. 74, recante interventi urgenti in favore delle popolazioni colpite dagli eventi sismici che hanno interessato il territorio delle province di Bologna, Modena, Ferrara, Mantova, Reggio Emilia e Rovigo, il 20 e il 29 maggio 2012 (in Italian)." Gazzetta Ufficiale n. 180 del 03/08/2012.

Luzi, L., Hailemikael, S., Bindi, D., Pacor, F., Mele, F., and Sabetta, F. (2008). "ITACA (ITalian ACcelerometric Archive): A web portal for the dissemination of Italian strong-motion data." *Seismological Research Letters*, 79(5), 716-722.

Magliulo, G., Capozzi, V., Fabbrocino, G., and Manfredi, G. (2011). "Neoprene-concrete friction relationships for seismic assessment of existing precast buildings." *Engineering Structures*, 33(2), 532-538.

Magliulo, G., Capozzi, V., and Manfredi, G. (2014). "Experimental shear test on beam-column pin connections of precast structures." *Earthquake Engineering & Structural Dynamics*, (under review).

Magliulo, G., Ercolino, M., Cimmino, M., Capozzi, V., and Manfredi, G. (2014). "FEM analysis of the strength of RC beam-to-column dowel connections under monotonic actions." *Constr Build Mater*, 69, 271-284.

Magliulo, G., Ercolino, M., Cimmino, M., Capozzi, V., and Manfredi, G. (2015). "Cyclic shear test on dowel beam-column connections." *Earthquakes and Structures*, 9(3), 541-562.

Magliulo, G., Ercolino, M., and Manfredi, G. (2015). "Influence of cladding panels on the first period of one-story precast buildings." *Bulletin of Earthquake Engineering*, 13(5), 1531-1555.

Magliulo, G., Ercolino, M., Petrone, C., Coppola, O., and Manfredi, G. (2014). "The Emilia Earthquake: Seismic Performance of Precast Reinforced Concrete Buildings." *Earthq Spectra*, 30(2), 891-912.

Magliulo, G., Ercolino, M., Petrone, C., Coppola, O., and Manfredi, G. (2014). "Emilia Earthquake: the Seismic Performance of Precast RC Buildings." *Earthquake Spectra*, 30(2), 891-912.

Magliulo, G., Fabbrocino, G., and Manfredi, G. (2008). "Seismic assessment of existing precast industrial buildings using static and dynamic nonlinear analyses." *Engineering Structures*, 30(9), 2580-2588.

Makris, N., and Constantinou, M. (1991). "Fractional-derivative Maxwell model for viscous dampers." *J. Struct. Eng.*, 117(9), 2708-2724.

Martinelli, P., and Mulas, M. G. (2010). "An innovative passive control technique for industrial precast frames." *Engineering Structures*, 32(4), 1123-1132.

Mazza, F. (2015). "Comparative study of the seismic response of RC framed buildings retrofitted using modern techniques." *Earthquake and Structures*, 9(1), 29-48.

McKenna, F., and Fenves, G. L. (2013). "OpenSees Manual http://opensees.berkeley.edu." (February 27, 2013, 2013).

Ozden, S., Akpinar, E., Erdogan, H., and Atalay, H. M. (2014). "Performance of precast concrete structures in October 2011 Van earthquake, Turkey." *Mag Concrete Res*, 66(11), 543-552.

Petrovcic, S., and Kilar, V. (2012). "Effects of Horizontal and Vertical Mass-Asymmetric Distributions on the Seismic Response of a High-Rack Steel Structure." *Advances in Structural Engineering*, 15(11), 1977-1988.

Psycharis, J., Mouzakis, H., and Carydis, P. (2006). "Experimental investigation of the seismic behaviour of prefabricated RC structures." *Proceeding of the 2nd International Conference, Fib, Naples*.

Saatcioglu, M., Mitchell, D., Tinawi, R., Gardner, N. J., Gillies, A. G., Ghobarah, A., Anderson, D. L., and Lau, D. (2001). "The August 17, 1999, Kocaeli (Turkey) earthquake — damage to structures." *Canadian Journal of Civil Engineering*, 28(4), 715-737.

Toniolo, G. (2012). "SAFECAST project: European research on seismic behaviour of the connections of precast structures." *15th World conference on earthquake engineering (15WCEE), Lisbon, Portugal*.

Toniolo, G. (2013). "Safecast Project: European Research on Seismic Behaviour of the Connections of Precast Structures." *COMPDYN 2013 4th ECCOMAS Thematic Conference on Computational Methods in Structural Dynamics and Earthquake Engineering, Kos Island, Greece, 12–14 June 2013*.

Toniolo, G., and Colombo, A. (2012). "Precast concrete structures: the lessons learned from the L'Aquila earthquake." *Struct Concrete*, 13(2), 73-83.

van der Harst, P., Zhang, W. H., Leach, I. M., Rendon, A., Verweij, N., Sehmi, J., Paul, D. S., Elling, U., Allayee, H., Li, X. Z., Radhakrishnan, A., Tan, S. T., Voss, K., Weichenberger, C. X., Albers, C. A., Al-Hussani, A., Asselbergs, F. W., Ciullo, M., Danjou, F., Dina, C., Esko, T., Evans, D. M., Franke, L., Goegele, M., Hartiala, J., Hersch, M., Holm, H., Hottenga, J. J., Kanoni, S., Kleber, M. E., Lagou, V., Langenberg, C., Lopez, L. M., Lyytikainen, L. P., Melander, O., Murgia, F., Nolte, I. M., O'Reilly, P. F., Padmanabhan, S., Parsa, A., Pirastu, N., Porcu, E., Portas, L., Prokopenko, I., Ried, J. S., Shin, S. Y., Tang, C. S., Teumer, A., Traglia, M., Ulivi, S., Westra, H. J., Yang, J., Zhao, J. H., Anni, F., Abdellaoui, A., Attwood, A., Balkau, B., Bandinelli, S., Bastardot, F., Benyamin, B., Boehm, B. O., Cookson, W. O., Das, D., de Bakker, P. I. W., de Boer, R. A., de Geus, E. J. C., de Moor, M. H., Dimitriou, M., Domingues, F. S., Doring, A., Engstrom, G., Eyjolfsson, G. I., Ferrucci, L., Fischer, K., Galanello, R., Garner, S. F., Genser, B., Gibson, Q. D., Girotto, G., Gudbjartsson, D. F., Harris, S. E., Hartikainen, A. L., Hastie, C. E., Hedblad, B., Illig, T., Jolley, J., Kahonen, M., Kema, I. P., Kemp, J. P., Liang, L. M., Lloyd-Jones, H., Loos, R. J. F., Meacham, S., Medland, S. E., Meisinger, C., Memari, Y., Mihailov, E., Miller, K., Moffatt, M. F., Nauck, M., Novatchkova, M., Nutile, T., Olafsson, I., Onundarson, P. T., Parracciani, D., Penninx, B. W., Perseu, L., Piga, A., Pistis, G., Pouta, A., Puc, U., Raitakari, O., Ring, S. M., Robino, A., Ruggiero, D., Ruokonen, A., Saint-Pierre, A.,

Sala, C., Salumets, A., Sambrook, J., Schepers, H., Schmidt, C. O., Sillje, H. H. W., Sladek, R., Smit, J. H., Starr, J. M., Stephens, J., Sulem, P., Tanaka, T., Thorsteinsdottir, U., Tragante, V., van Gilst, W. H., van Pelt, L. J., van Veldhuisen, D. J., Volker, U., Whitfield, J. B., Willemsen, G., Winkelmann, B. R., Wirnsberger, G., Algra, A., Cucca, F., d'Adamo, A. P., Danesh, J., Deary, I. J., Dominiczak, A. F., Elliott, P., Fortina, P., Froguel, P., Gasparini, P., Greinacher, A., Hazen, S. L., Jarvelin, M. R., Khaw, K. T., Lehtimaki, T., Maerz, W., Martin, N. G., Metspalu, A., Mitchell, B. D., Montgomery, G. W., Moore, C., Navis, G., Pirastu, M., Pramstaller, P. P., Ramirez-Solis, R., Schadt, E., Scott, J., Shuldiner, A. R., Smith, G. D., Smith, J. G., Snieder, H., Sorice, R., Spector, T. D., Stefansson, K., Stumvoll, M., Tang, W. H. W., Toniolo, D., Tonjes, A., Visscher, P. M., Vollenweider, P., Wareham, N. J., Wolffenbuttel, B. H. R., Boomsma, D. I., Beckmann, J. S., Dedoussis, G. V., Deloukas, P., Ferreira, M. A., Sanna, S., Uda, M., Hicks, A. A., Penninger, J. M., Gieger, C., Kooner, J. S., Ouwehand, W. H., Soranzo, N., and Chambers, J. C. (2012). "Seventy-five genetic loci influencing the human red blood cell." *Nature*, 492(7429), 369-+.

Vintzeleou, E. N., and Tassios, T. P. (1986). "Mathematical-Models for Dowel Action under Monotonic and Cyclic Conditions." *Magazine of Concrete Research*, 38(134), 13-22.

Yildirim, S., Kalyoncuoglu, A., Erkus, B., and Tonguc, Y. (2015). "Seismic Retrofit of Industrial Precast Concrete Structures Using Friction Dampers: Case Study from Turkey." *Improving the Seismic Performance of Existing Buildings and Other Structures 2015*, 693-705.

Zoubek, B., Fischinger, M., and Isakovic, T. (2015). "Estimation of the cyclic capacity of beam-to-column dowel connections in precast industrial buildings." *Bulletin of Earthquake Engineering*, 13(7), 2145-2168.

Zoubek, B., Isakovic, T., Fahjan, Y., and Fischinger, M. (2013). "Cyclic failure analysis of the beam-to-column dowel connections in precast industrial buildings." *Engineering Structures*, 52(0), 179-191.